Czech Technical University in Prague
Faculty of Mechanical Engineering
Department of Mechanics, Biomechanics and Mechatronics

APPROXIMATE METHODS FOR CALCULATING NOTCH TIP STRAINS AND STRESSES UNDER MULTIAXIAL CYCLIC LOADING

by

Ing. Maxim LUTOVINOV

Doctoral Study Programme: Mechanical Engineering
Study Field: Mechanics of Rigid and Deformable Bodies and Environment

Supervisors:
prof. Ing. Milan Růžička, CSc. and Ing. Jan Papuga, Ph.D.

A thesis submitted to
the Faculty of Mechanical Engineering, Czech Technical University in Prague,
in partial fulfilment of the requirements for the degree of Doctor.

Prague, March 2022

Thesis Supervisors:
prof. Ing. Milan Růžička, CSc. and
Ing. Jan Papuga, Ph.D.
Department of Mechanics, Biomechanics and Mechatronics
Faculty of Mechanical Engineering
Czech Technical University in Prague
Technická 4
166 07 Prague 6
Czech Republic

Abstract

This work deals with approximate methods for calculating elastic-plastic stresses and strains on the surface of notched samples. In order to expand the range of currently available experimental notch strain response data, specimens manufactured from the 2124-T851 aluminum alloy were subjected to various multiaxial cyclic loading combinations. Then a new approximate method based on the Abdel-Karim-Ohno cyclic plasticity model was proposed. The results of the approximations were verified on own experimental results, as well as on experimental results available in the literature. A comparison with estimates by other methods was also made. The new method provides competitive results and a good correlation with the experimental data.

Keywords: plasticity; multiaxial loading; pseudo stress; stress-strain estimation; 2124-T851.

Abstrakt

Tato práce se zabývá aproximačními metodami pro výpočet elasto-plastických deformací a napětí na povrchu kořene vrubu. Pro rozšíření současně dostupných experimentálních dat deformační odezvy v kořeni vrubu vzorky z hliníkové slitiny 2124-T851 byly zkoušeny různými kombinacemi axiální síly a kroutícího momentu. Poté byla navržena nová aproximační metoda založená na modelu cyklické plasticity Abdel-Karim-Ohno. Výsledky aproximačních výpočtů byly ověřené na vlastních experimentálních datech a experimentálních datech dostupných v literatuře. Bylo provedeno porovnání s výsledky výpočtů jiných aproximačních metod. Nová metoda poskytuje konkurenceschopné výsledky s dobrou shodou s experimentálními výsledky.

Klíčová slova: plasticita; víceosé namáhaní; pseudo napětí; aproximace napětí a deformace; 2124-T851.

Acknowledgements

I would like to thank my supervisors, Milan Růžička and Jan Papuga, who guided me for many years, my colleagues, Michal Bartošák and Jiří Kuželka, who carried out the experimental testing with me, Radim Halama, for his consultations on the plasticity theory, Martin Nesládek, from whom I learned so much in the FEA field, and Anastasiya Paulavets, who is always a tremendous support to me.

I would also like to thank the Czech Science Foundation for their support with grant No. GA15-18274S, and the Grant Agency of the Czech Technical University in Prague, who supported me with grant No. SGS14/181/OHK2/3T/12.

Declaration

I hereby declare that I am the sole author of this dissertation thesis and that I have not used any sources other than those listed in the bibliography and identified as references.

.....
Ing. Maxim Lutovinov
March 2022

Contents

List of Figures **9**

List of Tables **12**

1 Introduction **16**

2 State of the art **18**
2.1 Methods for monotonic loading 18
2.2 Methods for cyclic loading 19
2.3 Plasticity models 23
2.3.1 Mróz plasticity type models 25
2.3.2 Chaboche nonlinear kinematic hardening model 25
2.3.3 Jiang-Sehitoglu plasticity model 26
2.3.4 Ohno-Wang model II 27
2.3.5 Unified viscoplastic constitutive model by Li et al. 27

3 Aims of the thesis **28**

4 Used methods/ tools **30**
4.1 AKO model 30
4.2 Iteration algorithm 31
4.3 Implementation of the approximate method 35

5 Experiments **36**
5.1 DIC 36
5.1.1 Material and specimens 36
5.1.2 Tests realisation 38
5.1.3 Strain measurement 42
5.1.4 Evaluation in Matlab 42
5.2 FEM 44

6 A new method **47**
6.1 A new approximate method 47
6.1.1 Establishing pseudo stress material curve 48
6.1.2 Getting real strain and real stress 48
6.1.3 Equivalence of pseudo and real plastic strain tensors 49
6.1.4 Approximation method step by step 49

6.2 Results - own experiments 50
6.3 Predictions of other authors 55

7 Outcomes **59**

8 Conclusions and future work **60**
8.1 Conclusions 60
8.2 Future work 61

References **61**

Publications of the author related to the topic of the thesis **65**

A Estimates for 2124-T851 aluminum alloy **67**
A.1 U-notched specimen 67
A.2 Specimen with fillet 71

B Estimates comparison for 1070 steel **75**

C MATLAB code of the proposed method **81**
C.1 Main file 81
C.2 Functions 85
C.2.1 calc_alfa_and_dEpsPl 85
C.2.2 calc_alfa_and_Snp1 86
C.2.3 calc_alfa_and_Snp1 86
C.2.4 calc_C_gamma 87
C.2.5 calc_dp_AKO 87
C.2.6 calc_equiv_stress 89
C.2.7 material_curves 89
C.2.8 ramberg_osgood_coefficients 89
C.3 Scripts 90
C.3.1 calc_rel_error 90
C.3.2 define_notch_stress_inputs 91
C.3.3 elastic_region_solution 98
C.3.4 graphs 99
C.3.5 increase_number_of_load_cycles 102
C.3.6 prealocate_variables 104

List of Figures

2.1 Illustration of the pseudo stress-real plastic strain principle. 21
2.2 Experimental loading paths from literature: (A) Butterfly, (B) Circle, (C) ksi, (D) N, (E) NV, (F) Proportional, (G) Rotated V, (H) S, (I) Square, (J) V . F means force, M means moment. 23

4.1 Iteration algorithm for calculating accumulated plastic strain increment dp. 34

5.1 Specimen with U-notch. A and B in frames indicate surfaces based on which a datum axis for geometrical run-out tolerance is defined. 37
5.2 Specimen with fillet. A and B in frames indicate surfaces based on which a datum axis for geometrical run-out tolerance is defined. 37
5.3 Specimen with U-notched sprayed with two acryl paints for DIC measurement. 37
5.4 Loading paths: (top left) "7"; (top middle) Circle; (top right) NV; (middle left) proportional;(middle) Square; (middle right) uniaxial; (bottom) X. . . 39
5.5 Testing part of the experimental setup. Zoomed image of the specimen in a yellow dash frame demonstrates the notch shape, but is taken before the paint application. 41
5.6 Processed experimental axial strain values along the notch tip circuit for a uniaxial tension-compression test. Red dashed line represents mean value, black dashed lines represent 0.1% deviation from the mean value. 43
5.7 A segment of a U-notched test specimen from DIC meausrements. Notch tip circuit (red color) was used for selecting and averaging of notch tip axial strain ε_1. Axis y is parallel to the axis of the specimen. 44
5.8 Axisymmetric models of the U-notched specimen (left) and the specimen with a fillet (right) in Abaqus. u_x and u_y are translations in the x and y axes directions respectively; u_{rx}, u_{ry}, and u_{rz} are rotations about the x, y, and z axes respectively. 45
5.9 Comparison of experimental data and results of elastic–plastic FEA in Abaqus for paths "7" (left) and NV (right) 46

6.1 Pseudo stress–real plastic strain curve and cyclic stress–strain curve; points represent discrete versions of the curves based on the Hollomon parameters. 47
6.2 Influence of the ratcheting parameter μ_i on the prediction for Path "7". (a) just experiment; (b) $\mu_i = 0$; (c) $\mu_i = 0.1$; (d) $\mu_i = 1$ 52

A.1 Estimate for Path Circle, ratio of nominal axial to shear stresses is 1. . . . 67
A.2 Estimate for Path Circle, ratio of nominal axial to shear stresses is 1.73. . . 68
A.3 Estimate for Path NV, ratio of nominal axial to shear stresses is 1. 68
A.4 Estimate for Path NV, ratio of nominal axial to shear stresses is 1.73. . . . 69
A.5 Estimate for Path Proportional, ratio of nominal axial to shear stresses is 1. 69
A.6 Estimate for Path Uniaxial, nominal axial stress is 274.5 MPa. 70
A.7 Estimate for Path X, ratio of nominal axial to shear stresses is 1. 70
A.8 Estimate for Path X, ratio of nominal axial to shear stresses is 1.73. 71
A.9 Estimate for Path Circle, ratio of nominal axial to shear stresses is 1. . . . 71
A.10 Estimate for Path Circle, ratio of nominal axial to shear stresses is 1.73. . . 72
A.11 Estimate for Path NV, ratio of nominal axial to shear stresses is 1. 72
A.12 Estimate for Path Proportional, ratio of nominal axial to shear stresses is 1. 73
A.13 Estimate for Path Proportional, ratio of nominal axial to shear stresses is 1.73 73
A.14 Estimate for Path X, ratio of nominal axial to shear stresses is 1. 74
A.15 Estimate for Path X, ratio of nominal axial to shear stresses is 1.73. 74

B.1 Comparison of the proposed method and estimate by Tao et al. [13] for loading path ksi. 75
B.2 Comparison of the proposed method and estimate by Ince et al. [11] for loading path ksi. 76
B.3 Comparison of the proposed method and estimate by Tao et al. [13] for loading path N. 76
B.4 Comparison of the proposed method and estimates by Li et al. [12] and Ince et al. [11] for loading path N. 77
B.5 Comparison of the proposed method and estimate by Tao et al. [13] for loading path NV. 77
B.6 Comparison of the proposed method and estimate by Ince et al. [11] for loading path NV. 78
B.7 Comparison of the proposed method and estimate by Tao et al. [13] for proportional loading path. 78
B.8 Comparison of the proposed method and estimate by Tao et al. [13] for loading path S. 79
B.9 Comparison of the proposed method and estimates by Li et al. [12] and Ince et al. [11] for loading path S. 79

B.10 Comparison of the proposed method and estimates by Li et al. [12] and Ince et al. [11] for loading path Square (clockwise). 80
B.11 Comparison of the proposed method and estimate by Li et al. [12] for loading path V. 80

List of Tables

2.1 Materials used for validations of the approximate methods. 20
2.2 Experimental loading paths used for validations of the approximate methods. 23
2.3 Plasticity models used in the approximate methods. 24

5.1 Number of cycles till the break of 2124-T851 specimens. 40
5.2 Cyclic stress–strain curve used for elastic–plastic simulations. 46

6.1 Stress concentration factors of the aluminum alloy specimens. 50
6.2 Influence of parameter μ_i values on estimates for 2124-T851 aluminum. . . 53
6.3 Relative errors in percents between measured and calculated strain ranges for 2124-T851 U-notched specimens. $\mu_i = 0$. 54
6.4 Relative errors in percents between measured and calculated strain ranges for 2124-T851 single fillet specimens. $\mu_i = 0$. 54
6.5 Material data on 1070 steel used in the present work. 55
6.6 Relative errors between measured and calculated **axial** strain ranges for selected methods for 1070 steel in percents. 56
6.7 Relative errors between measured and calculated **shear** strain ranges for selected methods for 1070 steel in percents. 57
6.8 Relative errors between measured and calculated **combined** strain ranges for selected methods for 1070 steel in percents. 57
6.9 Influence of parameter μ_i values on estimates for 1070 steel. 58

Nomenclature

Symbols

$\boldsymbol{a}$	deviatoric part of backstress tensor	MPa
$\boldsymbol{a^{(i)}}$	the i^{th} part of deviatoric backstress tensor	MPa
$\overline{a^{(i)}}$	size of the i^{th} part of backstress tensor	MPa
$\boldsymbol{\alpha}$	backstress tensor	MPa
C_i	material parameter (i=1, 2, ..., M)	MPa
c_i	material parameter (i=1, 2, ..., M)	–
d	(following by a symbol) increment designation	–
d_i	distance to the i^{th} neighbour node (DIC)	mm
d_{min}	distance to the closest neighbour node (DIC)	mm
Δ	(following by a symbol) range designation	–
δ_{ij}	Kronecker delta	–
E	Young's modulus	MPa
E	(as superscript) equivalent strain energy density rule solution	
e	elastic solution designation	
ε_{ap}	plastic strain amplitude	
ε_{eq}	equivalent strain	
ε_{ij}	strain tensor component	
$\boldsymbol{\varepsilon_p}$	plastic strain tensor	–

f	yield surface function	
γ_i	material parameter (i=1, 2, ..., M)	–
ζ_i	material parameter (i=1, 2, ..., M)	–
h	plastic modulus	MPa
h_i	slope of a segment of a discretized stress-strain curve	MPa
i	auxiliary index	–
K'	strength coefficient from Hollomon's equation	MPa
K_{yz}	torsion stress concentration factor	–
K_z	axial stress concentration factor	–
K'_z	transverse stress concentration factor	–
k	index of iteration	–
l	index of yield surface	–
λ	plastic multiplier	–
M	number of backstress parts	–
μ_i	ratcheting parameter of Abdel-Karim-Ohno model	–
N	(as superscript) Neuber's rule solution	
n	index of estimation step	–
$\hat{\boldsymbol{n}}$	normal tensor	–
n'	strain hardening exponent from Hollomon's equation	–
ν	Poisson's ratio	–
ξ	Mróz model parameter	–
p	accumulated plastic strain	–
r_i	material parameter (i=1, 2, ..., M)	MPa
$\boldsymbol{s}$	deviatoric stress tensor	MPa

σ	stress in the uniaxial state case (stress-strain curve)	MPa
$\boldsymbol{\sigma}$	stress tensor	MPa
σ_0	constant of Mróz model	MPa
σ_a	stress amplitude	MPa
σ_{eq}	equivalent stress	MPa
σ_{ij}	stress tensor component	MPa
σ_y	yield strength	MPa
θ_i	correction multiplier	–
u_i	displacement of the i^{th} neighbour node	mm
$u_{smoothed}$	smoothed displacement	mm
χ_i	material parameter (i=1, 2, ..., M)	–
ω_i	correction multiplier	–

Abbreviations

AKO	Abdel-Karim-Ohno
DIC	digital image correlation
FE	Finite Element
FEA	Finite Element Analysis

Designations and operators

$\boldsymbol{X}$	second order tensos with components X_{ij}, where $i, j = 1, 2, 3$
$H(f_i)$	Heaviside step function ($H(f_i) = 1$ for $f_i > 0$ and $H(f_i) = 0$ for $f_i \leq 0$)
:	double contraction of tensors (by applying the Einstein summation convention it is possible to express $\boldsymbol{b} : \boldsymbol{c}$ as $b_{ij}c_{ij}$, where $i, j = 1, 2, 3$)

Chapter 1

Introduction

Most initially isotropic engineering materials exhibit elastic-plastic behavior. To evaluate the damage imposed on components made from such materials, one has to obtain strains and stresses of the components in question. Achieving this is possible with the help of experimental measurements, finite element analyses (FEA), or approximate calculation methods. Experimental approaches, although being most precise, are usually expensive and, for some applications, are quite difficult from realization point of view.

A less expensive way to obtain stresses and strains became available with the progress of computer performance capabilities and the invention of the finite element method. With the finite element method, limitations related to complexity of component geometries stopped being an issue.

Still, even with FEA, calculations of large assemblies, especially with non-elastic material behavior, could take up to several days. If several of such calculations need to be made, weeks could be consumed before the final result is achieved.

In order to speed up the process of obtaining stresses and strains, an approximate calculation might be carried out. The results would not be as precise as in the case of experimental measurements or finite element analyses, but they would be obtained faster. That is the motivation behind the approximate methods for stress and strain calculations.

This work deals with approximate methods that transform the initial solution of a problem, obtained from simulation with ideally elastic material behavior, into elastic-plastic estimates using basic material data.

The transformation might be achieved by different approaches. The first one is by creation of a pseudo material, which relate theoretical purely elastic material and real elastic-plastic equivalent. The second approach relies on the connection between linear-elastic and elastic-plastic strain energies.

It is worth noting that in the present time the approximate methods have a limitation on plane stress state. This is due to the plane stress condition being part of the estimations. Specifically, notch tips of specimens are considered whenever such approximate methods are being investigated.

The current state of the methods development will be reviewed in Chapter 2. The aims of thesis will be defined in Chapter 3.

Chapter 4 will deal with methods and tools used to achieve the results of the present work.

In Chapter 5 an experimental program that was carried out to expand the currently available experimental notch strain data will be described.

Chapter 6 will present the new method for the approximation of notch stresses and strains, and the evaluation procedures.

The last chapters 7 and 8 will state outcomes and conclusions of the work.

Chapter 2

State of the art

2.1 Methods for monotonic loading

The first group of approximate methods consists of those intended for monotonic loading and plane stress cases only [1–5]. The limitation of monotonic loading is given by the constitutive models that the approximate methods use, which do not describe the movement of the yield surface. The limitation of the plane stress cases is given by the fact that the methods are designed to estimate stresses and strains at the notch tips of specimens.

To obtain unknown stresses and strains, specifically $\sigma_{22}, \sigma_{23}, \sigma_{33}, \varepsilon_{11}, \varepsilon_{22}, \varepsilon_{23}$, and ε_{33}, a system of 7 equations is assembled. The first equation is based on the equality of strain energy densities at the notch tip of the actual and hypothetically elastic materials. Either generalized Neuber's rule for multiaxial loading

$$\begin{aligned} \sigma^e_{22}d\varepsilon^e_{22} + \sigma^e_{33}d\varepsilon^e_{33} + 2\sigma^e_{23}d\varepsilon^e_{23} + \varepsilon^e_{22}d\sigma^e_{22} + \varepsilon^e_{33}d\sigma^e_{33} + 2\varepsilon^e_{23}d\sigma^e_{23} \; = \\ \sigma^N_{22}d\varepsilon^N_{22} + \sigma^N_{33}d\varepsilon^N_{33} + 2\sigma^N_{23}d\varepsilon^N_{23} + \varepsilon^N_{22}d\sigma^N_{22} + \varepsilon^N_{33}d\sigma^N_{33} + 2\varepsilon^N_{23}d\sigma^N_{23} \end{aligned} \tag{2.1}$$

or the equivalent strain energy density (ESED) rule

$$\sigma^e_{22}d\varepsilon^e_{22} + \sigma^e_{33}d\varepsilon^e_{33} + 2\sigma^e_{23}d\varepsilon^e_{23} = \sigma^E_{22}d\varepsilon^E_{22} + \sigma^E_{33}d\varepsilon^E_{33} + 2\sigma^E_{23}d\varepsilon^E_{23} \tag{2.2}$$

is used. In Equations 2.1 and 2.2 index e means a solution with purely elastic material, N stands for Neuber's rule, and E means the ESED rule. Depending on which rule is used a different estimate is obtained. Rather than choosing one of them, they are usually considered as a lower and an upper limits of the actual notch tip stresses and strains [2–4].

Another four equations are obtained, depending on the approximate method, either by the Hencky relation [2]

$$\varepsilon_{ij} = \frac{1+\nu}{E}\sigma_{ij} - \frac{v}{E}\sigma_{kk}\delta_{ij} + \frac{3}{2}\frac{\varepsilon^p_{eq}}{\sigma_{eq}}s_{ij} \tag{2.3}$$

or by the Prandtl-Reuss relation [3]

$$d\varepsilon_{ij} = \frac{1+\nu}{E} d\sigma_{ij} - \frac{v}{E} d\sigma_{kk}\delta_{ij} + \frac{3}{2}\frac{d\varepsilon^p_{eq}}{\sigma_{eq}} s_{ij}. \tag{2.4}$$

In Equations 2.3 and 2.4, s_{ij} is a deviatoric stress, $\sigma_{eq} = \sqrt{\frac{3}{2} s_{ij} s_{ij}}$ is an equivalent stress, δ_{ij} is the Kronecker delta, ε^p_{eq} is an equivalent strain, $i = 1, 2, 3$ and the Einstein summation convention applies. The equivalent strain is a function of the equivalent stress, such as the plastic part of the Ramberg-Osgood relation:

$$\varepsilon^P_{eq} = \left(\frac{\sigma_{eq}}{K'}\right)^{1/n'}, \tag{2.5}$$

where K' and n' are Hollomon parameters.

The last two equations are provided by energy ratio assumptions in relation to a notch tip. For example, in the case of Singh's method [3], the energy equations are the two of

$$\sigma^e_{22} d\varepsilon^e_{22} + \varepsilon^e_{22} d\sigma^e_{22} = \sigma^N_{22} d\varepsilon^N_{22} + \varepsilon^N_{22} d\sigma^N_{22}, \tag{2.6}$$

$$\sigma^e_{33} d\varepsilon^e_{33} + \varepsilon^e_{33} d\sigma^e_{33} = \sigma^N_{33} d\varepsilon^N_{33} + \varepsilon^N_{33} d\sigma^N_{33}, \tag{2.7}$$

$$\sigma^e_{23} d\varepsilon^e_{23} + \varepsilon^e_{23} d\sigma^e_{23} = \sigma^N_{23} d\varepsilon^N_{23} + \varepsilon^N_{23} d\sigma^N_{23}. \tag{2.8}$$

In [2] it was noted that since the set of equations 2.1-2.8 is nonlinear, there is a possibility of having more than one solution, and if a numerical solver is used, it is important to select the correct solution. Unfortunately, no more details were discussed in [2] on the matter of choosing the right solution.

The methods [1–5] are suitable for calculating the notch tip stresses and strains of components subjected to various types of monotonic loading: uniaxial, multiaxial proportional, and non-proportional loading. To incorporate the ability to calculate the stress-strain response on cyclic loading, more complicated material constitutive models, than those represented by Equations 2.3 and 2.4, need to be combined with the notch correction parts (Equations 2.1, 2.2, and 2.6-2.8).

2.2 Methods for cyclic loading

In order to estimate stresses and strains for cyclic loading, researchers incorporated plasticity models into the approximate methods. This allowed to describe cyclic hardening and softening. Unlike finite-element analyses (FEA), the approximate methods do not deal with elastic–plastic stiffness matrices, but instead use an elastic solution that they convert into an elastic–plastic solution by using a relation either between pseudo material and real material or between linear–elastic and elastic–plastic strain energies.

Only a few methods are based on the equality of linear–elastic and elastic–plastic strain energies, as is in the case of the methods described in the previous section. The more popular approach is in creating a so-called pseudo material that allows to relate a theoretical purely elastic solution with the elastic-plastic one.

One of the first elastic–plastic stress–strain approximate methods for cyclic loading used yet another way to get the estimates [6], different from either strain energy density equality or pseudo material approaches. Barkey pointed out that plastic flow at the notch root behaves differently alongside different directions, and therefore, a notch element could be treated as an equivalent element of an anisotropic material. He used Hill's theory of anisotropic metal plasticity as a yield criterion and combined it with the normality flow rule. By this, Barkey expressed plastic notch strains as a function of nominal stresses and coefficients of Hill's yield criterion, which in turn are dependent on directional yield strengths.

To validate his estimates, Barkey carried out an extensive experimental program on solid round notched bars from 1070 steel and measured axial and shear notch strains. These data subsequently were used by many other authors to verify their own approximate methods (Table 2.1).

Table 2.1: Materials used for validations of the approximate methods.

Author	Material	Used data
Barkey [6]	1070 steel	[6]
Koettgen et al. [7]	steel	only FEA
Langlais [8]	1070 steel	[6]
Ye et al. [9]	S460N steel	[9]
Firat [10]	1070 steel	[6]
Ince et al. [11]	1070 steel	[6]
Li et al. [12]	1070 steel, S460N steel	[6, 9]
Tao et al. [13]	TC21 titanium alloy, 1070 steel	[6, 13]
Li et al. [14]	GH4169 superalloy	only FEA
Kraft et al. [15]	steel	only FEA

Two types of the pseudo material approach were presented in [7], a pseudo notch stress approach, and a pseudo notch strain approach. The essence of both methods was in relating entities from a purely elastic solution to the real elastic–plastic ones, e.g., the equivalent pseudo stress to the real plastic equivalent strain, creating a pseudo material by it (Figure 2.1). The behavior of the pseudo material was simultaneously characterized by stresses from the elastic solution and by plastic strains from the real elastic–plastic material response. By applying the Mróz model of plasticity on the pseudo stress or strain history, a real strain or stress was obtained, depending on which type of pseudo material approach was used. The estimates were verified against FEA results.

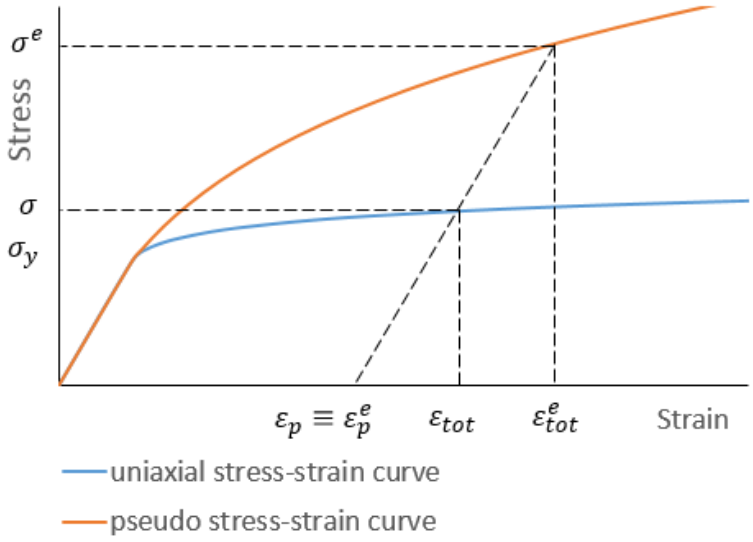

Figure 2.1: Illustration of the pseudo stress-real plastic strain principle.

In conjunction with Koettgen's model, Langlais [8] used the infinite surface hardening rule, which is a modification of the Mróz's model presented by Chu [16]. Instead of the flow rule, Langlais used Drucker's equation, which related the plastic strain rate and the generalized plastic modulus. Langlais reported that the same level of precision as in [6] and [7] was achieved.

Ye et al. [9] proposed a new unified expression based on a thermodynamic analysis of cyclic plastic deformation. The authors used this solution with the material constitutive model proposed by Jiang and Sehitoglu [17] to estimate the notch stresses and strains. New experimental data on the strain responses at the notch tip of S460N steel bar were presented. The mean relative errors were reported to be -3.5% for the axial strain component, and -3.9% for the shear strain component. The authors indicated that the unified expression developed in the article had the applicability range limited to the chosen geometries and loading conditions and that further verifications of the proposed approximate method were needed.

Firat [10] used a pseudo stress method similar to the method presented by Koettgen. The approach was combined with the rate-independent plasticity model by Chaboche [18]. The estimates were verified on the basis of the experimental results by Barkey and a high accuracy of the predicted values were reported. Unfortunately, only a general idea of the method was presented in the publication.

Ince et al. [11] combined the Prandtl–Reuss flow rule [19, 20], an assumption about the equivalence of increments of the total distortional strain energy density, and the Garud multisurface plasticity model [21]. The authors reported non-conservative estimates, as the strain ranges were predicted to be 4% to 15% smaller than the experimental results

that had been used for comparison. Regarding energy approaches, an overview of the development of the equivalent strain energy density (ESED) approach by Glinka et al. is described in [22].

One of the recent works on the topic of pseudo curve approaches was conducted by Li et al. [12]. They combined the pseudo strain method with the Jiang–Sehitoglu plasticity model. Both 1070 steel and S460N steel mentioned above [6, 9] were used for the validation of the method. The authors reported reasonable results under multiaxial cyclic loading.

The approach in [13] used tangent moduli of pseudo and real curves to calculate the real stress history. The Garud plasticity model was used to describe the behavior of the material. New experimental notch strain data were presented for samples manufactured from the TC21 titanium alloy. To the authors' knowledge, it is the first work in which the estimates of a notch stress–strain approximation method were validated on other materials than steel. Estimates for 1070 steel were also carried out.

Similarly to [13], Li et al. [14] used tangent moduli for stress estimation, but their method also took into account the influence of temperature. This was achieved by incorporating the Ramberg–Osgood equation in high-temperature form [23]. As a study case material, the authors chose the Ni-based superalloy GH4169, probably due to the availability of its thermal and mechanical material constants. A unified viscoplastic constitutive model proposed by the authors was applied to account the material behaviour under high temperature condition [24]. FEA was used to validate the estimates.

Kraft and Vormwald [15] combined the unified expression of Ye et al. [9] with the Ohno–Wang plasticity model [25]. The integration algorithm used to calculate the elastic–plastic variables was described in depth. A steel material was used for the FEA to assess the precision of the estimates.

Table 2.2 and Figure 2.2 summarize the loading paths that were used by different authors for the evaluation of their estimates. Only experimentally obtained paths are included.

Loading paths that were calculated using FEA only and are not listed in Table 2.2, include such loading paths as rhombus-shaped, X-shaped, and an ellipse-shaped paths. Barkey carried out some asymmetric loading paths using FEA calculations. The path in a shape of the number "7" (Figure 5.4) seems to be a good candidate for the ratcheting study, as it provides a response with accumulation of plastic deformation.

Table 2.2: Experimental loading paths used for validations of the approximate methods.

	Reference in Figure 2.2	Barkey [6] 1070 steel	Ye et al.[9] S460N	Tao et al. [13] TC21 titanium alloy
Butterfly	A		*	
Circle	B		*	
ksi	C	*		*
N	D	*		*
NV	E	*		*
Proportional	F	*	*	*
Rotated V	G	*		*
S	H	*		*
Square	I	*	*	
V	J	*		*

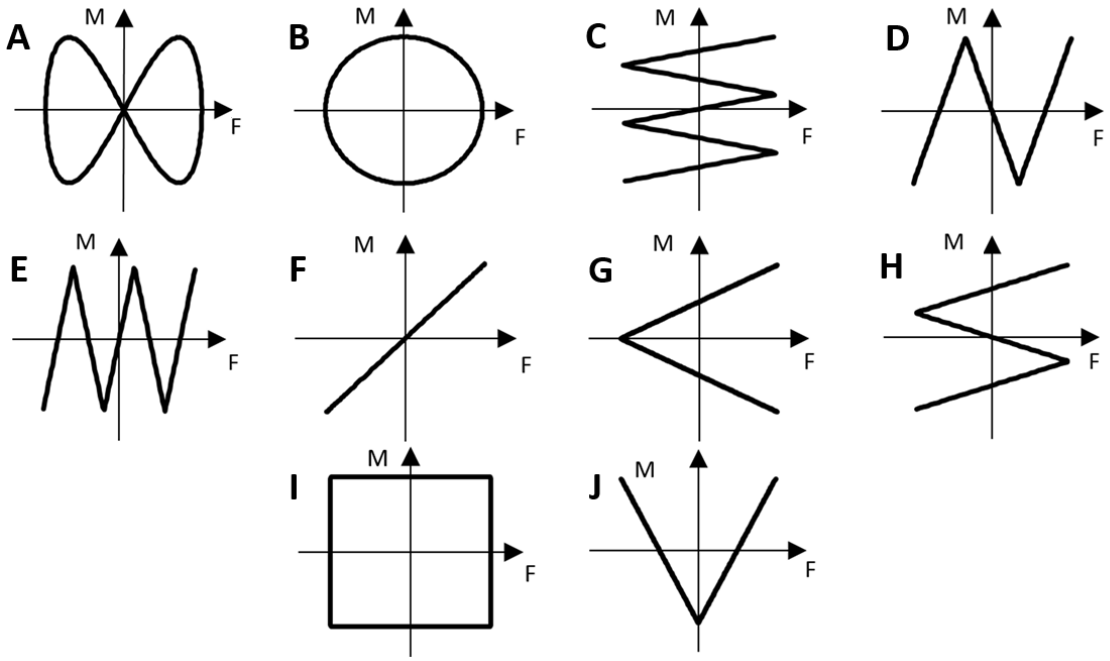

Figure 2.2: Experimental loading paths from literature: (A) Butterfly, (B) Circle, (C) ksi, (D) N, (E) NV, (F) Proportional, (G) Rotated V, (H) S, (I) Square, (J) V . F means force, M means moment.

2.3 Plasticity models

In this section, plasticity models mentioned in Section 2.2 are briefly described. The overview of which plasticity model was used in each approximate method is presented

in Table 2.3. Although this work does not deal with thermo-mechanical loading, Li's plasticity model is described for completion. Before the plasticity models description, some of the typical phenomena for plastic behavior of materials are explained.

Plastic hardening or softening occurs when a material exceeds its yield surface. As a result of this phenomenon, the material hardens or softens, its initial yield surface value changes, and after unloading, a higher stress is needed for the material to start plasticize again. The hardening is called non-proportional when the material hardens under a non-proportional loading, which is characterized by changes in the direction of the principal stresses during the loading.

Based on the way the yield surface changes during the plasticization process, it is possible to divide plastic hardening into isotropic hardening and kinematic hardening. In the case of kinematic hardening, the difference between the yield surface and the center of the yield surface, also known as backstress, stays constant. This distance between the yield surface and the backstress is also called radius of the yield surface, as the yield surface often has the form of a sphere.

In the case of isotropic hardening, the radius of the yield surface changes. The change is driven either by a set of yield surfaces values (multi-surface models) or by a continuous function that is dependent on material parameters.

Ratcheting is an accumulation of plastic strain, while maximal values of cycling loading with a mean stress stay the same. In addition to mean stress, load conditions, stress amplitude values, stress ratios, and the load history influence the magnitude of the ratcheting [26, 27].

Table 2.3: Plasticity models used in the approximate methods.

Author	Plasticity model						
	Chaboche	Garud	Jiang	Li	Mróz	Modified Mróz	Ohno-Wang II
Barkey [6]					*		
Koettgen et al. [7]					*		
Langlais [8]						*	
Ye et al. [9]			*				
Firat [10]	*						
Ince et al. [11]		*					
Li et al. [12]			*				
Tao et al. [13]	*						
Li et al. [14]				*			
Kraft et al. [15]							*

2.3.1 Mróz plasticity type models

The Mróz plasticity model is a multiple yield surface model from 1967 [28]. The number of surfaces is finite, and a constant hardening modulus corresponds to each surface. When a yield surface representing the current state comes into contact with the next surface, the plastic modulus of a larger yield surface in contact is used. The surfaces are not supposed to intersect and could only have a tangential contact at the current stress point [6, 8, 28].

The movement of the active surface is described by

$$d\alpha_{ij}^{(l)} = \frac{d\xi}{\sigma_0^{(l)}}[(\sigma_0^{(l+1)} - \sigma_0^{(l)})\sigma_{ij}^{(l)} - (\alpha_{ij}^{(l)}\sigma_0^{(l+1)} - \alpha_{ij}^{(l+1)}\sigma_0^{(l)})] \tag{2.9}$$

where index l denotes the currently active surface, $l+1$ denotes the next surface. The parameter ξ is a function of the consistency condition

$$d\xi = \frac{\partial f/\partial\sigma_{ij} d\sigma_{ij}}{\partial f/\partial\sigma_{kl}(\sigma_{kl}^{(l+1)} - \sigma_{kl}^{(l)})} \tag{2.10}$$

Chu [16] improved the Mróz plasticity model by changing the discrete number of the yield surfaces to infinite. He also improved the implementation so the model uses less parameters, and thus saves storage capacities required.

Garud [21] pointed out that the consistency condition of the Mróz model is not always satisfied and that the yield surfaces might intersect for a certain loading. He then proposed an improvement.

Several researchers pointed out drawbacks of multiple surface models in view of ratcheting phenomenon [17, 21, 28]. According to them, multiple surface models cannot predict ratcheting for proportional loading at all and predict much larger ratcheting for non-proportional loading compared to experimental results.

2.3.2 Chaboche nonlinear kinematic hardening model

Chaboche [18] had a huge impact on plasticity theory in general with his proposal to calculate backstress as a sum of additive parts, which many plasticity models adapted later on:

$$\boldsymbol{\alpha} = \sum_{i}^{M} \boldsymbol{\alpha^{(i)}} \tag{2.11}$$

where $\boldsymbol{\alpha^{(i)}}$ is the i^{th} part of the total backstress composed of M parts. Each of the backstress parts follows Armstrong-Frederick hardening rule:

$$\boldsymbol{d\alpha^{(i)}} = \frac{2}{3} C_i \boldsymbol{d\varepsilon_p} - \gamma_i \boldsymbol{\alpha^{(i)}} dp \tag{2.12}$$

where C_i and γ_i are material parameters that could be calculated based on the discretization of the cyclic stress-strain curve:

$$C_i = \frac{\sigma_{a(i)} - \sigma_{a(i-1)}}{\varepsilon_{ap(i)} - \varepsilon_{ap(i-1)}} - \frac{\sigma_{a(i+1)} - \sigma_{a(i)}}{\varepsilon_{ap(i+1)} - \varepsilon_{ap(i)}} \text{ for } i \neq M, \tag{2.13}$$

$$C_M = \frac{\sigma_{a(M)} - \sigma_{a(i-1)}}{\varepsilon_{ap(M)} - \varepsilon_{ap(i-1)}}, \tag{2.14}$$

$$\gamma_i = \frac{1}{\varepsilon_{ap(i)}} \text{ for all } i, \tag{2.15}$$

where $\sigma_{a(i)}$ is the stress amplitude and $\varepsilon_{ap(i)}$ is the plastic strain amplitude of the i-th point of the cyclic stress-strain curve.

Jiang and Sehitoglu pointed out [29] that although the transient ratcheting predicted by the model is consistent with experiments, the duration of the transient response is short-lived. After the transient part, the model predicts a constant ratcheting rate.

2.3.3 Jiang-Sehitoglu plasticity model

The Jiang-Sehitoglu plasticity model was used in the approximate methods by Ye et al. [9] and by Li et al. [12]. Since Ye et al. indicated that the material parameters for his method were taken from [30] the, it seems that the original form from [17] was used. In this form, the kinematic hardening rule is proposed according to Equation 2.16:

$$\boldsymbol{da^{(i)}} = c_i r_i \left[\hat{\boldsymbol{n}} - \left(\frac{|\boldsymbol{a^{(i)}}|}{r_i} \right)^{\chi_i + 1} \frac{\boldsymbol{a^{(i)}}}{|\boldsymbol{a^{(i)}}|} \right] dp \tag{2.16}$$

where c_i, r_i and χ_i are sets of material parameters. r_i represents the radii of the limiting surfaces, and c_i is dependent on five other material constants, which have to be determined by a parameter optimization procedure. Parameter χ_i is calculated based on another set of material parameters.

Li et al. [12] used a simplified version by replacing the dependence of c_i and r_i on the material parameters with the relations represented by Equations 2.17 and 2.18, and the parameter χ_i is set to a constant value.

$$c_i = \frac{2\sqrt{\frac{2}{3}}}{\Delta\varepsilon_{p(i)}} \tag{2.17}$$

$$r_i = \frac{2}{3} \frac{h_i - h_{i+1}}{c_i} \ (i = 1, 2, ..., M), \tag{2.18}$$

where

$$h_i = \frac{\Delta\sigma_{(i)} - \Delta\sigma_{(i-1)}}{\Delta\varepsilon_{p(i)} - \Delta\varepsilon_{p(i-1)}}. \tag{2.19}$$

2.3.4 Ohno-Wang model II

The Ohno-Wang model II [25] was used by Kraft in his approximate method [15]. The model is an extension of Ohno-Wang model I and covers the solution by Ohno-Wang model I as its special case.

The evolution of the backstress tensor is described according to Equation 2.20:

$$\boldsymbol{da^{(i)}} = \zeta_i \left[\frac{2}{3} r_i \boldsymbol{d\varepsilon_p} - \left(\frac{|\boldsymbol{a^{(i)}}|}{r_i} \right)^{\chi_i} \langle \boldsymbol{d\varepsilon_p} : \boldsymbol{k_i} \rangle \boldsymbol{a^{(i)}} \right], \tag{2.20}$$

here, r_i has the same meaning as in the case of the Jinag-Sehitoglu model, and the exponent χ_i affects the magnitude and trajectory of ratcheting. $\boldsymbol{k_i}$ is the backstress $\boldsymbol{a^{(i)}}$ divided by its size $|\boldsymbol{a^{(i)}}|$.

The Ohno-Wang model exhibits a ratcheting rate decay for a number of cycles, and then a constant ratcheting is predicted. The predictions are consistent with experiments for non-proportional loading, but inconsistent with proportional loading, including the asymmetric tension-compression case.

2.3.5 Unified viscoplastic constitutive model by Li et al.

Li et al [24] have extend the Chaboche's time-dependent combined hardening plasticity model [31] in order to address the effects of non-proportional hardening and dynamic strain aging.

The total strain rate $\dot{\boldsymbol{\varepsilon}}_{\boldsymbol{t}}$ is divided into elastic $\dot{\boldsymbol{\varepsilon}}_{\boldsymbol{e}}$ and inelastic $\dot{\boldsymbol{\varepsilon}}_{\boldsymbol{in}}$ parts:

$$\dot{\boldsymbol{\varepsilon}}_{\boldsymbol{t}} = \dot{\boldsymbol{\varepsilon}}_{\boldsymbol{e}} + \dot{\boldsymbol{\varepsilon}}_{\boldsymbol{in}}, \tag{2.21}$$

where the inelastic strain tensor is defined with the flow rule as

$$\dot{\boldsymbol{\varepsilon}}_{\boldsymbol{in}} = \frac{3}{2} \dot{p} \frac{\boldsymbol{s} - \boldsymbol{a}}{|\boldsymbol{s} - \boldsymbol{a}|}. \tag{2.22}$$

The total backstress is composed of two sub-parts by the additive rule (Equation 2.11) and is defined as

$$\dot{\boldsymbol{a}}_{\boldsymbol{i}} = C_i \left[\frac{2}{3} (1 + \Phi F) Y_i \dot{\boldsymbol{\varepsilon}}_{\boldsymbol{in}} - L \boldsymbol{a}_{\boldsymbol{i}} \dot{p} \right] \tag{2.23}$$

where Y_i is an asymptotic value for the backstresses; F, the rotation factor, and Φ, the non-proportional hardening coefficient, serve to describe the non-proportional hardening effect, and L is the dynamic strain aging influence factor.

The main aim of Li's unified viscoplastic plasticity model is to account for the influence of non-proportional loading and strain aging on some materials under multiaxial thermo-mechanical loading.

Chapter 3

Aims of the thesis

One of the drawbacks of the current state of the approximate methods, which becomes obvious when a researcher is trying to recreate the methods, is the lack of detailed descriptions of how the plasticity part and the notch correction part are combined. This was also noticed by other authors in [12]. That might be the probable reason for why the methods have not gained wide practical use, despite the fact that some of them were invented several decades ago. There are many works on plasticity models by themselves, but since the approximate methods work on different principles, a lot of guesswork remains when a notch correction and a plasticity model must be combined.

The capability of the previously proposed methods to predict the ratcheting precisely remains unverified, as experimental loading paths with mean stress have not been measured and used for the validation of the methods estimates. Such loading paths cause, depending on the material, a noticeable ratcheting response and provide the possibility to evaluate the precision of the ratcheting estimates.

Another drawback of the current development of the approximate methods is a very limited amount of experimental data of the notch strain responses. Beside steels, only titanium alloy and GH4169 superalloy were used for the validations so far. These types of experiments might be not so popular due to their specific utilization in notch tip strain testing and a complicated way of measurement.

Based on these observations, the main target of this thesis is set as the development of a novel pseudo-curve-based approximate method for calculating notch tip elastic-plastic stresses and strains under multiaxial cyclic loading condition.

The task consists of the following sub-tasks:

1. Develop a methodology on how to combine a notch correction and a plasticity model, which will be the main parts of the novel approximate method for notch tip stresses and strains estimation. Provide a detailed description and an implementation code.

2. Propose a new and original approximate method for calculating elastic-plastic stresses

and strains at the notch tip under multiaxial cyclic loading that provides results of better or of similar precision compared to the other existing methods.

3. Obtain new and original experimental data of notch tip strains to validate the method predictions on specimens manufactured from a different than steel material. The experimental program must include a loading path with a mean stress.

Chapter 4

Used methods/ tools

4.1 AKO model

The plasticity model of Abdel-Karim-Ohno (AKO), in addition to requiring only a few material parameters, also represents other plasticity models as its special cases, depending on its settings.

The nonlinear kinematic rule for the AKO model has the following form:

$$\boldsymbol{da^{(i)}} = \frac{2}{3} C_i \boldsymbol{d\varepsilon_p} - \mu_i \gamma_i \boldsymbol{a^{(i)}} dp - \gamma_i H(f_i) \langle d\lambda_i \rangle \boldsymbol{a^{(i)}}, \tag{4.1}$$

where term

$$f_i = \frac{3}{2} \boldsymbol{a^{(i)}} : \boldsymbol{a^{(i)}} - \left(\frac{C_i}{\gamma_i} \right)^2 \tag{4.2}$$

is responsible for a dynamic recovery of backstress, and $d\lambda$ is a plastic multiplier, which is defined as

$$d\lambda_i = \boldsymbol{d\varepsilon_p} : \frac{\boldsymbol{a^{(i)}}}{C_i/\gamma_i} - \mu_i dp. \tag{4.3}$$

In Equations 4.1-4.3, $\boldsymbol{a^{(i)}}$ is the i^{th} part of the total backstress $\boldsymbol{a}$; C_i and γ_i are material parameters calculated according to Equations 2.13-2.15; symbol $\langle x \rangle$ represents Macaulay brackets ($\langle x \rangle = (x + |x|)/2$) and $H(f_i)$ is the Heaviside step function. μ_i is the ratcheting parameter. The same value of the ratcheting parameter is usually set for all backstress parts, and its value varies between 0 and 1. When it is set to 0 for all i, the model corresponds to the multilinear model of Ohno and Wang type I. When μ_i is set to 1 for all i, the model corresponds to Chaboche's kinematic hardening model of plasticity.

The total backstress is then represented by the sum of additive backstress parts according to the Chaboche's proposal (Equation 2.11).

Another advantage of the AKO model is an easy way to obtain model parameters C_i and γ_i, which is identical to the method used for Chaboche's model (Equations 2.13-2.15).

For a description of the yield surface movement, the von Mises criterion is used:

$$f(\boldsymbol{\sigma}) = \sqrt{\frac{3}{2}(\boldsymbol{s}-\boldsymbol{a}) : (\boldsymbol{s}-\boldsymbol{a})} - \sigma_y = 0, \tag{4.4}$$

where $\boldsymbol{s}$ represents the stress deviator and σ_y represents the radius of the yield surface and the yield strength for this specific formulation of the AKO model without isotropic hardening.

4.2 Iteration algorithm

The important part of an approximate method for cyclic loading is a substitution algorithm that allows to solve the non-linear scalar equation for accumulated plastic strain. The algorithm used for the combined AF and OW model in [32] is used in this work and is depicted in Diagram 4.1.

In Diagram 4.1, k denotes the index of iteration, n is the index of solution increment, at which all stresses, strains, and backstresses are known, and i indicates backstress part. $\boldsymbol{d\varepsilon_p}$ is the plastic strain increment between states n and $n+1$. Besides material parameters C_i, γ_i and μ_i, the deviatoric stress $\boldsymbol{s_{n+1}}$ and the backstress $\boldsymbol{a_n}$, consisting of i parts $\boldsymbol{a_n^{(i)}}$, are used as inputs for the iteration algorithm.

The nonlinearity of the expression for the accumulated plastic strain (Equation 4.6) lies in the parameter θ_i, which is a function of dp. To solve it, θ_i is set to 1 for all i for the first iteration. Besides that, a critical state, when f_i in Equation 4.2 is equal to 0, is assumed not to be reached. The critical state will be included later. If $f_i < 0$, the third term on the right side of Equation 4.1 is zero. The i^{th} part of the backstress $\boldsymbol{a}$ at state $n+1$ is expressed as

$$\boldsymbol{a_{n+1}^{(i)}} = \boldsymbol{a_n^{(i)}} + \frac{2}{3}C_i\boldsymbol{d\varepsilon_p} - \mu_i\gamma_i\boldsymbol{a_{n+1}^{(i)}}dp, \tag{4.5}$$

$$\boldsymbol{a_{n+1}^{(i)}} = \frac{\boldsymbol{a_n^{(i)}} + \frac{2}{3}C_i\boldsymbol{d\varepsilon_p}}{1+\mu_i\gamma_i dp} = \theta_i\left(\boldsymbol{a_n^{(i)}} + \frac{2}{3}C_i\boldsymbol{d\varepsilon_p}\right). \tag{4.6}$$

By applying Chaboche's additive backstress parts proposal (Equation 2.11) the tensor $\boldsymbol{s_{n+1}} - \boldsymbol{a_{n+1}}$ became

$$\boldsymbol{s_{n+1}} - \boldsymbol{a_{n+1}} = \boldsymbol{s_{n+1}} - \sum_i \theta_i\left(\boldsymbol{a_n^{(i)}} + \frac{2}{3}C_i\boldsymbol{d\varepsilon_p}\right). \tag{4.7}$$

By substituting $\boldsymbol{d\varepsilon_p}$ from the flow rule relation

$$\boldsymbol{d\varepsilon_p} = \frac{3}{2}dp\frac{\boldsymbol{s_{n+1}} - \boldsymbol{a_{n+1}}}{\sigma_y} \tag{4.8}$$

and rearranging Equation 4.7 so that the tensor $\boldsymbol{s_{n+1}} - \boldsymbol{a_{n+1}}$ appears only on the left side of the equation, the relation

$$\boldsymbol{s_{n+1}} - \boldsymbol{a_{n+1}} = \frac{\sigma_y \left(\boldsymbol{s_{n+1}} - \sum_i \theta_i \boldsymbol{a_n^{(i)}}\right)}{\sigma_y + \sum_i C_i \theta_i dp} \tag{4.9}$$

is obtained. Equation 4.9 allows to calculate the tensor $\boldsymbol{s_{n+1}} - \boldsymbol{a_{n+1}}$ for state $n+1$ based on variables at state n and θ_i. The accumulated plastic strain is calculated by substituting Equation 4.9 into the von Mises yield function (Equation 4.4) and rearranging it so that

$$dp = \frac{\sqrt{\frac{3}{2}\left(\boldsymbol{s_{n+1}} - \sum_i \theta_i \boldsymbol{a_n^{(i)}}\right) : \left(\boldsymbol{s_{n+1}} - \sum_i \theta_i \boldsymbol{a_n^{(i)}}\right)} - \sigma_y}{\sum_i C_i \theta_i}. \tag{4.10}$$

To incorporate the critical state $f_i = 0$, θ_i defined in Equation 4.6 is marked as ω_i:

$$\omega_i = \frac{1}{1 + \mu_i \gamma_i dp}. \tag{4.11}$$

By defining

$$\boldsymbol{a_{n+1}^{*(i)}} = \boldsymbol{a_n^{(i)}} + \frac{2}{3} C_i \boldsymbol{d\varepsilon_p}, \tag{4.12}$$

Equation 4.6 takes the following form:

$$\boldsymbol{a_{n+1}^{\#(i)}} = \omega_{n+1}^i \boldsymbol{a_{n+1}^{*(i)}}. \tag{4.13}$$

The equivalent value of $\boldsymbol{a_{n+1}^{\#(i)}}$ is expressed as

$$\overline{a_{n+1}^{\#(i)}} = \sqrt{\frac{3}{2} \boldsymbol{a_{n+1}^{\#(i)}} : \boldsymbol{a_{n+1}^{\#(i)}}}, \tag{4.14}$$

and it is equal to C_i/γ_i for the critical state based on Equation 4.2. Expressing the equivalent value of the right side of Equation 4.13 gives

$$\omega_i \boldsymbol{a_{n+1}^{*(i)}} = \sqrt{\frac{3}{2} \omega_i \boldsymbol{a_{n+1}^{*(i)}} : \omega_i \boldsymbol{a_{n+1}^{*(i)}}} = \omega_i \sqrt{\frac{3}{2} \boldsymbol{a_{n+1}^{*(i)}} : \boldsymbol{a_{n+1}^{*(i)}}} = \omega_i \overline{a_{n+1}^{*(i)}}. \tag{4.15}$$

Transforming Equation 4.13 into equivalent values form by applying Equations 4.14-4.15 and substituting $\overline{a_{n+1}^{\#(i)}}$ with C_i/γ_i, a relation for calculating ω_i for the critical state is obtained

$$\omega_i = \frac{C_i}{\gamma_i \overline{a_{n+1}^{*(i)}}} \tag{4.16}$$

Expanding the new relation for both critical and non-critical states gives

$$\theta_i = \omega_i + H(f_{n+1}^{\#i})(\frac{C_i}{\gamma_i \overline{a_{n+1}}^{*(i)}} - \omega_i) \tag{4.17}$$

With updated θ_i the algorithm proceeds to the next iteration according to Diagram 4.1. Aitken's Δ^2 process is utilized to speed up the convergence [32].

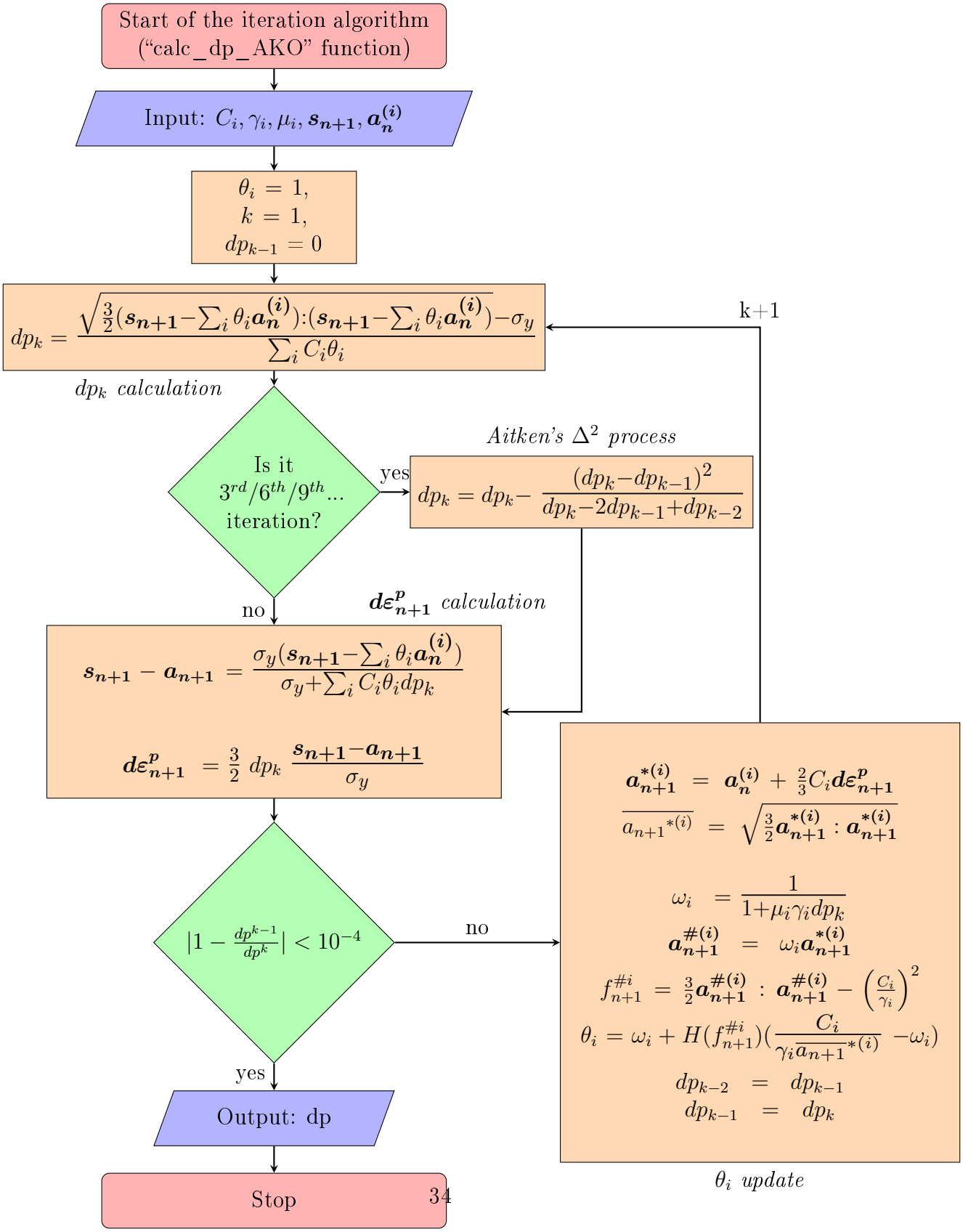

Figure 4.1: Iteration algorithm for calculating accumulated plastic strain increment dp.

4.3 Implementation of the approximate method

The approximate method presented in Chapter 6 was implemented in MATLAB. The only input for the program was the stress history at the notch tip from the elastic FEA and the material data presented in Section 5.1. The cyclic stress–strain material curve was defined using Hollomon parameters for five sections of plastic strain with a step of 0.02 and the first value corresponding to a cyclic yield strength of 330 MPa. The pseudo curve was established according to the process described in Section 6.1.1.

The parameters of the plasticity model C_i and γ_i were calculated according to Equations 2.13-2.15.

The code is available in Appendix C.

Chapter 5

Experiments

5.1 DIC

5.1.1 Material and specimens

To verify the proposed method, fatigue experiments were carried out on two types of notched samples (Figures 5.1 and 5.2) manufactured from the aluminum alloy 2124-T851. Young's modulus of the material is 73100 MPa [33], Poisson's number is 0.33, Hollomon parameters for the Ramberg–Osgood relation (Equation 2.5) are $K' = 646MPa$ and $n' = 0.089$. The cyclic yield strength σ_y of 330 MPa was used for the FEA simulation (Section 5.2) and for the approximate method (Section 6.1). The source of the material data was an extensive report on the static and cyclic characteristics of the material [34]. The only exception was Young's modulus, in case of which the value from [33] led to better results for the initial loading than the values presented in [34] values of 61550 MPa for monotonic and of 65540 MPa for cyclic loading.

Aluminum 2124-T851 was a part of studies on the mean stress effect in stress-life fatigue predictions and on data sets usable for validating multiaxial fatigue [A1, A2]. In [A3] fatigue data on 2124-T851 for different types of notches are presented.

To prepare specimens for digital image correlation (DIC) measurements, notch regions of specimens were first covered with a white acryl paint to prevent light reflections. Next, the same regions were sprayed with a black acryl paint to create a spotted texture that would allow the DIC method to correlate images from specimens testing. An example of sprayed specimens is shown in Figure 5.3.

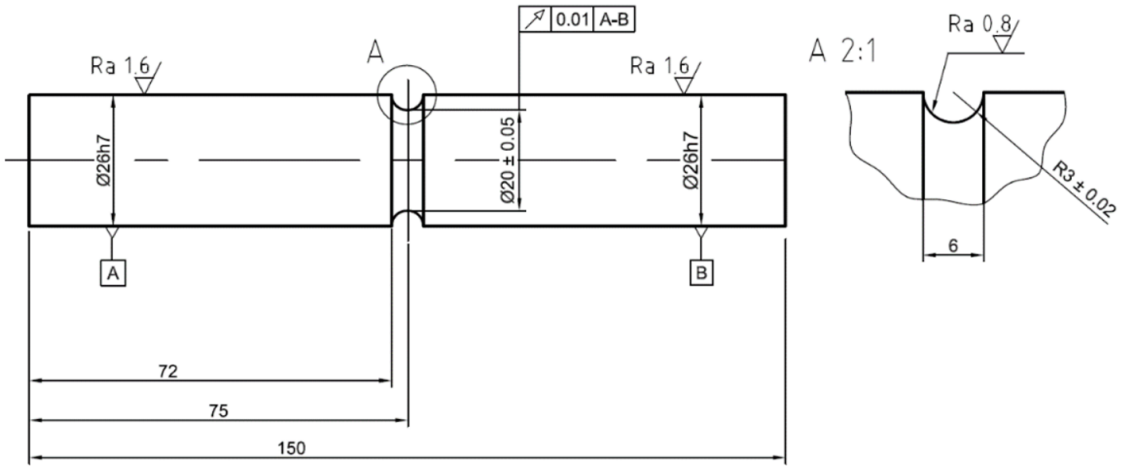

Figure 5.1: Specimen with U-notch. A and B in frames indicate surfaces based on which a datum axis for geometrical run-out tolerance is defined.

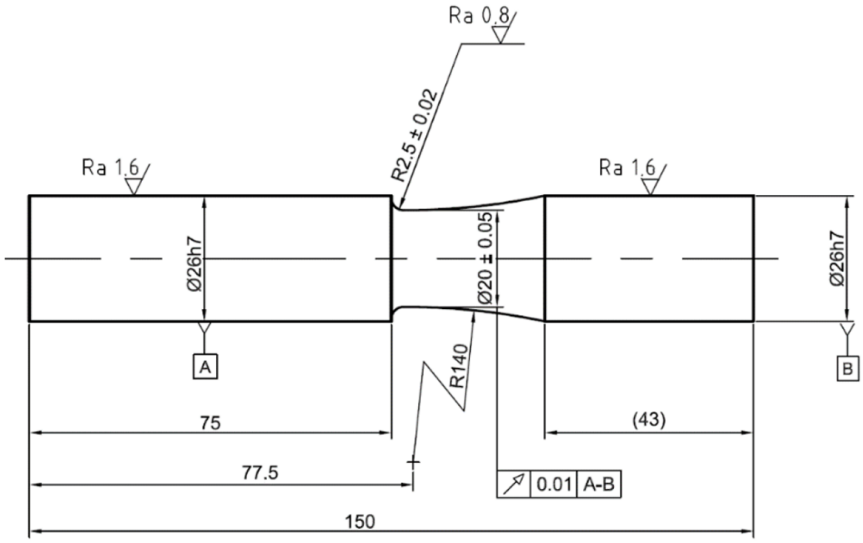

Figure 5.2: Specimen with fillet. A and B in frames indicate surfaces based on which a datum axis for geometrical run-out tolerance is defined.

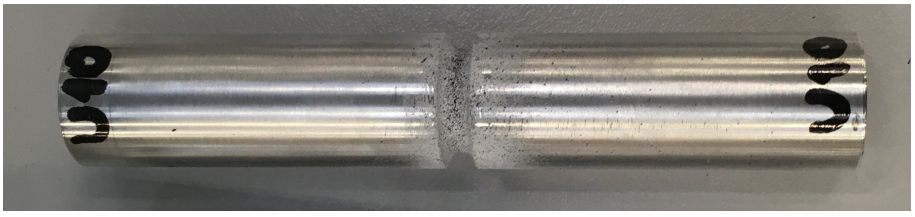

Figure 5.3: Specimen with U-notched sprayed with two acryl paints for DIC measurement.

5.1.2 Tests realisation

The aim of the experiments was to measure the notch tip strains, specifically the axial and shear strain components. These components are commonly used to compare estimates with experimental results [6–15].

The test machine used for the experiments was INOVA FU 250 (distributed by Inova Praha s.r.o.), multiaxial tension-compression and torsion load frame with hydraulic actuator for dynamic loading. The maximal value of the axial force channel of the machine is 250 kN, and the maximum moment is 2000 Nm.

The experiments were carried out under force and moment control. The first reason for the load-controlled experiments was the possibility of recalculating the loading forces and moments into the local elastic notch stress history using the stress concentration factors as described in [10]. The second reason for using force control was that the strain control of notched specimens would require complex real-time notch strain measurement and processing.

The stress ratio of nominal axial stress to shear stress was 1 for all paths (Figure 5.4) used for the experimental program. Additionally, the stress ratio 1.73 was applied. The evaluation of measured data on path Square was not successful for the specimen under the stress ratio 1.73 and therefore was excluded from the results. The unsuccessful evaluation was due to the presence of light reflections on the specimen notch surface, which prevented the algorithm of the software for digital image correlation in the comparison of the captured images.

For the stress ratio 1, the maximum force was 65.8 kN, and the maximum moment was 329 Nm. For the 1.73 ratio, the maximum force was 100.5 kN and the maximum moment was 290 Nm. To samples under uniaxial tension-compression loading, maximal forces of 86.25 kN (Figure A.6) and 100.472 kN (Table 6.9) were applied. Experiments were carried out at room temperature.

Path "7" represents the loading by a constant torque in one channel and a sinusoidal tension-compression waveform in the other. The loading frequency when measuring the strains was 0.1 Hz. Path "7" was used for validation in [6, 7] but only in the form of FEA simulations.

Path Circle consists of two sinusoidal waveforms of axial force and torque with a phase shift of 90°. The loading frequency was 0.1 Hz. The path has so far been only presented in [9] as an experimental loading path and in [6] and [15] as FEA.

To achieve NV path, both channels had sinusoidal waveforms with the loading frequency of the torsion channel five times faster than the loading frequency of the tension-compression channel. For the digital image correlation (DIC) measurement, the frequencies were 0.004 Hz for the torque channel and 0.02 Hz for the force channel. Other authors used this path to validate their approximate methods [6–8, 11, 13, 14].

Path Square was achieved by multiaxial loading by trapezoidal waveforms of force and moment signals with a mutual phase shift of 90°. The common load frequency for the

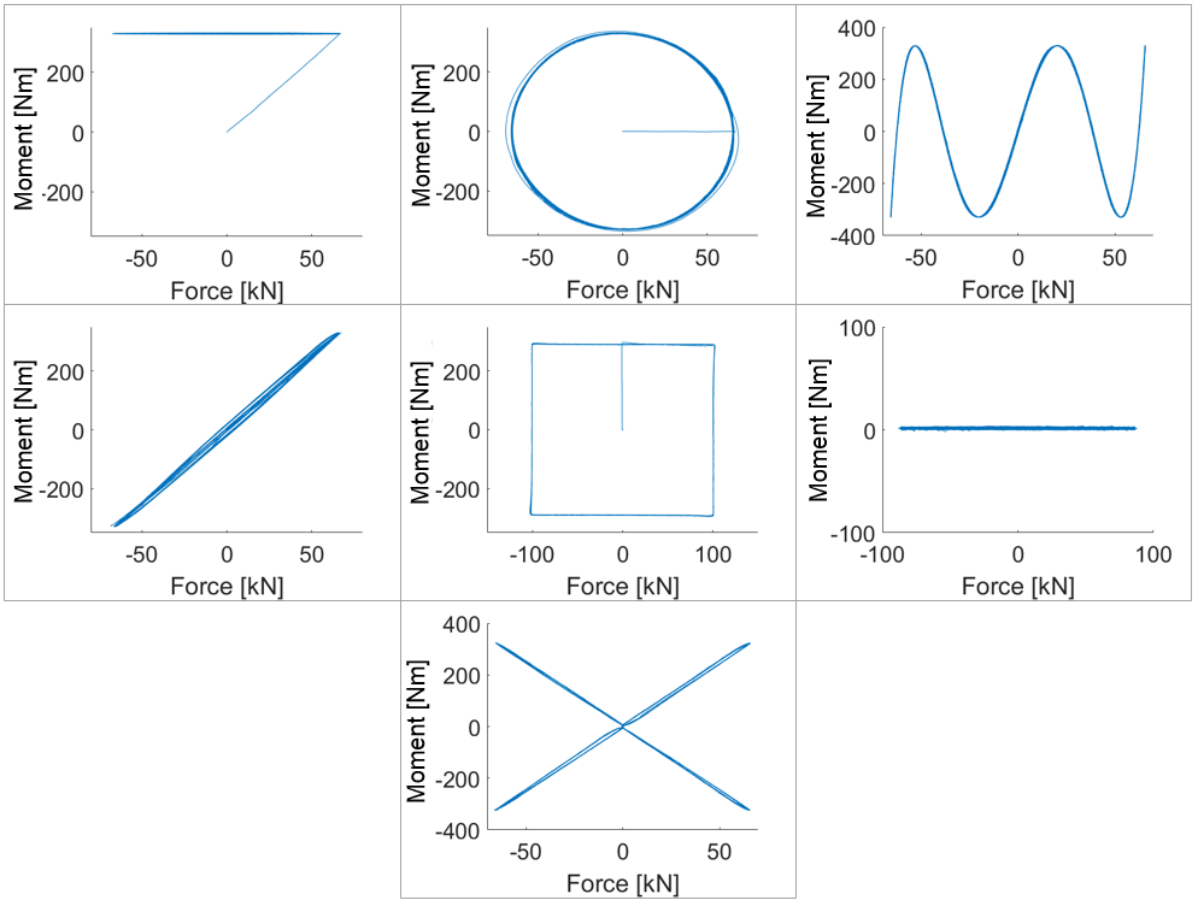

Figure 5.4: Loading paths: (top left) "7"; (top middle) Circle; (top right) NV; (middle left) proportional;(middle) Square; (middle right) uniaxial; (bottom) X.

entire test was 0.0417 Hz. Other authors used the path to validate their estimates [6, 8–15].

Path X represents four linear segments that go from 0 to maximum loading in each quadrant. The quadrants are switched in a clockwise manner. This path was used as FEA in [6, 7].

The loading frequencies were set according to the ability of the testing machine to maintain the loading paths on each channel without distortions. The sampling frequency of the DIC cameras was also taken into account, as the loading frequencies had to be 20 times smaller than the sampling frequency of the cameras to avoid aliasing.

Each specimen was tested till the complete break, which corresponded to a state, when a crack propagated through the whole net section. The number of cycles till the break are presented in Table 5.1. The crack initiation was not measured, but in a few cases the crack was observed approximately at half of the specimens life. In the case of

the U-notched specimen under uniaxial tension-compression with a nominal stress 319.8 MPa, the crack was already visible after 500 cycles, while the complete breaking of the specimen occurred at the 1016 cycle. Another example was in the case of the single fillet specimen loaded by the path Circle with the ratio of nominal stresses equal to 1, when an asymmetric decrease in the axial strain measured between cycles 350 to 400 indicated the presence of crack (Figure A.9).

Table 5.1: Number of cycles till the break of 2124-T851 specimens.

Path	σ_{nom}[MPa]/ τ_{nom} [MPa]	Number of cycles till break	
		U-notched specimens	Single fillet specimens
7	209.5/209.5	—	10165
Circle	209.5/209.5	578	592
Circle	319.8/184.9	247	403
NV	209.5/209.5	120	235
NV	319.8/184.9	94	—
Proportional	209.5/209.5	585	661
Proportional	319.8/184.9	—	365
Square	209.5/209.5	233	—
Uniaxial	274.5/ —	2027	—
Uniaxial	319.8/ —	1016	—
X	209.5/209.5	309	460
X	319.8/184.9	142	171

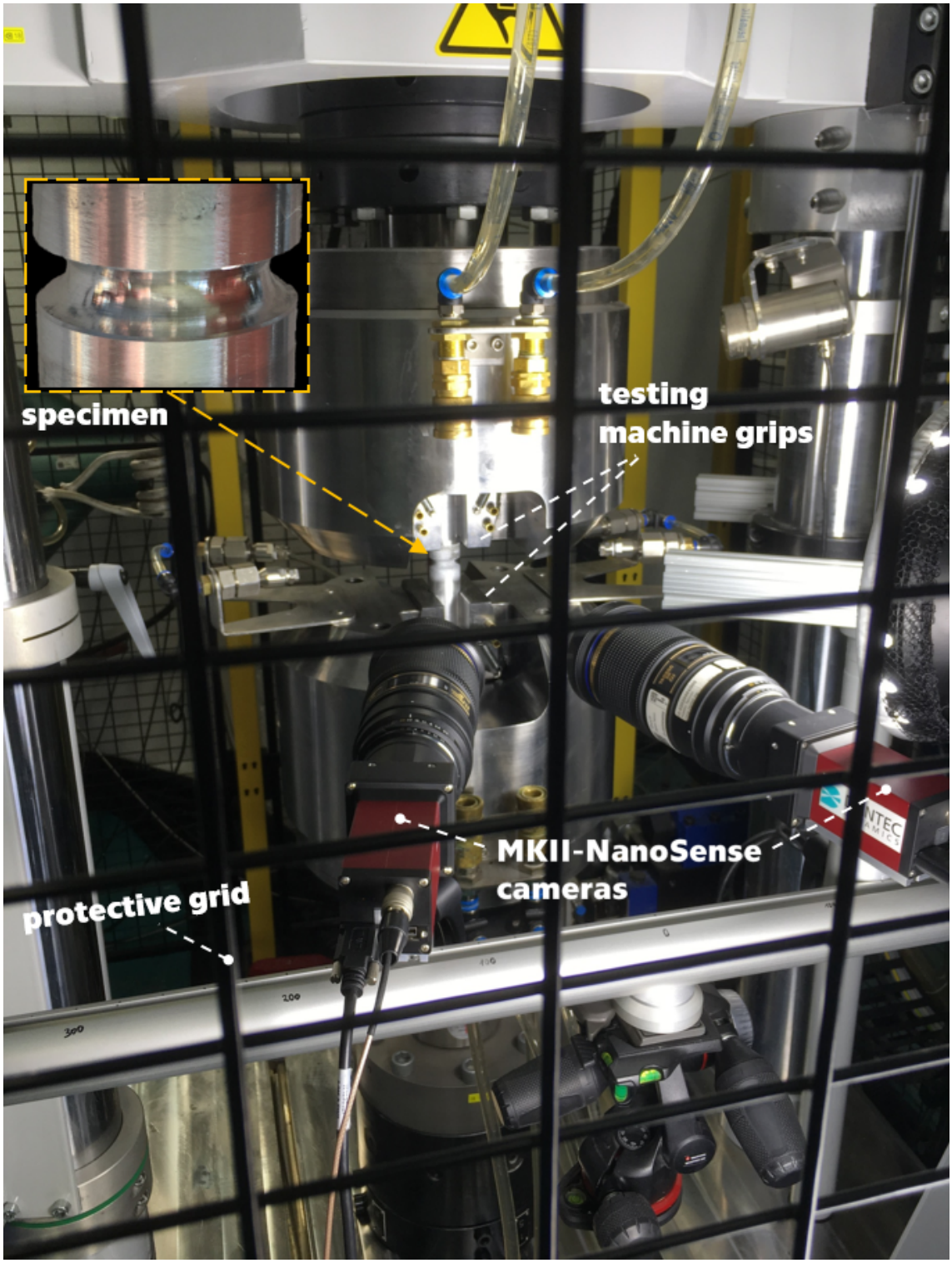

Figure 5.5: Testing part of the experimental setup. Zoomed image of the specimen in a yellow dash frame demonstrates the notch shape, but is taken before the paint application.

5.1.3 Strain measurement

The Dantec Dynamics 3D Q-450 high-speed image correlation system was used for the DIC measurement. The system consists of MKII-NanoSense cameras with a CCD sensor with a resolution of 1024 × 1280 pixels and Istra 4-D software (version 4.4.3.414). The software was used for calibration, measurement, displacement evaluation, and displacement export.

The first 100 cycles were the primary target range for the DIC measurements. Additionally, from 50 to 100 cycles were measured after several hundred cycles. For U-notched specimens, which were tested before the specimens with single fillets, the second range for the measurements was after 500 initial cycles. The choice was based on investigations on the 2124-T751 aluminum alloy in [34] and aimed to measure strains approximately at the half-life of the specimens. Since many U-notched specimens had broken before the chosen range of cycles, the second range for measurements on the specimens with single fillets was set between 350 and 400 cycles.

The results of the experimental measurements are available in Appendix A. They were also previously published in [A4].

5.1.4 Evaluation in Matlab

To calculate axial and shear strains based on exported displacements from Istra 4D, a program was written in MATLAB language. The reason for processing the data outside the DIC system was the possibility of applying a higher level of automation and more control over displacement smoothing.

The displacement were smoothed according to the next equation:

$$u_{smoothed} = \frac{u_{smoothed} + \sum_i \frac{d_{min}}{d_i} u_i}{\sum_i \frac{d_{min}}{d_i} + 1}, \tag{5.1}$$

where u_i means a displacement vector of a neighbor i, d_{min} means the minimum distance from the distances u_i between the node, displacements of which are being smoothed, and its neighbors. $u_{smoothed}$ on the right side of the "=" sign is equal to the initial unsmoothed displacement in the case of the first smoothing iteration, and to the previous result of smoothing for the next smoothing iterations.

The calculated strains along the notch tip circuit (Figure 5.7) were within a reasonable deviation interval. In Figure 5.6 a strain distibution histogram along the notch tip circuit is presented. The presented state corresponds to a uniaxial tension-compression loading at its pick of the 10th cycle. More than 85% of processed strain values lie within the 0.1% deviation interval from the mean value. The strain distribution also suggests that no unwanted additional bending was present, as the strain along the notch tip circuit are evenly distributed. The median value from all values within the notch tip circuit in

each time step was used as the final result and input for validations in Chapter 6 and Appendix A.

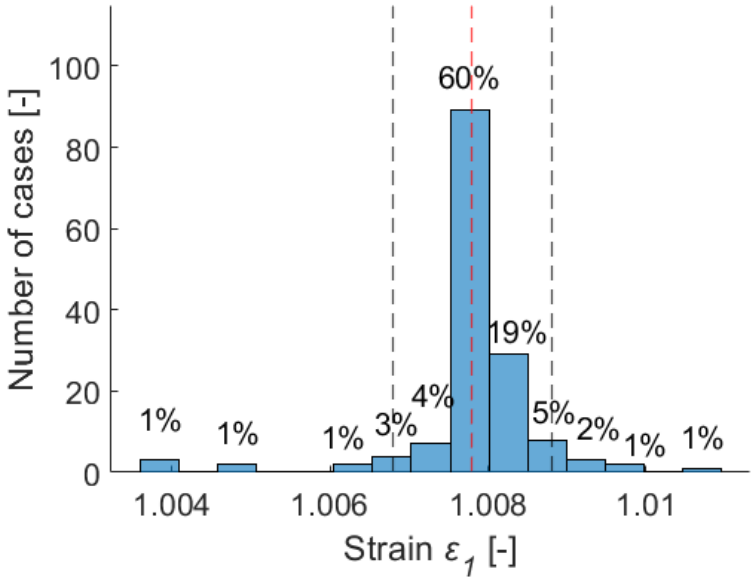

Figure 5.6: Processed experimental axial strain values along the notch tip circuit for a uniaxial tension-compression test. Red dashed line represents mean value, black dashed lines represent 0.1% deviation from the mean value.

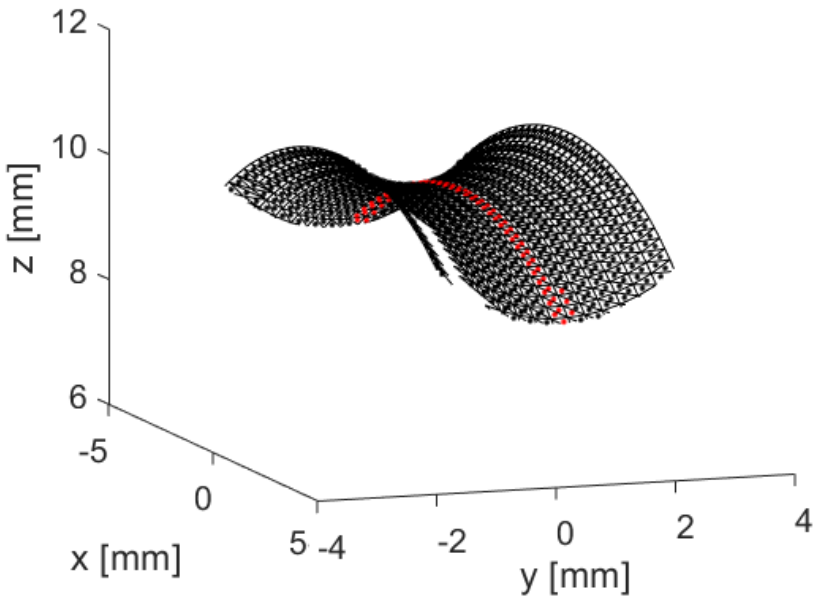

Figure 5.7: A segment of a U-notched test specimen from DIC meausrements. Notch tip circuit (red color) was used for selecting and averaging of notch tip axial strain ε_1. Axis y is parallel to the axis of the specimen.

5.2 FEM

FE analyzes with purely elastic and elastic–plastic materials were performed in Abaqus v6.14-5. The elastic material model served to obtain stress concentration factors, which were later used for the notch tip stress histories calculation. Analyses with elastic–plastic material data were performed to verify the correspondence of the material data and the experimental results.

Specimens were modeled as axisymmetric. The same mesh was used for both elastic and elastic-plastic analyzes. The final mesh size of the quadratic axisymmetric stress elements CGAX8R (8-node biquadratic, reduced integration) was 0.1 mm (Figure 5.8). Attempts to further decrease the element size did not affect the results by more than 0.007%. All elements passed the mesh quality check without errors and warnings.

For elastic–plastic analyzes, the combined hardening behavior was chosen with the stabilized data type. The number of backstresses was set to 5. The cyclic stress–strain curve used in the model was calculated based on the Hollomon parameters presented in Section 5.1. Its values are listed in Table 5.2.

The boundary conditions for both elastic and elastic-plastic analyzes were the same. In Figure 5.8, the blue dashed line indicates the boundary condition applied to the specimens to prevent their axes from moving away from the axis of the axisymmetry. The gray dashed line simulates the displacement by the bottom grips of the testing machine.

The torque was applied to a reference point from which it was distributed to the specimens. Tension-compression was applied as a negative pressure to the upper surface of the specimens.

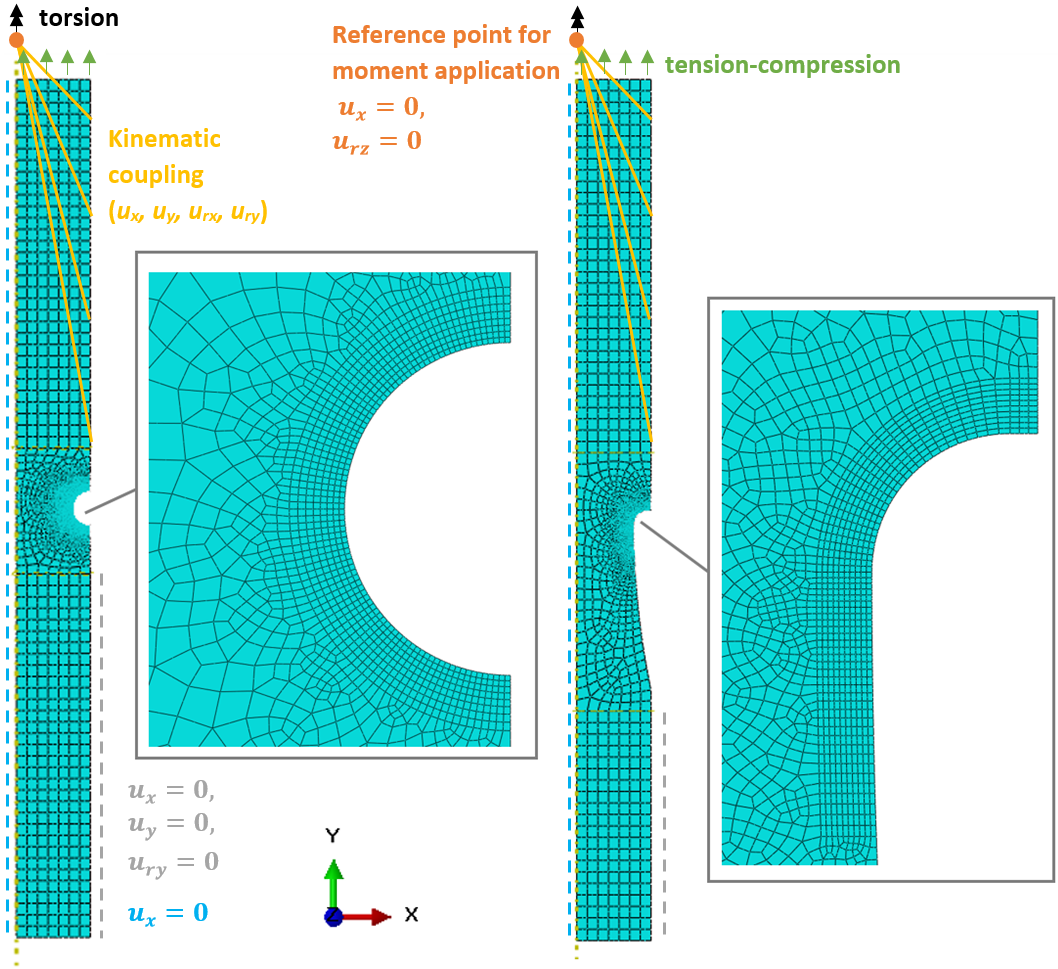

Figure 5.8: Axisymmetric models of the U-notched specimen (left) and the specimen with a fillet (right) in Abaqus. u_x and u_y are translations in the x and y axes directions respectively; u_{rx}, u_{ry}, and u_{rz} are rotations about the x, y, and z axes respectively.

The coincidence of the responses from the experiments and from the FEA (Figure 5.9) at the initial loading and at the beginning of cyclic loading suggests that the elastic data are valid. There are small differences in the cyclic regions that could have been caused by the absence of a ratcheting parameter in the combined hardening model of plasticity in Abaqus 6.14.

Table 5.2: Cyclic stress–strain curve used for elastic–plastic simulations.

Stress [MPa]	Plastic strain [-]
330	0.000
371.56	0.002
395.19	0.004
409.72	0.006
420.35	0.008
428.78	0.010
435.79	0.012
441.81	0.014
447.09	0.016
451.81	0.018

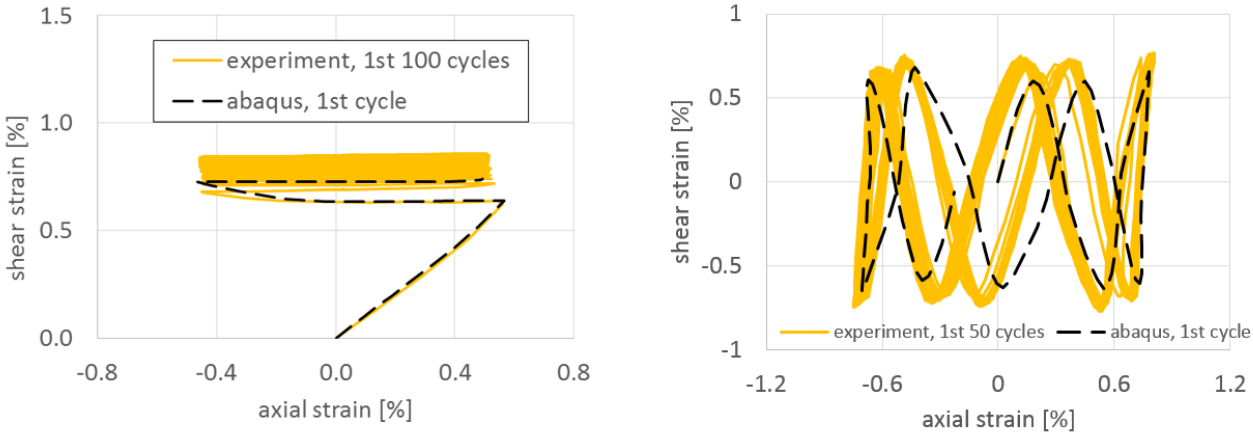

Figure 5.9: Comparison of experimental data and results of elastic–plastic FEA in Abaqus for paths "7" (left) and NV (right)

Chapter 6

A new method

6.1 A new approximate method

Pseudo material approaches are based on material behavior that couples either elastic stress with elastic-plastic strain or elastic strain with elastic-plastic stress. The behavior of the material can be represented by a pseudo curve that is analogous to the static/cyclic stress–strain curve (Figure 6.1). In case of the pseudo stress–real plastic strain curve, which is used in this work, the pseudo material experiences stresses that correspond to stresses related to a purely elastic solution, while it plasticizes according to its real material response at the same time.

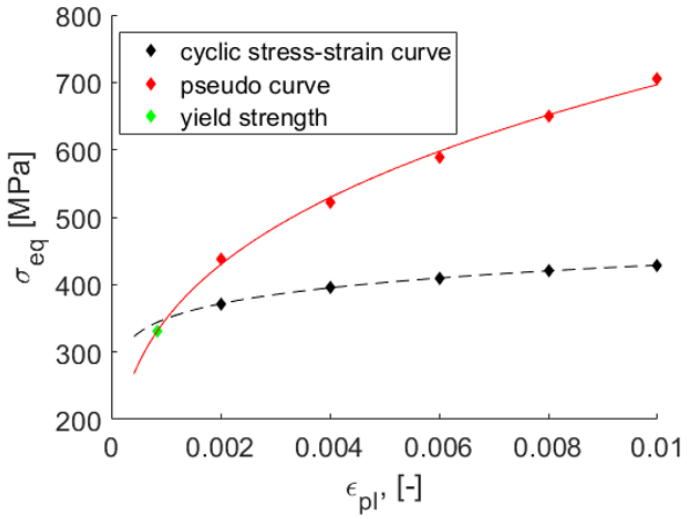

Figure 6.1: Pseudo stress–real plastic strain curve and cyclic stress–strain curve; points represent discrete versions of the curves based on the Hollomon parameters.

There are two types of pseudo stress approaches. In the first approach, pseudo stress

is paired with the total strain [12]; in the second type, pseudo stress is paired with the plastic strain [7, 10]. The main difference between the two approaches is in the strain component that is obtained when a plasticity model is applied to the pseudo stress history, that is, if it is a total strain tensor or a plastic strain tensor. In the present paper, the second type of solution is used.

6.1.1 Establishing pseudo stress material curve

A pseudo curve is established by combining elastic stress with plastic strain. The plastic strain values are the same as the plastic strain values of the real cyclic stress–strain (CSS) curve. The CSS curve could be obtained by the Ramberg–Osgood expression using Hollomon parameters (values are presented in Section 5.1). Since the number of selected plastic strain values is finite, both curves are discrete. Elastic stress is calculated on the basis of the modification of the Neuber rule:

$$\sigma_e = \sqrt{\sigma(\varepsilon_p + \frac{\sigma}{E})E}, \tag{6.1}$$

where σ and ε_p are real stress and plastic strain described by the cyclic stress–strain curve, respectively, and E is Young's modulus. When the curve is established, the parameters of the plasticity model C_i and γ_i are calculated (Equations 2.13-2.15). The number of intervals between discrete points i of pseudo or real curves affects the number of back-stresses used in the approximations, because pairs of C_i and γ_i parameters are calculated for each discrete interval of the pseudo or the real curve, and the number of pairs of C_i and γ_i define the number of backstress parts.

During the approximation process, the curves are represented solely by the C_i and γ_i parameters. They are not referenced in any other way.

6.1.2 Getting real strain and real stress

When two pairs of parameters C_i and γ_i representing the pseudo and the real curves are defined, the plasticity model is applied to the elastic stress history. Elastic stress history can be obtained, e.g., for a chosen loading path from an elastic FEA. Because of the way the pseudo curve is built, this step provides a real plastic stress tensor and accumulated plastic strain as its outputs. Detailed analysis of this property of pseudo material is presented in Section 6.1.3.

Once the plastic strain tensor is obtained, the plasticity model is applied again and the real stress and the real total strain are estimated. However, this time, the iteration algorithm (Section 4.2) to acquire the accumulated plastic strain is not involved, since the accumulated plastic strain has been calculated already in the previous step.

6.1.3 Equivalence of pseudo and real plastic strain tensors

The key part in calculating the real response from the pseudo variables is the equivalence of the accumulated plastic strain dp of the pseudo curve and of the real stress–strain curve. This is ensured by the way the pseudo curve is established (Section 6.1.1).

Unlike in the case of accumulated plastic strain, the equivalence of the pseudo plastic strain tensor and of the real plastic strain tensor is not explicitly stated in [7] or in [10], where similar approaches are used. However, it is stated in [7] that applying the plasticity model to the pseudo stress history results in a real plastic strain tensor. This statement supports the claim of plastic strain tensor equivalence.

Justification can be found by analyzing the widely used relationship between the accumulated plastic strain increment dp and the plastic strain tensor increment $\boldsymbol{d\varepsilon_p}$

$$dp = \sqrt{\frac{2}{3}\boldsymbol{d\varepsilon_p} : \boldsymbol{d\varepsilon_p}}, \tag{6.2}$$

and the flow rule:

$$\boldsymbol{d\varepsilon_p} = \frac{3}{2} dp \frac{\boldsymbol{s} - \boldsymbol{a}}{\sigma_y}, \tag{6.3}$$

where $\boldsymbol{s}$ is the deviatoric part of the stress tensor, $\boldsymbol{a}$ is the deviatoric part of the backstress, and $\boldsymbol{\sigma_y}$ is the yield strength. Note that dp and $\boldsymbol{\sigma_y}$ are identical for the real curve and the pseudo curve.

Due to the intrinsic difference between the elastic and elastic–plastic material behavior of isotropic materials, the real stress is smaller than the pseudo stress under the same load. Backstress $\boldsymbol{a}$ follows the stress while maintaining the radius of the yield sphere during the kinematic hardening. Because of this, it is safe to assume that the tensors $\boldsymbol{s} - \boldsymbol{a}$ for the real and the pseudo material change similarly; more specifically, the corresponding components of $\boldsymbol{s} - \boldsymbol{a}$ change in a similar manner for both materials. If one component increases for the pseudo material, the corresponding component of the real material also increases. The increments should have at least the same sign.

The increment of plastic strain is obtained by a multiplication of $\boldsymbol{s} - \boldsymbol{a}$. Therefore, the same assumptions as for the $\boldsymbol{s} - \boldsymbol{a}$ tensor are valid for the increment of plastic strain. However, then, if all the corresponding components of the real/pseudo plastic strain change in a similar manner by either increasing or decreasing, they could not provide the same dp in Equation 6.2 unless they are equal. Hence, the components of pseudo and real plastic strains had to be the same.

6.1.4 Approximation method step by step

This section summarizes the approximate method described in Sections 6.1.1 and 6.1.2:

1. The pseudo material curve is established.

2. The pseudo stress history is obtained either by elastic FEA or using stress concentration factors.

3. The plasticity model is applied to the pseudo stress history. In this step, plasticity parameters C_i and γ_i obtained for the pseudo material are used. The plastic strain tensor and the accumulated strain are calculated.

4. The plasticity model is applied to the obtained plastic strain tensor and to the accumulated strain. In this step, the plasticity parameters C_i and γ_i for the real material are used. Real stress and real backstress are calculated.

6.2 Results - own experiments

In this section estimates made for the loading paths used on Al2124-T821 specimens (Figure 5.4) are presented. Local notch elastic stresses used as input for the method were obtained using stress concentration factors (Equations 6.4), which in turn were calculated based on FEA described in Section 5.2.

$$\begin{aligned} {}^{e}\sigma_z &= K_z \cdot S_z, \\ {}^{e}\sigma_y &= K'_z \cdot S_z, \\ {}^{e}\sigma_{yz} &= K_{yz} \cdot S_{yz}, \end{aligned} \tag{6.4}$$

In Equation 6.4 S_z and S_{yz} are nominal axial and shear stresses. The values of stress concentration factors for U-notched and specimens with fillets are presented in Table 6.1.

Table 6.1: Stress concentration factors of the aluminum alloy specimens.

Specimen	K_z	K'_z	Kyz
U-notched	2.04	0.54	1.39
Single fillet	1.79	0.39	1.29

The estimates for the first 100 numbers of cycles were plotted against the corresponding experimental responses (Figure 6.2, Table 6.2, Appendix A). Exceptions were estimates of loading path NV for U-notched specimens, for which the numbers of cycles till the specimens break were small (Table 5.1) and the strains increased rapidly after 50 cycles due to the presence of a crack. For these specimens, only the first 42 (Figure A.4) and 50 cycles (Figure A.3) were plotted. In several cases, the experimental response between cycles 350 and 400, and cycles between 501 and 600 was plotted (Table 6.2, Figures A.6, A.9, and A.12). Note that the first 100 cycles were chosen as the primary range for the validation of estimates, as experimental measurements at the beginning of

the tests are less likely to be affected by the presence of a crack. The ratcheting rate after the first 100 cycles seems to be quite slow, and the strains in higher cycles do not differ greatly from the strains during the first 100 cycles (Figures 6.2, A.6, and A.12).

Although for uniaxial and proportional paths the best results were achieved when parameter μ_i was set to 1, estimates of other paths with this value were worse (see Table 6.2). The value μ_i set to 0 showed itself as a better option, as it provided better results overall, despite being slightly less precise in the case of uniaxial and proportional paths.

Relative errors of strain ranges were calculated according to Equation 6.5:

$$RE = \frac{Calculated\,strain\,range - measured\,strain\,range}{measured\,strain\,range}. \tag{6.5}$$

Positive values of relative errors mean that the estimated strain range is greater than the measured strain range. Such a result is considered conservative. The relative error values for axial and shear strain ranges, as well as combined values, are presented. The combined values are calculated as the square root of the corresponding axial and shear components.

In Tables 6.3 and 6.4 values of the relative errors are presented for the first 100 number of cycles (50 and 42 in the case of path NV for U-notched samples). The green filling of cells mean that the absolute value of the relative error is within the 0-10% interval. The yellow filling corresponds to 10-20% of the relative errors, and the orange color means a higher relative error.

The precision of the estimates for the axial and shear components is different. In the case of the axial component, 94% of the studied cases lie within 20% of the relative error in absolute values. The shear component for the same range shows a slightly lower value of 87.5%.

If the precision range is lowered to 10% of the relative error, then 67% of the axial strain estimates fall into this limit, and 44% in the case of the shear component.

The greatest error is 24.7% for the combined strain range.

The influence of the ratcheting parameter on the prediction for Path "7" is shown in Figure 6.2. The value of $\mu_i = 1$ corresponding to the Chaboche's plasticity model (Figure 6.2 d) resulted in an excessive accumulation of plastic shear strain from the first cycle. The value of $\mu = 0.1$ (Figure 6.2 c) provided a better prediction of the evolution of the shear strain in the first cycle, but the prediction after saturation of the response is worse than that of OWI (Figure 6.2 d). Thus, the best prediction of ratcheting is obtained for the limit value of the ratcheting parameter $\mu = 0$, which corresponds to the Ohno–Wang I model. However, the ratcheting response remained exaggerated for the 2124-T851 aluminum alloy.

The graphical representation of the estimates, that have not been shown in this section can be found in Appendix A. A discussion of the results can also be found in [A4].

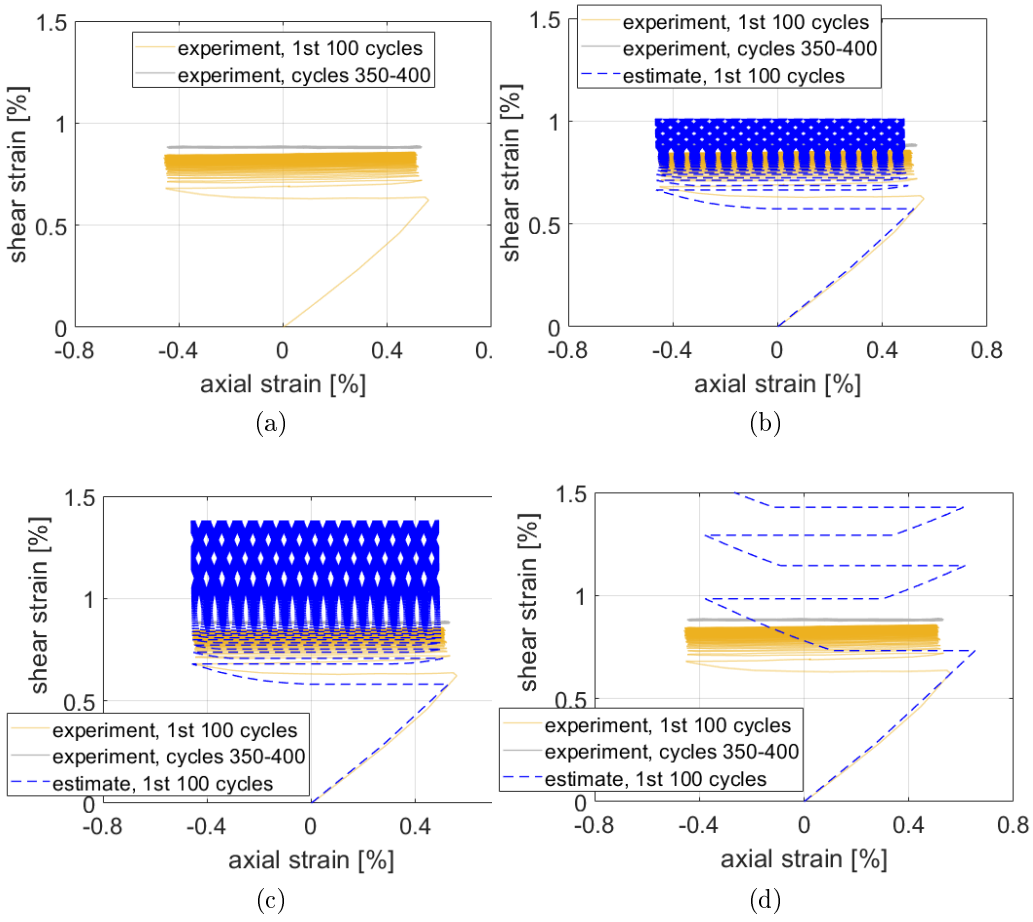

Figure 6.2: Influence of the ratcheting parameter μ_i on the prediction for Path "7". (a) just experiment; (b) $\mu_i = 0$; (c) $\mu_i = 0.1$; (d) $\mu_i = 1$

Table 6.2: Influence of parameter μ_i values on estimates for 2124-T851 aluminum.

μ_i	Path Square	uniaxial path
0	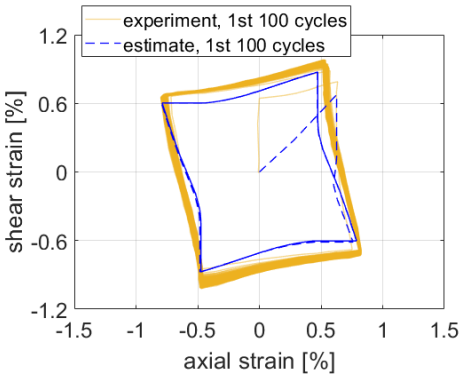	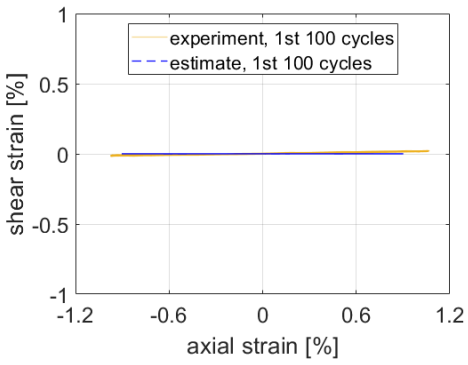
0.1	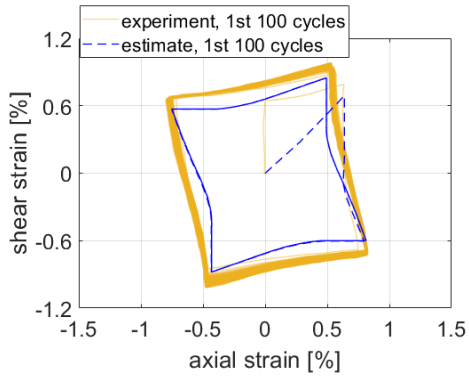	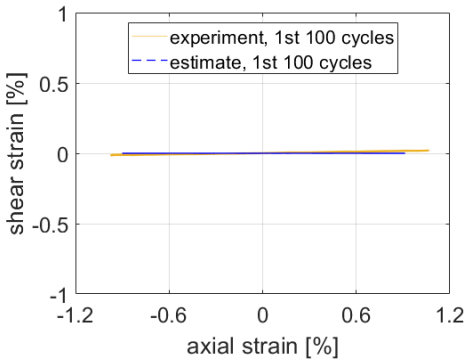
0.5	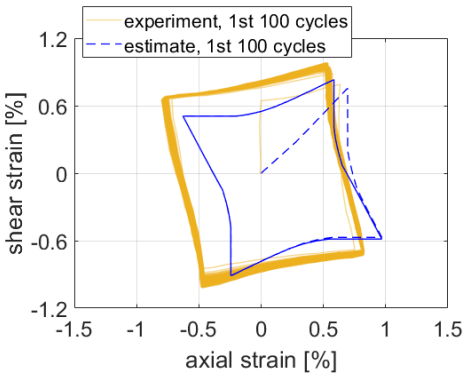	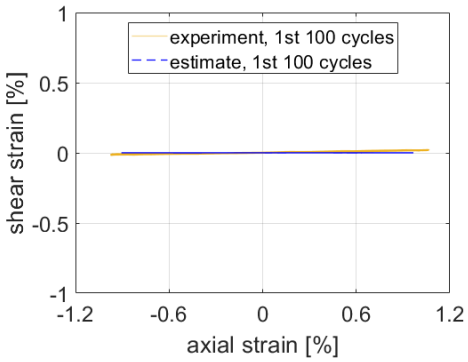
1	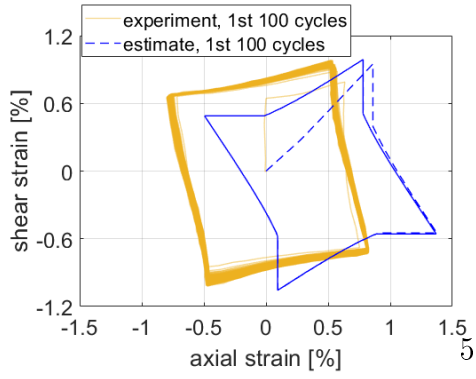	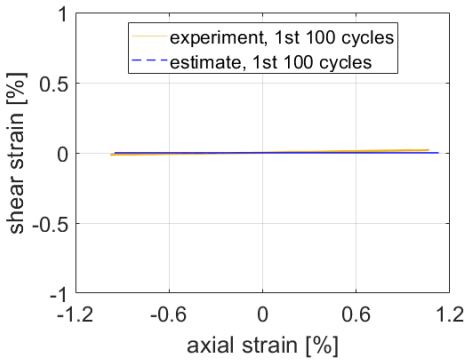

Table 6.3: Relative errors in percents between measured and calculated strain ranges for 2124-T851 U-notched specimens. $\mu_i = 0$.

Path	σ_{nom}[MPa]/ τ_{nom} [MPa]	number of cycles	axial	shear	total
Circle	1	100	−6	−12.2	13.6
Circle	1.73	100	−7.6	−4.7	8.9
NV	1	50	−6.8	−13.9	15.5
NV	1.73	42	−1.2	−5.4	5.5
Proportional	1	100	−6.7	−21.9	22.9
Square	1	100	−2.8	−12.6	12.9
Uniaxial	274.5/ −	100	−13.5	−	13.5
Uniaxial	319.8/ −	100	−11.8	−	11.8
X	1	100	−0.2	−4	4
X	1.73	100	3.1	−2.2	3.8

Table 6.4: Relative errors in percents between measured and calculated strain ranges for 2124-T851 single fillet specimens. $\mu_i = 0$.

Path	$\sigma_{nom}[MPa]$/ τ_{nom} [MPa]	number of cycles	axial	shear	total
7	1	100	−2.8	17.7	17.9
Circle	1	100	9	−4.8	10.2
Circle	1.73	100	−10	−11.1	14.9
NV	1	100	5.7	−2.9	6.4
Proportional	1	100	−6.8	−14.3	15.8
Proportional	1.73	100	−12.6	−21.2	24.7
X	1	100	20.3	7.2	21.5
X	1.73	100	−13.9	−11.5	18.0

6.3 Predictions of other authors

In this chapter, estimates by the proposed method are compared to the estimates by other methods found in the literature. The comparison is made for 1070 steel, as it is the most frequently used material for the validations of the approximate methods. Moreover, all approximations made on this material are based on the same experimental program by Barkey [6], so predictions of several methods can be also compared.

The specimen used by Barkey for his experimental program was a solid 1070 steel bar with a circumferential notch, a net diameter of 25.4 mm and a notch radius of 12.7 mm. The values of the stress concentration factors used to identify the elastic local stress input history are $K_z = 1.42$, $K'_z = 0.3$, and $K_{yz} = 1.15$. The values of nominal stresses are given for each loading path in Tables 6.6-6.8. The material data of 1070 steel are presented in Table 6.5.

Table 6.5: Material data on 1070 steel used in the present work.

Young's modulus	Poisson's ratio	Ramberg-Osgood parameters		Cyclic yield strength	Ratcheting parameter
[GPa]	[-]	K [MPa]	n [-]	[MPa]	$\mu_i[-]$
210	0.3	1736	0.199	286	0.01

The parameters of the plasticity model C_i and γ_i were obtained based on the material data with the function *calc_ C_ gamma* (Appendix C). The cyclic yield strength for 1070 steel was calculated as $\sqrt{3} \cdot$ *cyclic yield strength in shear* (165 MPa) presented for the same material in [29], and resulted in 286 MPa. The calculated value led to better results than that of the initial yield strength of 242 MPa used for the Garud model of plasticity in [13]. The original plots from [11–13] were recreated using an online tool [35].

Only estimates validated on experimental data were selected. Completeness of information about loading was also a necessary requirement.

The values of the relative errors were already given for the estimates by Ince and Tao. The relative error values of the predictions by Li et al. were calculated based on the data from the plots presented in [12]. The signs of the relative error values of Ince's predictions were altered, so they match the sign convention used in the present work (described in Section 6.2).

Relative errors for axial and shear strain ranges are presented in Tables 6.6 and 6.7, and combined values, again calculated as the square root of the corresponding axial and shear components, are presented in Table 6.8.

In Tables 6.6-6.8, the highlighted cells mark the lowest relative error for each loading case. The proposed method provides the best predictions in the 6 out of 13 cases. However, since the estimates of other authors are not available for every studied case, the conclusion should be taken with reservations.

The geratest relative errors were made for the shear component of path Square . The lowest errors could be achieved by changing the value of parameter μ_i, but this would negatively affect the estimates for paths V and rotated V (Table 6.9) .

The graphical representation of the estimates by the proposed method and the estimates from the literature can be found in Appendix B and in [A4].

Table 6.6: Relative errors between measured and calculated **axial** strain ranges for selected methods for 1070 steel in percents.

Path	σ_{nom}[MPa]/ τ_{nom} [MPa]	Li et al. [12]	Ince et al. [11]	Tao et al. [13]	proposed method
ksi	258/168	–	–	–1.45	–1.5
ksi	296/193	–	–4.5	–	–4.5
N	258/168	–	–	–4.62	1.1
N	296/193	6.5	–6.4	–	–4.8
NV	258/168	–	–	–5.29	3.3
NV	296/193	–	–4.2	–	–5
Proportional	296/193	–	–	–1.67	–8.8
Rotated V	296/193	4.9	–	–	–1.4
S	258/168	–	–	–1.87	–1.3
S	296/193	–0.7	–6.6	–	–8.3
Square	296/193	8.7	–4	–4.98	–8
Square (clockwise)	296/193	10.4	–4.1	–	–7.2
V	296/193	11.4	–	–	1.4

Table 6.7: Relative errors between measured and calculated **shear** strain ranges for selected methods for 1070 steel in percents.

Path	σ_{nom}[MPa]/ τ_{nom} [MPa]	Li et al. [12]	Ince et al. [11]	Tao et al. [13]	proposed method
ksi	258/168	–	–	−10.33	2.7
ksi	296/193	–	−8.8	–	−8.9
N	258/168	–	–	−8.24	1.1
N	296/193	−4.5	−11.4	–	−10.7
NV	258/168	–	–	−2.85	4.1
NV	296/193	–	−4.7	–	−8.6
Proportional	296/193	–	–	−7.91	−16
Rotated V	296/193	11.8	–	–	1.5
S	258/168	–	–	−7.06	1.8
S	296/193	−0.8	−12.5	–	−10.5
Square	296/193	−0.3	−11.2	−14.71	−18.2
Square (clockwise)	296/193	2.5	−15.3	–	−16.4
V	296/193	2.2	–	–	−4.1

Table 6.8: Relative errors between measured and calculated **combined** strain ranges for selected methods for 1070 steel in percents.

Path	σ_{nom}[MPa]/ τ_{nom} [MPa]	Li et al. [12]	Ince et al. [11]	Tao et al. [13]	proposed method
ksi	258/168	–	–	10.4	3.1
ksi	296/193	–	9.9	–	10
N	258/168	–	–	9.4	1.6
N	296/193	7.9	13.1	–	11.7
NV	258/168	–	–	6	5.3
NV	296/193	–	6.3	–	9.9
Proportional	296/193	–	–	8.1	18.3
Rotated V	296/193	12.8	–	–	2.1
S	258/168	–	–	7.3	2.2
S	296/193	1.1	14.1	–	13.4
Square	296/193	8.7	11.9	15.5	19.9
Square (clockwise)	296/193	10.7	15.8	–	17.9
V	296/193	11.6	–	–	4.3

Table 6.9: Influence of parameter μ_i values on estimates for 1070 steel.

μ_i	Path Square	Path Rotated V
0.01	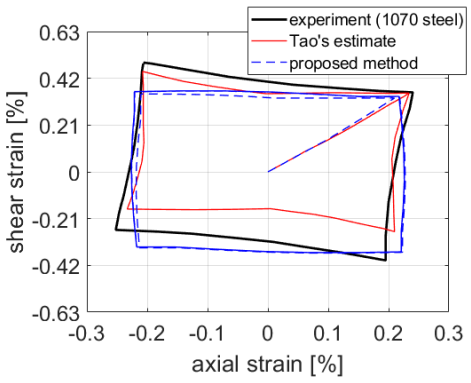	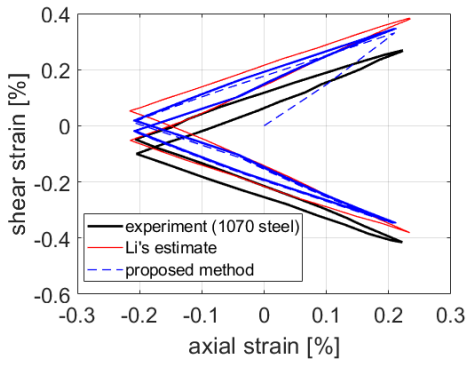
0.1	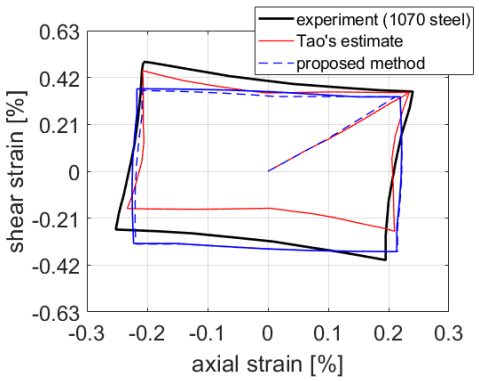	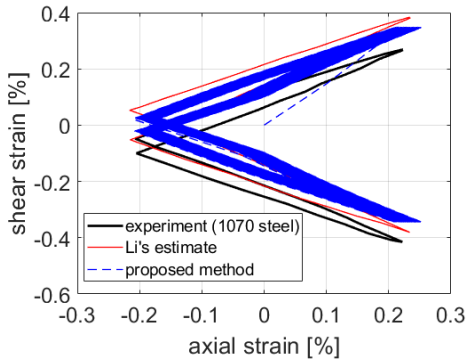
0.3	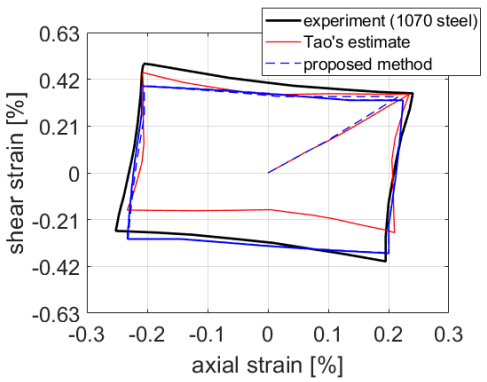	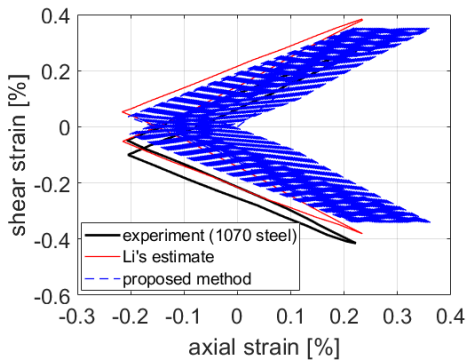
1	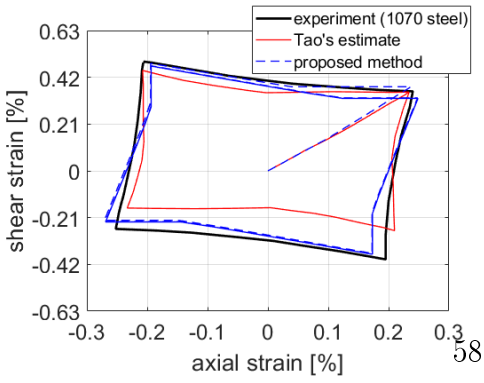	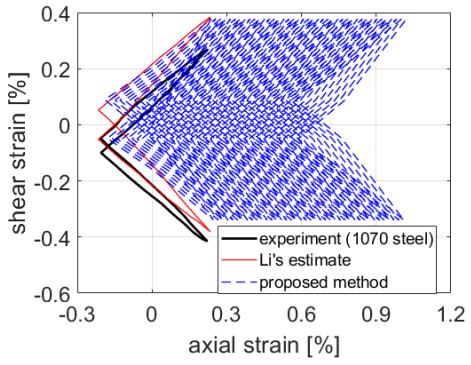

Chapter 7

Outcomes

Experimental data on the notch tip strains are very limited to this day. The presented experimental data obtained on 2124-T851 aluminum alloy specimens expand the set of currently available data. Responses to a wide variety of loading paths have been measured and presented. Path "7" represents an especially valuable addition as a path with a constant mean stress, since it allows to study the ratcheting effect and to tune the models' ratcheting parameters. The new experimental data are available in Appendix A, Figure 5.9, and [A4], and can be acquired by means of WebPlotDigitizer.

An overview of approximate methods for monotonic loading, as well as recommendations of which method to use, were published in [A5] and [A6].

As for the methods for cyclic loading, a code of the proposed approximate method written in the MATLAB programming language is available in Appendix C and in [A4]. Since details on combinations of notch correction methods and plasticity models represent a key value for researchers starting to deal with the stress-strain approximation methods, the published code allows researchers to better understand the method principle and recreate the method by themselves. The new method provides estimates with a relative error under 25% for many loading cycles without the need to carry out time-consuming elastic-plastic finite element analyses. The method was also presented in [A4] .

The code in its entirety can be used to obtain elastic-plastic stress-strain estimates. A stress history from the elastic solution at a critical location can be used as input for the code to estimate elastic-plastic stress-strain solution. That could speed up a design process or other stress assessment tasks.

Chapter 8

Conclusions and future work

8.1 Conclusions

The target of the thesis was to develop a novel pseudo curve based approximate method for calculating elastic-plastic stresses and strains at the notch tip under multiaxial cyclic loading condition. Each defined steps to achieve the target, as the target itself, was fulfilled:

1. A methodology on how to combine a notch correction and a plasticity model was developed and described in detail in Sections 4.2 and 6.1-6.1.4. The implementation code, which is available in Appendix C, provides a benefit to researchers dealing with the approximate methods for notch tip stress and strain calculation during the process of recreation of the proposed method. The methodology and the implementation code were published in [A4].

2. A new and original approximate method for calculating the elastic-plastic stresses and strains at the notch tip under multiaxial cyclic loading was proposed and published in [A4]. Its novelty lies in the ability to incorporate three plasticity models, Abdel-Karim-Ohno, Ohno-Wang, and Chaboche's model, as its special cases. The approximate method provides results of competitive precision to other existing methods and allows fast estimates of stress and strain responses on cyclic multiaxial loading.

3. New and original experimental data of notch tip strains were measured on aluminum 2124-T851 specimens for a variety of loading paths. A total number of 18 experimental loading cases is presented in this work. Both frequently and infrequently used loading paths from literature were chosen. A loading path with a mean stress was included in the experimental program. The path provides a ratcheting response that is useful for studying its effects. In preceding research publications, only FE

analyses of this specific path were used. To author's knowledge, it is the first time an experimental notch strain response has been published for a loading path with a mean stress. The experimental results were also published in [A4].

8.2 Future work

A future development in a practical way might be the implementation of the approximate method in an FE solver as a plugin. This would speed up the estimation process, as it would spare the time otherwise spent exporting stresses from elastic FE analyses. The accessibility directly from FE software would help the method to gain a wider use. The implementation would also allow to apply the method on all surface nodes of a model, which in turn would allow to study the method precision outside of a stress concentration region.

If higher precision needs to be achieved, a changeable value of the ratcheting parameter might be implemented. It should help capture ratcheting changes more accurately.

It is possible to expand the method by including the Calloch-Marquis non-proportional parameter, which would allow a non-proportional hardening to be taken into account, appearing, for example in the cases of stainless steels and coppers [36, 37].

Another way to improve the precision might be found by in-depth analyzes of differences between AKO and Jiang-Sehitoglu plasticity models, which showed itself as the most precise for the majority of its studied cases.

Finally, since thermo-mechanical loading is a common part of loading states and a need to calculate stresses and strains in such cases is as great as for mechanical loading under constant temperatures, the possibility to expand the method for thermo-mechanical loading might be investigated in the future.

References

1. Hoffmann, M. & Seeger, T. in (eds Brown, M. & Miller, K.) 3–24 (Mechanical Engineering Publications, London, 1989).
2. Moftakhar, A., Buczyński, A. & Glinka, G. Calculation of elasto-plastic strains and stresses in notches under multiaxial loading. *International Journal of Fracture* **70,** 357–373 (1995).
3. Singh, M., Glinka, G. & Dubey, R. Elastic-plastic stress-strain calculation in notched bodies subjected to non-proportional loading. *International Journal of Fracture* **76,** 39–60 (1996).
4. Buczynski, A. & Glinka, G. *Elastic-plastic stress-strain analysis of notches under non-proportional loading* in *Proceedings of the 5th International Conference on Biaxial/Multiaxial Fatigue and Fracture* (Cracow, Poland, 1997 September), 461–479.
5. Reinhardt, W., Moftakhar, A. & Glinka, G. An Efficient Method for Calculating Multiaxial Elasto-Plastic Notch Tip Strains and Stresses under Proportional Loading. *Fatigue and Fracture Mechanics* **27,** 613–629 (1997).
6. Barkey, M. E. *Calculation of notch strains under multiaxial nominal loading* PhD thesis (University of Illinois, USA, 1993).
7. Koettgen, V., Barkey, M. & Socie, D. Pseudo stress and pseudo strain based approaches to multiaxial notch analysis. *Fatigue & Fracture of Engineering Materials & Structures* **18,** 981–1006 (1995).
8. Langlais, T. E. *Computational methods for multiaxial fatigue analysis* PhD thesis (University of Minnesota, USA, 1999).
9. Ye, D., Hertel, O. & Vormwald, M. A unified expression of elastic–plastic notch stress–strain calculation in bodies subjected to multiaxial cyclic loading. *International Journal of Solids and Structures* **45,** 6177–6189 (2008).
10. Firat, M. A notch strain calculation of a notched specimen under axial-torsion loadings. *Materials & Design* **32,** 3876–3882 (2011).

11. Ince, A., Buczynski, A. & Glinka, G. Computational modeling of multiaxial elasto-plastic stress–strain response for notched components under non-proportional loading. *International Journal of Fatigue* **62,** 42–52 (2014).

12. Li, J., Zhang, Z. & Li, C. A coupled Armstrong-Frederick type plasticity correction methodology for calculating multiaxial notch stresses and strains. *Journal of Failure Analysis and Prevention* **17,** 706–716 (2017).

13. Tao, Z.-Q., Shang, D.-G. & Sun, Y.-J. New pseudo stress correction method for estimating local strains at notch under multiax-ial cyclic loading. *International Journal of Fatigue* **103,** 280–293 (2017).

14. Li, D.-H., Shang, D.-G., Xue, L., Li, L.-J., Wang, L.-W. & Cui, J. Notch stress-strain estimation method based on pseudo stress correction under multiaxial thermo-mechanical cyclic loading. *International Journal of Solids and Structures* **199,** 144–157 (2020).

15. Kraft, J. & Vormwald, M. Energy driven integration of incremental notch stress-strain approximation for multiaxial cyclic loading. *International Journal of Fatigue* **145,** 106043. ISSN: 0142-1123. `https://www.sciencedirect.com/science/article/pii/S0142112320305752` (2021).

16. Chu, C.-C. A three-dimensional model of anisotropic hardening in metals and its application to the analysis of sheet metal forming. *Journal of the Mechanics and Physics of Solids* **32,** 197–212 (1984).

17. Jiang, Y. & Sehitoglu, H. Modeling of Cyclic Ratchetting Plasticity, Part I: Development of Constitutive Relations. *Journal of Applied Mechanics* **63,** 720–725. ISSN: 0021-8936. `https://doi.org/10.1115/1.2823355` (Sept. 1996).

18. Chaboche, J. Constitutive equations for cyclic plasticity and cyclic viscoplasticity. *International Journal of Plasticity* **5,** 247–302. ISSN: 0749-6419. `https://www.sciencedirect.com/science/article/pii/0749641989900156` (1989).

19. Prandtl, W. *Spannungsverteilung in plastischen kerpern* in *Proceedings of the first international congress on applied mechanics* (1924).

20. Reuss, A. Berücksichtigung der elastischen Formänderung in der Plastizitätstheorie. *ZAMM - Journal of Applied Mathematics and Mechanics / Zeitschrift für Angewandte Mathematik und Mechanik* **10,** 266–274. eprint: `https://onlinelibrary.wiley.com/doi/pdf/10.1002/zamm.19300100308`. `https://onlinelibrary.wiley.com/doi/abs/10.1002/zamm.19300100308` (1930).

21. Garud, Y. S. A New Approach to the Evaluation of Fatigue Under Multiaxial Loadings. *Journal of Engineering Materials and Technology* **103,** 118–125. ISSN: 0094-4289. `https://doi.org/10.1115/1.3224982` (Apr. 1981).

22. Glinka, G., Roostaei, A. A. & Jahed, H. in *Cyclic Plasticity of Metals* (eds Jahed, H. & Roostaei, A. A.) 283–323 (Elsevier, 2022). ISBN: 978-0-12-819293-1. https://www.sciencedirect.com/science/article/pii/B978012819293100019X.

23. Nagode, M., Hack, M. & Fajdiga, M. Low cycle thermo-mechanical fatigue: Damage operator approach. *Fatigue & Fracture of Engineering Materials & Structures* **33,** 149–160 (2010).

24. Li, D.-H. *et al.* Unified viscoplastic constitutive model under axial-torsional thermo-mechanical cyclic loading. *International Journal of Mechanical Sciences* **150,** 90–102. ISSN: 0020-7403. https://www.sciencedirect.com/science/article/pii/S0020740318314796 (2019).

25. Ohno, N. & Wang, J.-D. Kinematic hardening rules with critical state of dynamic recovery, part I: formulation and basic features for ratchetting behavior. *International Journal of Plasticity* **9,** 375–390. ISSN: 0749-6419. https://www.sciencedirect.com/science/article/pii/074964199390042O (1993).

26. Halama, R., Parma, S., Sedlák, J. & Šofer, M. *Cyclic plasticity* tech. rep. FAD/11/003 (FME, VŠB-TU in Ostrava, Dec. 2011).

27. Abdollahi, E. & Chakherlou, T. N. Numerical and experimental study of ratcheting in cold expanded plate of Al-alloy 2024-T3 in double shear lap joints. *Fatigue & Fracture of Engineering Materials & Structures* **41,** 41–56. https://onlinelibrary.wiley.com/doi/abs/10.1111/ffe.12643 (2018).

28. Mróz, Z. On the Description of Anisotropic Workhardening. *Journal of the Mechanics and Physics of Solids* **15,** 163–175 (1967).

29. Jiang, Y. & Sehitoglu, H. Cyclic ratcheting of 1070 steel under multiaxial stress states. *International Journal of Plasticity* **10,** 579–608 (1994).

30. Hertel, O., Vormwald, M., Seeger, T., Döring, R. & Hoffmeyer, J. Notch stress and strain approximation procedures for application with multiaxial nonproportional loading. *Materials Testing* **47,** 268–277 (May 2005).

31. Chaboche, J. A review of some plasticity and viscoplasticity constitutive theories. *International Journal of Plasticity* **24.** Special Issue in Honor of Jean-Louis Chaboche, 1642–1693. ISSN: 0749-6419. https://www.sciencedirect.com/science/article/pii/S0749641908000582 (2008).

32. Kobayashi, M. & Ohno, N. Implementation of cyclic plasticity models based on a general form of kinematic hardening. *International Journal for Numerical Methods in Engineering* **53,** 2217–2238. https://onlinelibrary.wiley.com/doi/abs/10.1002/nme.384 (2002).

33. ASM Aerospace Specification Metals, I. *ASM Aerospace Specification Metals website* Dec. 2021. http://asm.matweb.com/search/SpecificMaterial.asp?bassnum=MA2124T851.

34. Papuga, J. *et al. Summary of experiments on 2124-T851 realized within FADOFF project* tech. rep. FAD/14/001 (FME, CTU in Prague, FME, VŠB-TU in Ostrava, and Evektor spol. s r.o., Dec. 2014).

35. Rohatgi, A. *Web Based Tool to Extract Data from Plots, Images, and Maps* Jan. 2022. https://apps.automeris.io/wpd/.

36. Halama, R., Markopoulos, A., Šmach, J. & Govindaraj, B. in (ed Anghel, C.) submitted. Chap. Theory, application and implementation of modified Abdel-Karim-Ohno model for uniaxial and multiaxial fatigue loading (Elsevier, Amsterdam, The Netherlands, 2022).

37. Calloch, S. & Marquis, D. Triaxial tension–compression tests for multiaxial cyclic plasticity. *International Journal of Plasticity* **15,** 521–549. ISSN: 0749-6419. https://www.sciencedirect.com/science/article/pii/S0749641999000054 (1999).

Publications of the author related to the topic of the thesis

A1. Papuga, J., Vízková, I., Lutovinov, M. & Nesládek, M. Mean stress effect in stress-life fatigue prediction re-evaluated. English. *MATEC Web of Conferences* **165,** 8 pages. https://www.matec-conferences.org/articles/matecconf/pdf/2018/24/matecconf_fatigue2018_10018.pdf (May 2018).

A2. Papuga, J., Kaľavský, A., Lutovinov, M., Vízková, I., Parma, S. & Nesládek, M. Evaluation of data sets usable for validating multiaxial fatigue strength criteria. English. *International Journal of Fatigue* **145,** 18 pages. https://www.sciencedirect.com/science/article/pii/S0142112320306253 (Apr. 2021).

A3. Papuga, J., Karkulín, A., Hanžl, O. & Lutovinov, M. Comparison of several methods for the notch effect quantification on specimens from 2124-T851 aluminum alloy. *Procedia Structural Integrity* **19.** Fatigue Design 2019, International Conference on Fatigue Design, 8th Edition, 405–414. ISSN: 2452-3216. https://www.sciencedirect.com/science/article/pii/S2452321619305128 (2019).

A4. Lutovinov, M., Halama, R., Papuga, J., Bartošák, M., Kuželka, J. & Růžička, M. An Approximate Method for Calculating Elastic-Plastic Stress and Strain on Notched Specimens. *Materials* **15,** 22 pages. ISSN: 1996-1944. https://www.mdpi.com/1996-1944/15/4/1432 (2022).

A5. Lutovinov M.; Papuga, J. *A Verification of Methods for Calculating Notch Tip Stresses and Strains* in *19th Workshop of Applied Mechanics* (Czech Technical University in Prague, Faculty of Mechanical Engineering, 2015), 4 pages. ISBN: 978-80-01-05918-0.

A6. Lutovinov, M., Černý, J. & Papuga, J. A comparison of methods for calculating notch tip strains and stresses under multiaxial loading. *Frattura ed Integrita Strutturale* **38,** 237–243 (2016).

Appendix A

Estimates for 2124-T851 aluminum alloy

Parameter μ_i is set to 0 for all cases.

A.1 U-notched specimen

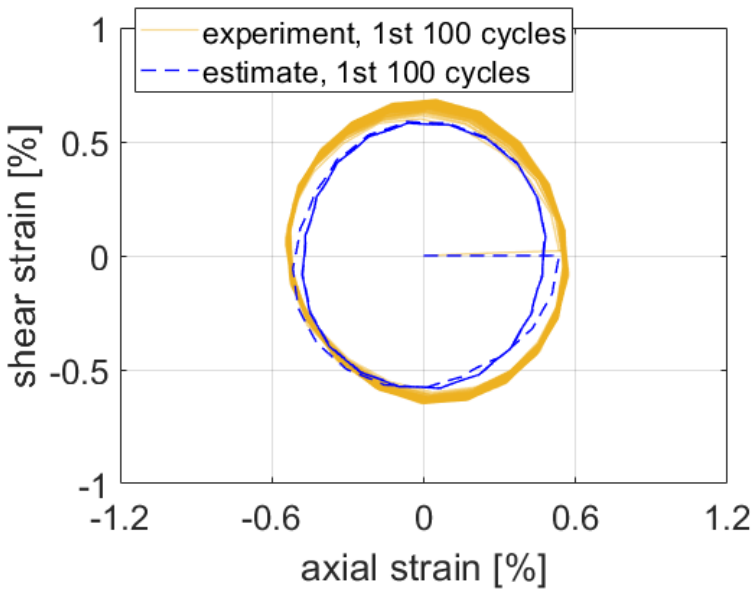

Figure A.1: Estimate for Path Circle, ratio of nominal axial to shear stresses is 1.

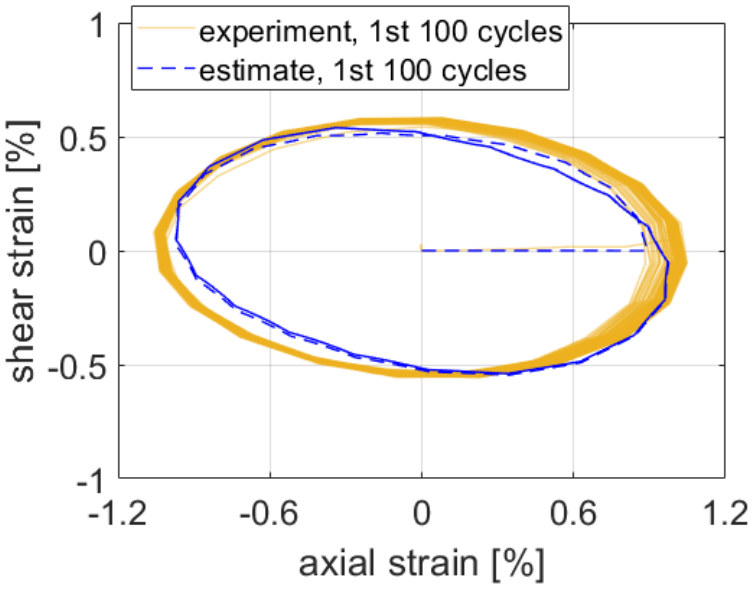

Figure A.2: Estimate for Path Circle, ratio of nominal axial to shear stresses is 1.73.

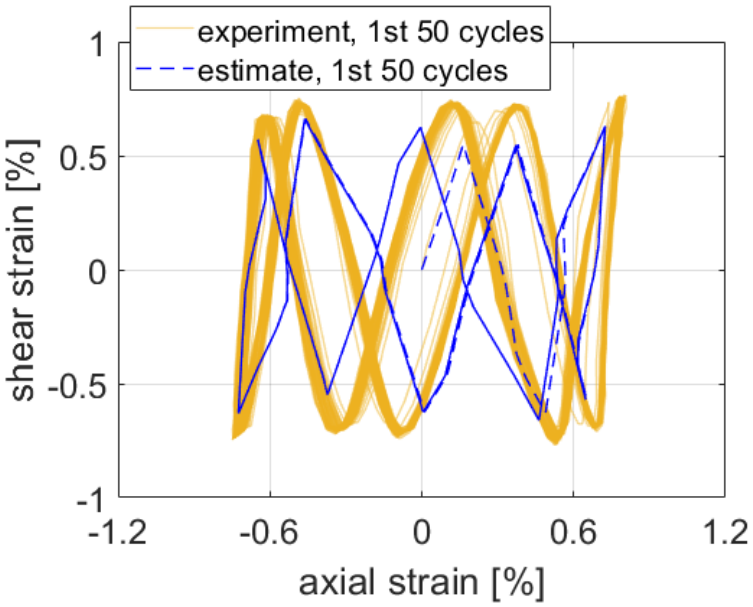

Figure A.3: Estimate for Path NV, ratio of nominal axial to shear stresses is 1.

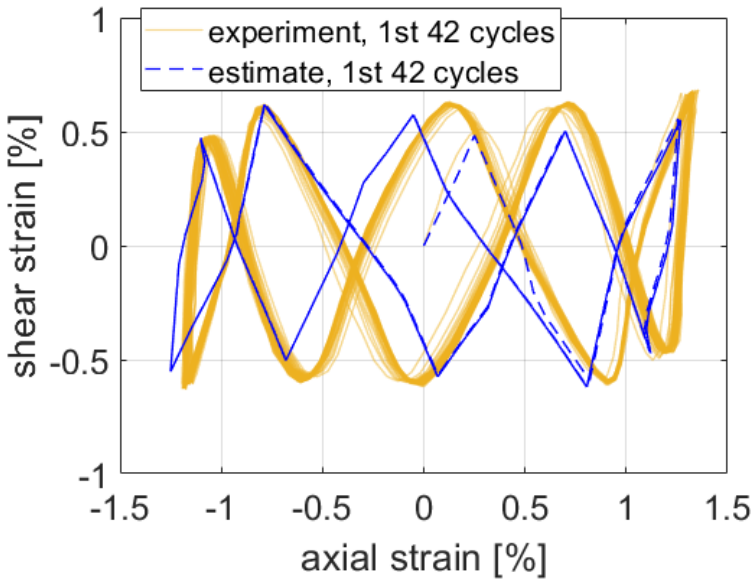

Figure A.4: Estimate for Path NV, ratio of nominal axial to shear stresses is 1.73.

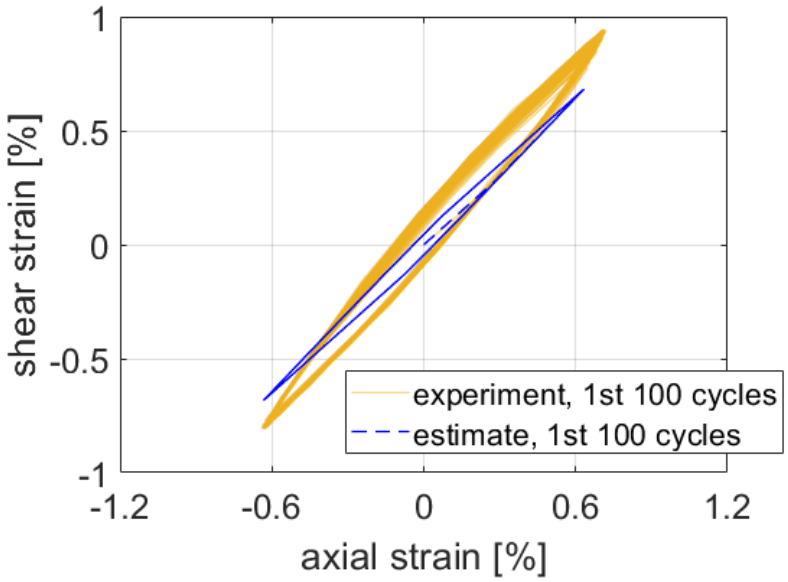

Figure A.5: Estimate for Path Proportional, ratio of nominal axial to shear stresses is 1.

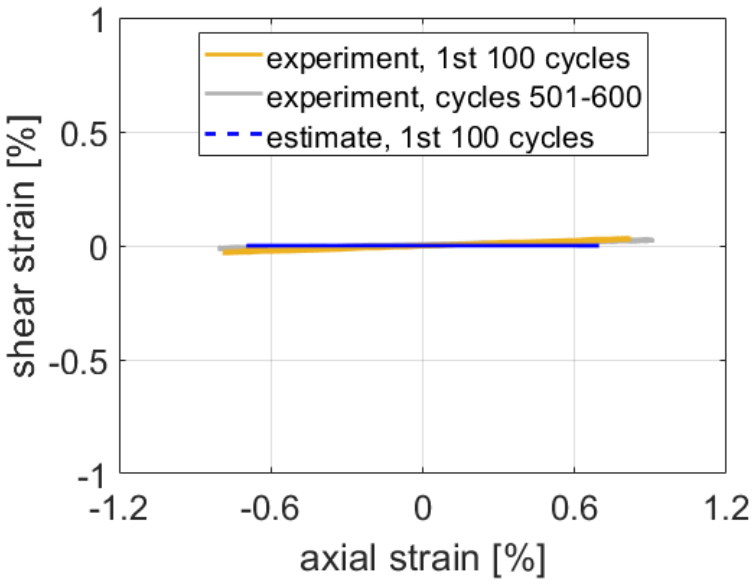

Figure A.6: Estimate for Path Uniaxial, nominal axial stress is 274.5 MPa.

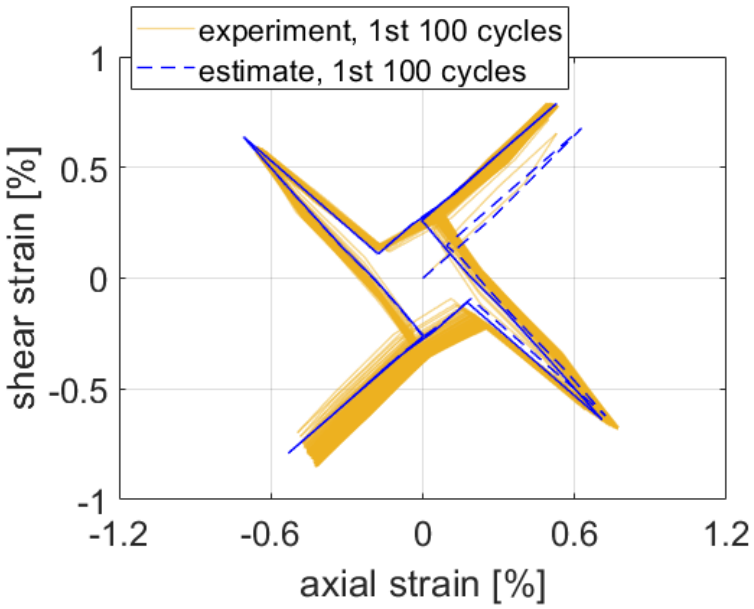

Figure A.7: Estimate for Path X, ratio of nominal axial to shear stresses is 1.

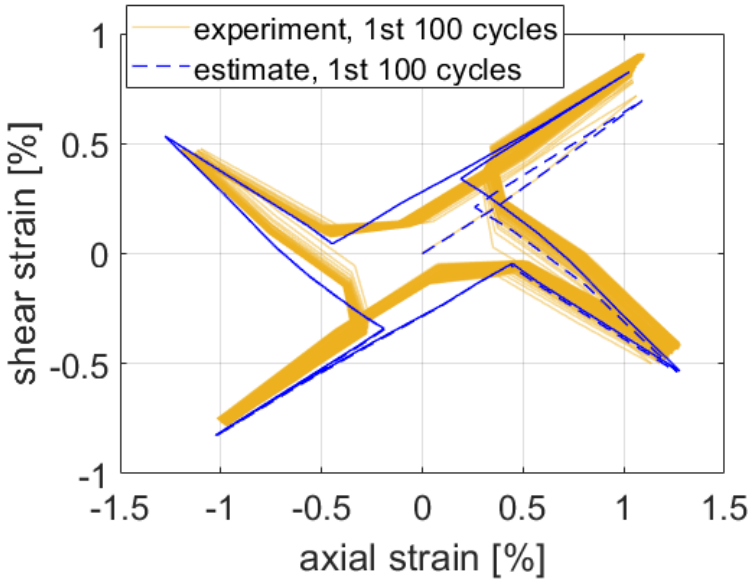

Figure A.8: Estimate for Path X, ratio of nominal axial to shear stresses is 1.73.

A.2 Specimen with fillet

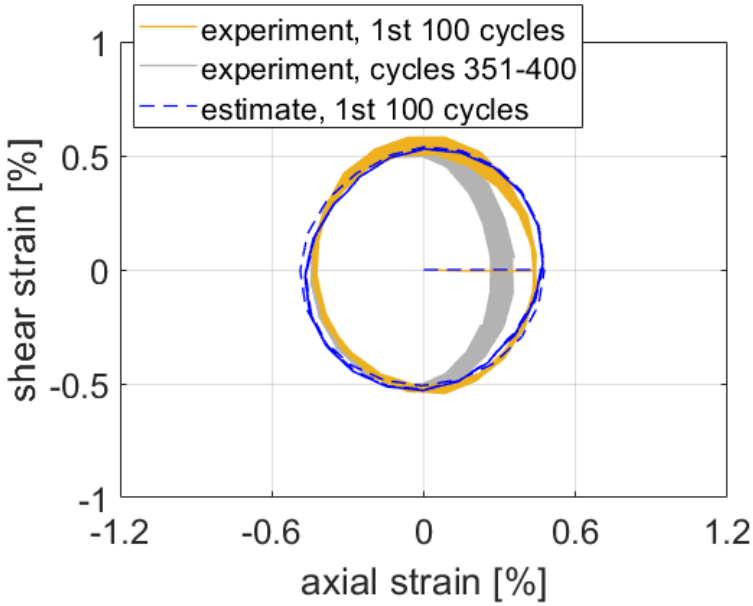

Figure A.9: Estimate for Path Circle, ratio of nominal axial to shear stresses is 1.

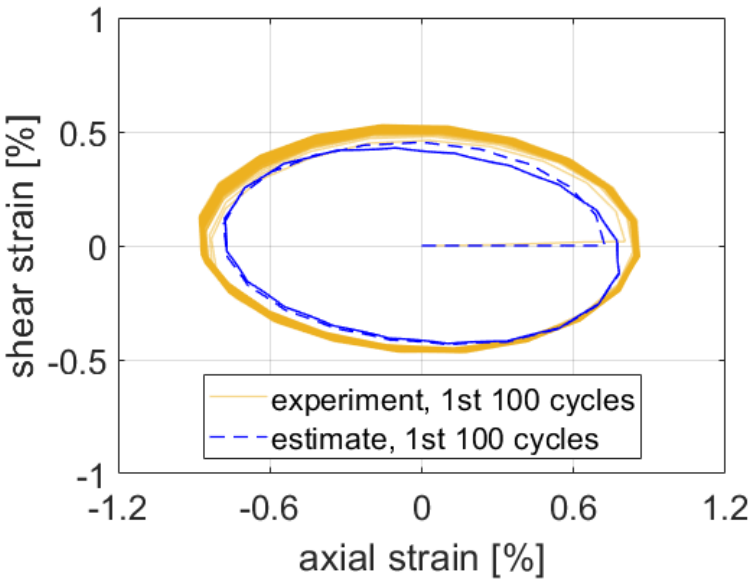

Figure A.10: Estimate for Path Circle, ratio of nominal axial to shear stresses is 1.73.

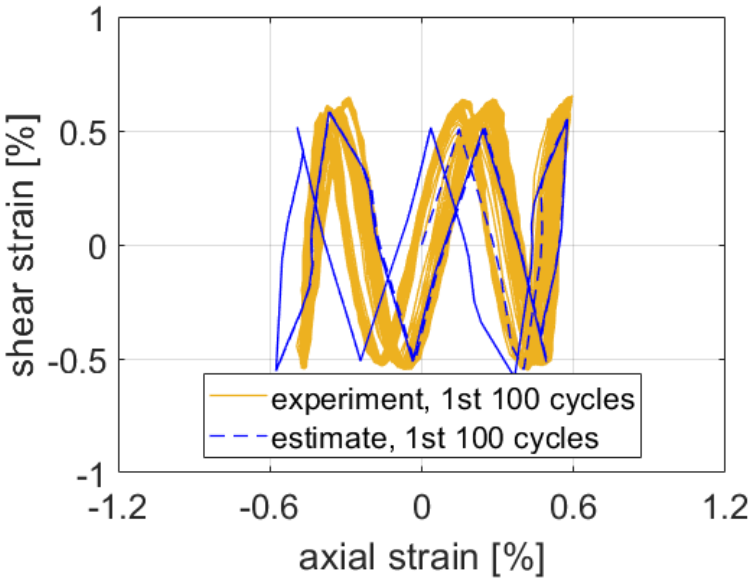

Figure A.11: Estimate for Path NV, ratio of nominal axial to shear stresses is 1.

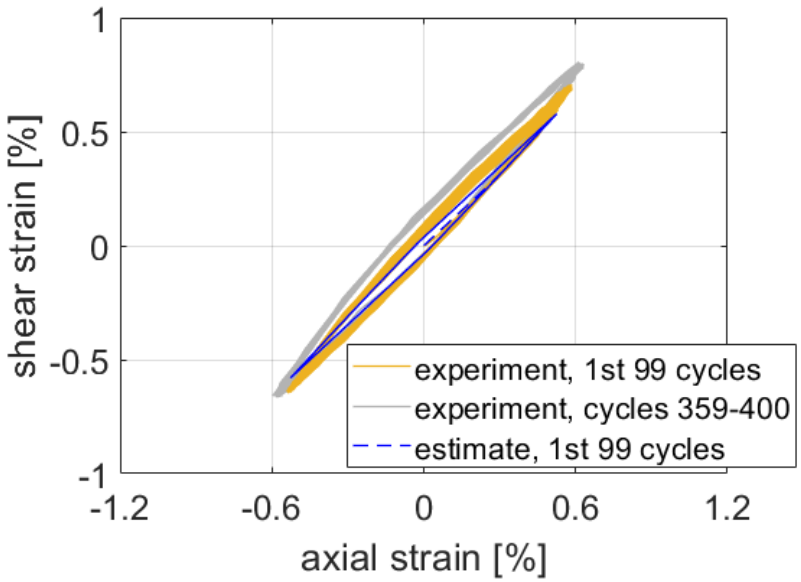

Figure A.12: Estimate for Path Proportional, ratio of nominal axial to shear stresses is 1.

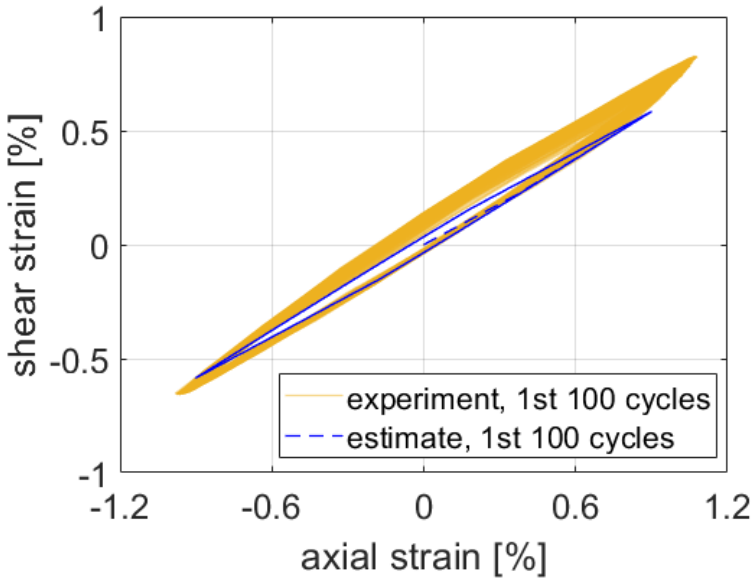

Figure A.13: Estimate for Path Proportional, ratio of nominal axial to shear stresses is 1.73

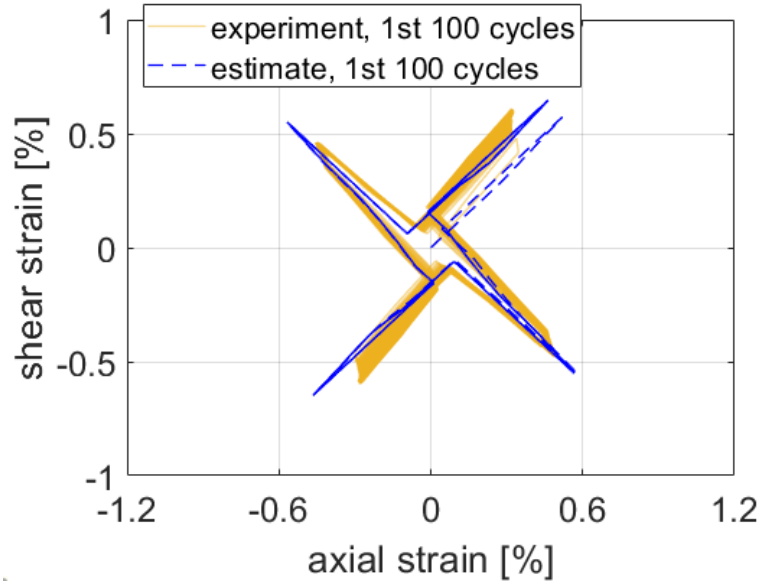

Figure A.14: Estimate for Path X, ratio of nominal axial to shear stresses is 1.

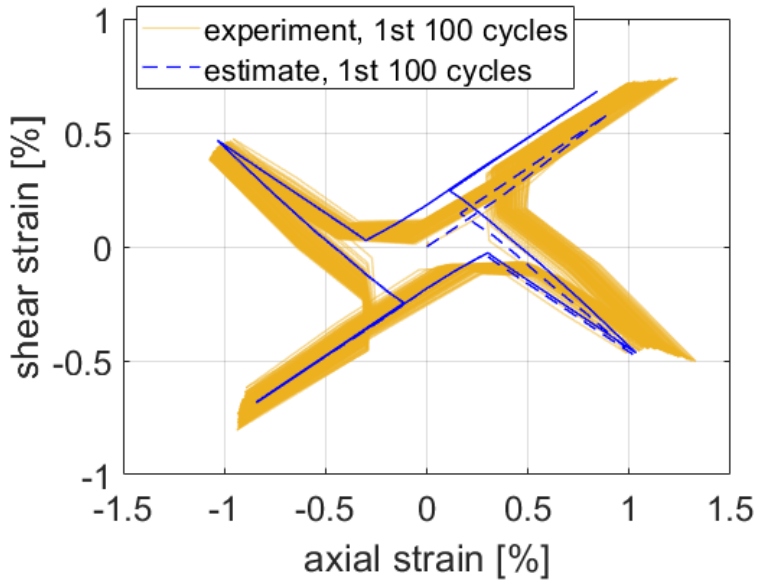

Figure A.15: Estimate for Path X, ratio of nominal axial to shear stresses is 1.73.

Appendix B

Estimates comparison for 1070 steel

Parameter μ_i is set to 0.01 for all cases.

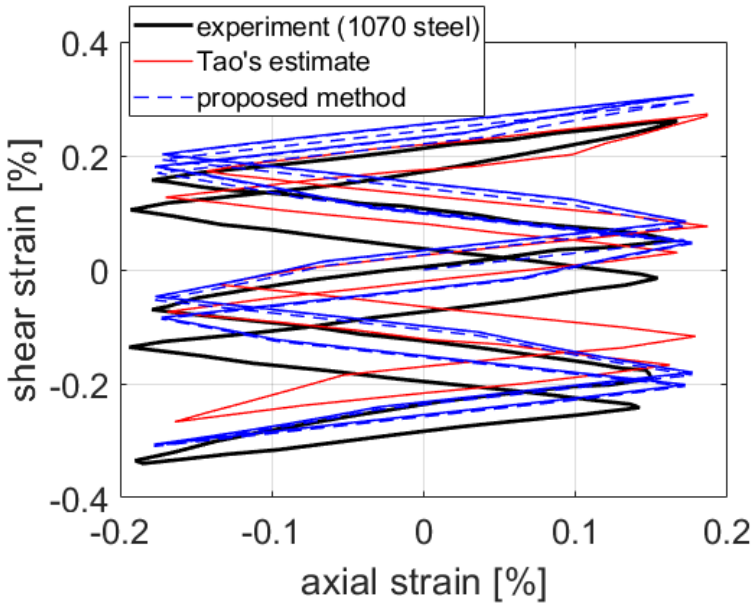

Figure B.1: Comparison of the proposed method and estimate by Tao et al. [13] for loading path ksi.

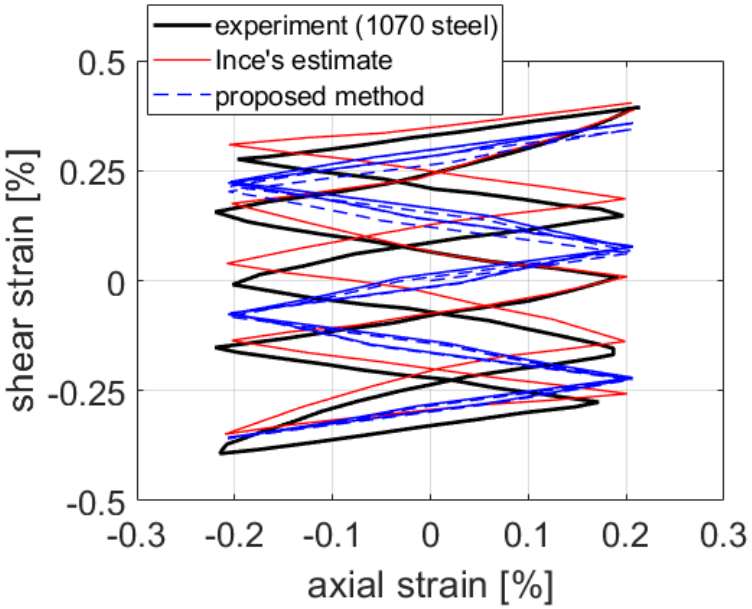

Figure B.2: Comparison of the proposed method and estimate by Ince et al. [11] for loading path ksi.

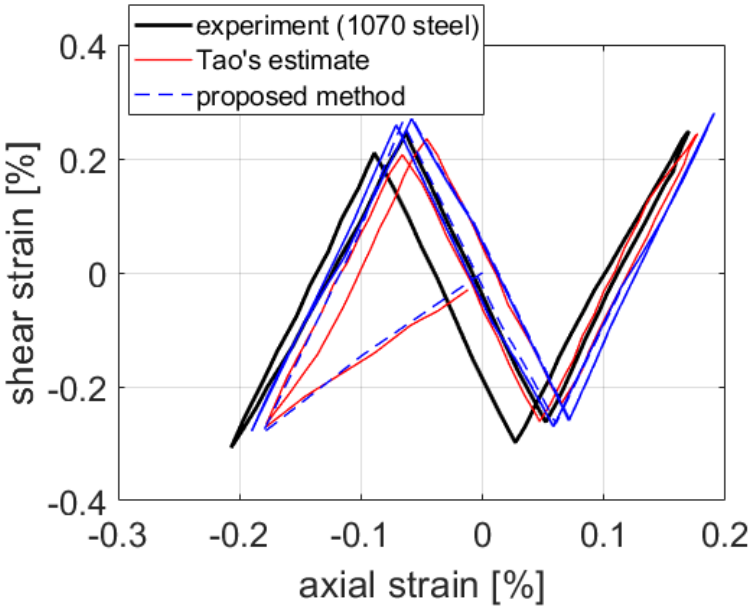

Figure B.3: Comparison of the proposed method and estimate by Tao et al. [13] for loading path N.

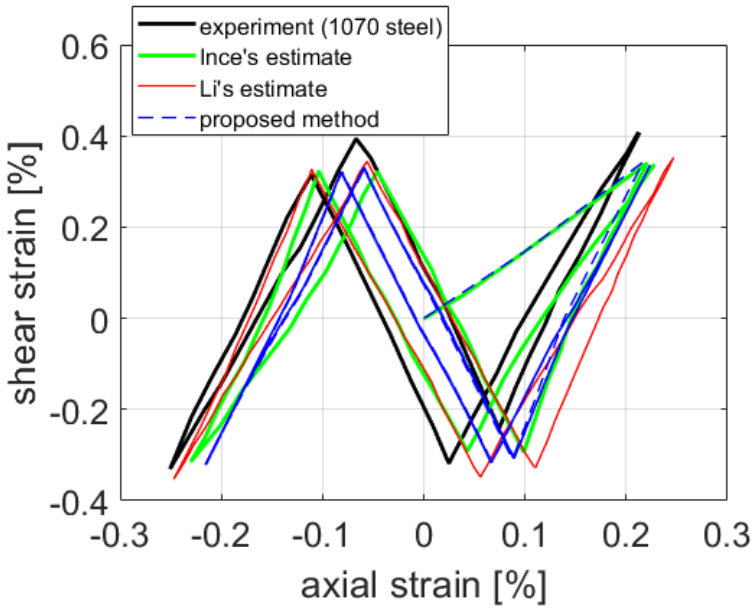

Figure B.4: Comparison of the proposed method and estimates by Li et al. [12] and Ince et al. [11] for loading path N.

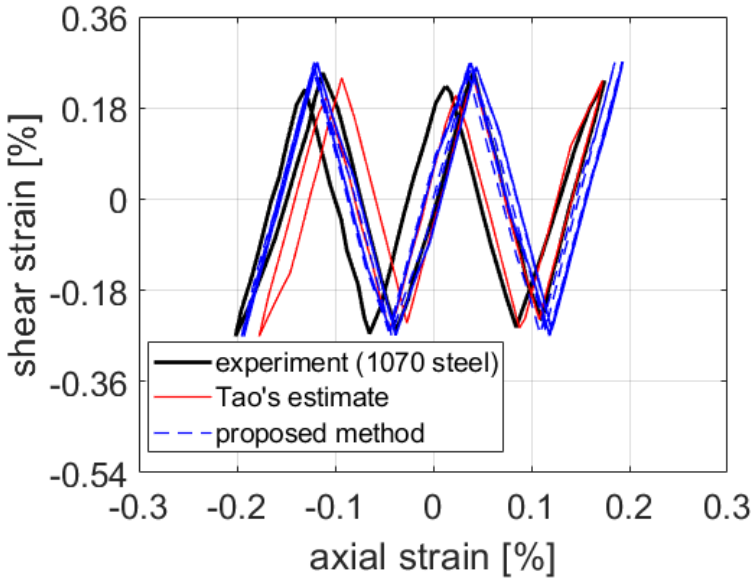

Figure B.5: Comparison of the proposed method and estimate by Tao et al. [13] for loading path NV.

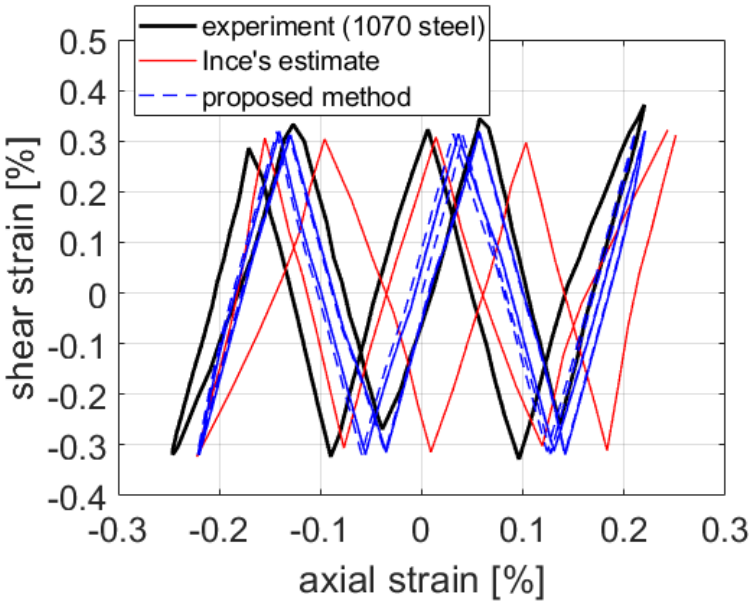

Figure B.6: Comparison of the proposed method and estimate by Ince et al. [11] for loading path NV.

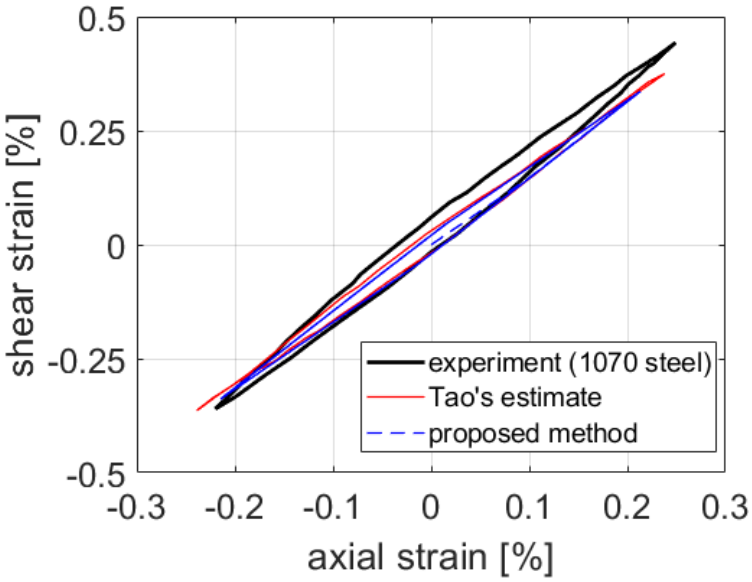

Figure B.7: Comparison of the proposed method and estimate by Tao et al. [13] for proportional loading path.

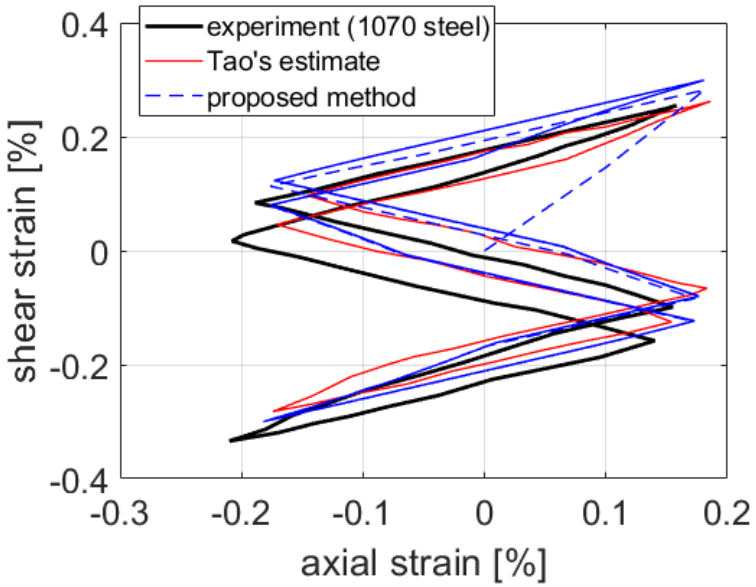

Figure B.8: Comparison of the proposed method and estimate by Tao et al. [13] for loading path S.

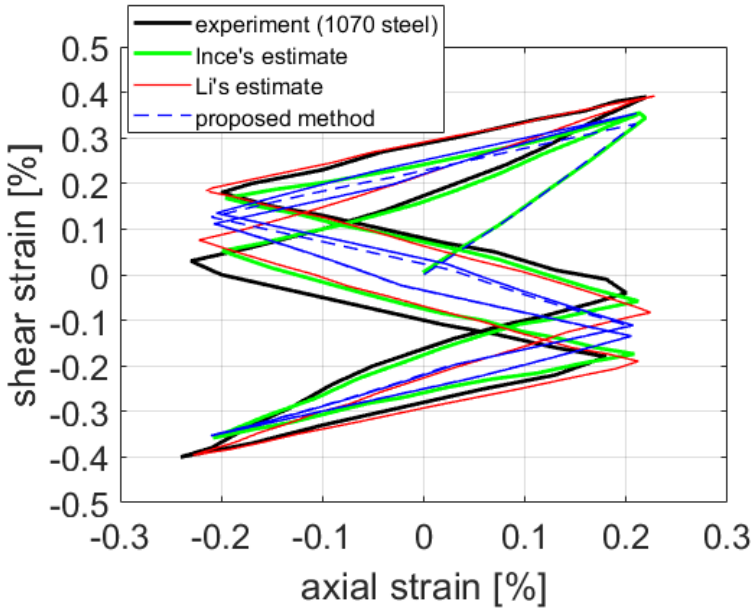

Figure B.9: Comparison of the proposed method and estimates by Li et al. [12] and Ince et al. [11] for loading path S.

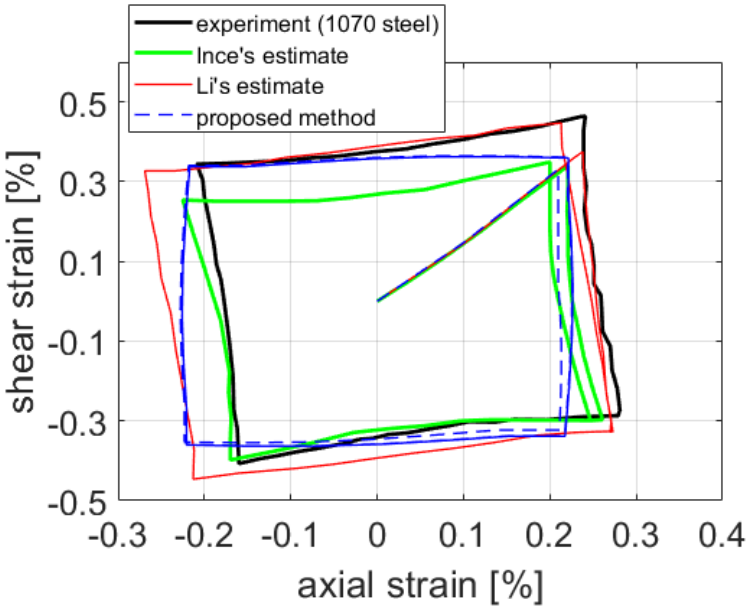

Figure B.10: Comparison of the proposed method and estimates by Li et al. [12] and Ince et al. [11] for loading path Square (clockwise).

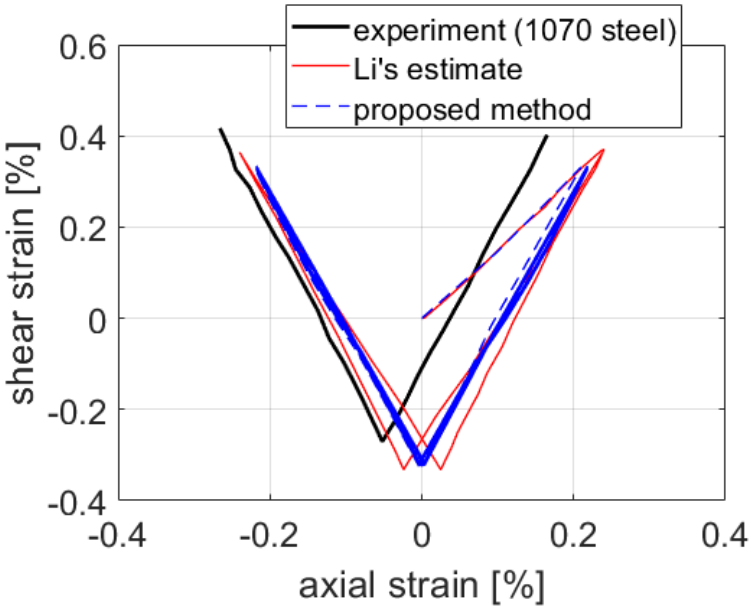

Figure B.11: Comparison of the proposed method and estimate by Li et al. [12] for loading path V.

Appendix C

MATLAB code of the proposed method

C.1 Main file

```
clear all; close all; clc;
%% %%%%%%%%%%%%%%%%%%%%%%%% GLOBAL VARIABLES
global yieldStrength
%% %%%%%%%%%%%%%%%%%%%% MATERIAL DATA
useAluminum = 1;
if useAluminum == 1
    plotExperiments = 1;
    E = 73100; ny = 0.33; G = E/2/(1+ny);
    K = 646; % MPa, Hollomon's parameters for RO curve
    nRO = 0.089;
    yieldStrength = 330;
else
    %steel 1070
    plotExperiments = 0;
    E = 210000; ny = 0.3; G = E/2/(1+ny);
    K = 1736; % MPa, Hollomon parameters for RO curve
    nRO = 0.199;
    yieldStrength = 286;
end

% ratcheting parameter; 0 ... OWI; 0.1 ... AKO; 1 ... CHAB
mu1 = 0;

%% %%%%%%%%%%%%%%%%%%%%%%%%%%%%%% DEFINE MATERIAL CURVES
[ePlRC, sRC, ePlPC, sPC] = material_curves(E, K, nRO);
[KPC, nPC] = ramberg_osgood_coefficients(ePlPC, sPC);

%% %%%%% %%%%%%%%%%%%%%%%%% PLASTICITY MODEL PARAMETERS - C and gamma
[gPC, cPC] = calc_C_gamma(ePlPC,sPC,KPC,nPC);
```

```
30 [gRC, cRC] = calc_C_gamma(ePlRC,sRC,K,  nRO);
31
32 %% %%%%%%%%%%%%%%%%%%%%% LOADING PATH
33 path_name = '7';
34 %fillet specimen                    u notched specimen
35 %'7'
36 %'circle_f7', 'circle_1p73_f8'     'circle','circle_1p73',
37 % NV_f11                           'NV','NV_1p73'
38 %proportional_f3  proportional_f4  'proportional_u11';
39 %----                              'square',
40 %----                              'uniaxial_u5'; %'uniaxial_u9';
41 %X_f5         X_1p73_f6           'X', 'X_1p73%'
42
43 define_notch_stress_inputs;
44 increase_number_of_load_cycles;
45 %% %%%%%%%%%%%%%%%%%% READ EXPERIMENTAL DATA FOR COMPARISON
46 if plotExperiments == 1
47     load(strcat(pwd,'/experiments_for_comparison/',test_spcm, ...
48                 '_notch_strains_and_info.mat'));
49 end
50 %% %%%%%%%%%%%%%%%%%% PREALOCATING VARIABLES
51 incPerPlR = 5; % increments per plastic range
52 prealocate_variables;
53
54 %% %%%%%%%%%%%%%%%%%%%%%%%% THE ESTIMATION PROCEDURE
55 ii = 1; % index of estimation step, all matrixes at 1 consist of zeros
56
57 for i = 2:1:(length(sigYyFI))
58     % i ...  index through loading steps
59     SPsStart = SPs; % deviatoric pseudo stress at the beginning of ...
           the step
60     alfaPsI = alfaPs; % I as initial
61
62     ii = ii+1;
63
64     sigPs = [0   0           0;
65              0   sigYyFI(i)  sigYzFI(i);
66              0   sigYzFI(i)  sigZzFI(i);];
67     SPs   = sigPs  - trace(sigPs)/3*eye(3);  % deviator
68
69     % find the start of the plasticization
70     tol = 1;   %[MPa], tolerance
71     beginAt = 0.01;
72     for i2=beginAt:beginAt/10:1
73         SInt = SPsStart+(SPs-SPsStart) * i2;
74         sEq = calc_equiv_stress(SInt-alfaPsI);
75         if (sEq - yieldStrength) < tol && (sEq - yieldStrength) > 0
76             elastic_part_instep = 1;   break;
77
```

```
78          elseif (sEq - yieldStrength) > 0
79              % no purely elastic loading during the step
80              elastic_part_instep = 0;   break;
81          end
82      end
83
84      % check if elastic loading/unloading has occurred
85      if i2 ≠ beginAt
86          %% PURELY ELASTIC region solution
87          dSigYPs =  (sigYyFI(i)-sigYyFI(i-1))*i2;
88          dSigZPs =  (sigZzFI(i)-sigZzFI(i-1))*i2;
89          dSigYzPs = (sigYzFI(i)-sigYzFI(i-1))*i2;
90
91          elastic_region_solution; % >> function
92
93          epsXxPl(ii) = epsXxPl(ii-1);
94          epsYyPl(ii) = epsYyPl(ii-1);
95          epsZzPl(ii) = epsZzPl(ii-1);
96          epsYzPl(ii) = epsYzPl(ii-1);
97
98      else
99          % no purely ela stic loading during the step
100         sigYPs( ii)=sigYyFI(i-1);
101         sigZPs( ii)=sigZzFI(i-1);
102         sigYzPs(ii)=sigYzFI(i-1);
103         ii= ii-1; % in order not to skip index when elastic ...
104                   % variables weren't calculated
105     end
106
107     %% plastic region solution (elastic+plastic stresses and strains)
108     if i2 < 1
109         % plasticization has occurred
110
111         % pseudo notch stresses increments till the end of current step
112         dSigYPs =  (sigYyFI(i) - sigYPs( ii))/incPerPlR;
113         dSigZPs =  (sigZzFI(i) - sigZPs( ii))/incPerPlR;
114         dSigYzPs = (sigYzFI(i) - sigYzPs(ii))/incPerPlR;
115
116         for j = 1:1:incPerPlR
117             %% cycle trough increments of plastic range
118
119             % index of increment in calculated matrixes
120             ii = ii + 1;
121
122             % pseudo stress
123             sigYPs(ii) = sigYPs(ii-1)+dSigYPs;
124             sigZPs(ii) = sigZPs(ii-1)+dSigZPs;
125             sigYzPs(ii) = sigYzPs(ii-1)+dSigYzPs;
126
```

```
127             sigPs = [0   0            0;
128                      0   sigYPs(ii)   sigYzPs(ii);
129                      0   sigYzPs(ii)  sigZPs(ii)];
130             % deviator of pseudo stress
131             SPs   = sigPs  - trace(sigPs)/3*eye(3);
132
133             [dp,theta] = calc_dp_AKO(gPC,cPC,SPs,alfa_partPs,mu1);
134
135             [alfaPs, alfa_partPs, dEpsPlPs] = ...
136                      calc_alfa_and_dEpsPl(dp,gPC,  cPC,  ...
                            alfa_partPs,SPs, theta);
137
138             dEpsPl = dEpsPlPs;
139
140             [alfa,   alfa_part, SReal]   = ...
141                      calc_alfa_and_Snp1(dp,gRC,cRC,alfa_part,  dEpsPl);
142
143             %% update pseudo material variables
144
145             %% non-deviatoric stress components
146             sigRealH = -SReal(1,1);
147             sigReal = SReal + sigRealH*eye(3);
148
149             sigY(ii) = sigReal(2,2);
150             sigZ(ii) = sigReal(3,3);
151             sigYz(ii) = sigReal(2,3);
152
153             dSigY = sigY(ii) - sigY(ii-1);
154             dSigZ = sigZ(ii) - sigZ(ii-1);
155             dSigYz = sigYz(ii) - sigYz(ii-1);
156
157             %% storing calculated strains
158             % plastic components increments
159             x(1) = dEpsPl(1,1);
160             x(2) = dEpsPl(2,2);
161             x(3) = dEpsPl(3,3);
162             x(4) = dEpsPl(2,3) ; % here, the tensorial shear strain ...
                    is calculated!!!
163
164             % elastic strain
165             dEpsXxE = 1/E * (-ny) * (dSigY + dSigZ);
166             dEpsYyE = 1/E * (dSigY + (-ny) * dSigZ);
167             dEpsZzE = 1/E * (dSigZ + (-ny) * dSigY);
168
169             dGammaYzE = 1/G* dSigYz;
170             dEpsYzE = dGammaYzE/ 2;
171
172             epsXxE(ii) = epsXxE(ii-1) + dEpsXxE;
173             epsYyE(ii) = epsYyE(ii-1) + dEpsYyE;
```

```
174             epsZzE(ii) = epsZzE(ii-1) + dEpsZzE;
175             epsYzE(ii) = epsYzE(ii-1) + dEpsYzE;
176
177             % plastic strain
178             epsXxPl(ii) = epsXxPl(ii-1) + x(1);
179             epsYyPl(ii) = epsYyPl(ii-1) + x(2);
180             epsZzPl(ii) = epsZzPl(ii-1) + x(3);
181             epsYzPl(ii) = epsYzPl(ii-1) + x(4);
182
183             % total strain (elastic total + plastic total)
184             epsXx(ii) = epsXxE(ii) + epsXxPl(ii);
185             epsYy(ii) = epsYyE(ii) + epsYyPl(ii);
186             epsZz(ii) = epsZzE(ii) + epsZzPl(ii);
187             epsYz(ii) = epsYzE(ii) + epsYzPl(ii);
188         end %j = 1:1:(incPerPlR)
189     end
190 end
191
192 graphs; % function for plotting results
193 calc_rel_error;
```

C.2 Functions

C.2.1 calc_alfa_and_dEpsPl

```
1  function [alfa, alfa_part, dEpsPl] = ...
2        calc_alfa_and_dEpsPl(dp,gamma,cMatrix,alfa_part,S,theta)
3
4      global yieldStrength
5      m2 = size(gamma,1); % number of backstress parts
6      aMatrix = zeros(3,3);
7      alfa = zeros(3,3);
8
9      aNum = 0;
10     for i = 1:m2
11         aMatrix =aMatrix + theta(i)*alfa_part(:,:,i);
12         aNum = aNum + cMatrix(i)*theta(i);
13     end
14
15     % calculate plastic strain tensor
16      SminusA = yieldStrength/(yieldStrength+aNum*dp)*(S-aMatrix);
17      dEpsPl = 3/2*dp*SminusA/yieldStrength;
18
19     % calculate backstress parts (for the next iteration)
20     for i = 1:m2
```

```
21          alfa_part(:,:,i) = ...
                (alfa_part(:,:,i)+2/3*cMatrix(i)*dEpsPl)*theta(i);
22          alfa = alfa + alfa_part(:,:,i);
23      end
24
25
26  end
```

C.2.2 calc_alfa_and_Snp1

```
1   function [alfa, alfa_part, Snp1] = ...
2         calc_alfa_and_Snp1(dp,gamma,cMatrix,alfa_part,dEpsPl)
3       global yieldStrength
4
5       m2 = size(gamma,1); % number of backstress parts
6       alfa = zeros(3,3);
7       % calculate backstress parts
8       for i = 1:m2
9           alfa_part(:,:,i) = ...
                (alfa_part(:,:,i)+2/3*cMatrix(i)*dEpsPl)/(1+gamma(i)*dp);
10          alfa = alfa + alfa_part(:,:,i);
11
12      end
13
14      % calculate stress
15      Snp1 = dEpsPl*yieldStrength*2/3/dp + alfa;
16
17
18  end
```

C.2.3 calc_alfa_and_Snp1

```
1   function [alfa, alfa_part, Snp1] = ...
2         calc_alfa_and_Snp1(dp,gamma,cMatrix,alfa_part,dEpsPl)
3       global yieldStrength
4
5       m2 = size(gamma,1); % number of backstress parts
6       alfa = zeros(3,3);
7       % calculate backstress parts
8       for i = 1:m2
9           alfa_part(:,:,i) = ...
                (alfa_part(:,:,i)+2/3*cMatrix(i)*dEpsPl)/(1+gamma(i)*dp);
10          alfa = alfa + alfa_part(:,:,i);
```

```
11
12      end
13
14      % calculate stress
15      Snp1 = dEpsPl*yieldStrength*2/3/dp + alfa;
16
17
18  end
```

C.2.4 calc_C_gamma

```
1   function [gamma, cMatrix] = calc_C_gamma(epsPl,stress,K,n)
2       global yieldStrength
3       slope = zeros(size(epsPl,1),1);
4       gamma = zeros(size(epsPl,1)-1,1);
5       cMatrix = zeros(size(epsPl,1)-1,1);
6       epsPlAtYS = (yieldStrength/K)^(1/n);
7       nn = size(epsPl,1);
8       for i=1:nn
9           if i == 1
10              slope(1) = (stress(1)-yieldStrength)/(epsPl(i)-epsPlAtYS);
11          else
12              slope(i) = (stress(i)-stress(i-1))/(epsPl(i)-epsPl(i-1));
13          end
14      end
15      slope(nn+1) = 0;
16      for i=1:nn
17          gamma(i) = 1/epsPl(i);
18          cMatrix(i) = slope(i) - slope(i+1);
19      end
20  end
```

C.2.5 calc_dp_AKO

```
1       function [dp,theta] = calc_dp_AKO(gamma,cMatrix,S,alfa_part,mu1)
2       global yieldStrength
3       n = size(gamma,1); % vectors prealocation
4       theta = ones(1,n);
5
6       %% model parameters
7
8       dpkm1 = 0; % variables to check convergence
9       dpkm2 = 0;
```

```
10
11      for k =1:100
12          aMatrix = zeros(3,3); % a supportive variable for the ...
               calculation
13          aNum = 0;
14          for i2 = 1:n
15               aMatrix = aMatrix + theta(i2)*alfa_part(:,:,i2);
16               aNum = aNum + cMatrix(i2)*theta(i2);
17          end
18          aNum2 = calc_equiv_stress(S-aMatrix);
19
20          dp = (aNum2 - yieldStrength)/aNum; % dp from the first iteration
21
22          % The Aitken's Δ^2 process to shorten the convergence -----
23          if mod(k,3) == 0
24              con = dp-(dp-dpkm1)^2/(dp-2*dpkm1+dpkm2);
25              if con > 0
26                 dp = con;
27              end
28          end % ------------------------------------------------------------
29
30          SminusA = yieldStrength/(yieldStrength+aNum*dp)*(S-aMatrix);
31          dEpsPl = 3/2*dp*SminusA/yieldStrength;
32
33          if abs(1-dpkm1/dp) < 10^(-4)
34              break; % solution found
35          end
36
37          for i2 = 1:n
38                aMatrix = zeros(3,3);
39                alnp1_st(:,:,i2) = ...
                     alfa_part(:,:,i2)+2/3*cMatrix(i2)*dEpsPl;
40                alnp1_dash(i2) = calc_equiv_stress(alnp1_st(:,:,i2));
41
42                mu(i2) = mu1;
43
44                c(i2) = 1/(1+mu(i2)*gamma(i2)*dp);
45
46                alnp1_hash(:,:,i2) = c(i2)*(alnp1_st(:,:,i2));
47
48                fnp1_hash = ...
                     calc_equiv_stress(alnp1_hash(:,:,i2))^2-(cMatrix(i2)/gamma(i2))^2;
49                theta(i2)=c(i2)+heaviside(fnp1_hash)*...
50                          (cMatrix(i2)/gamma(i2)/alnp1_dash(i2)-c(i2));
51
52          end
53
54          dpkm2 = dpkm1;
55          dpkm1 = dp;
```

```
56
57          if k == 200
58               error('Error: number of iterations has exceeded the ...
                     allowed value');
59               k
60          end
61      end
62  end
```

C.2.6 calc_equiv_stress

```
1  function equivalent_stress = calc_equiv_stress(A)
2      aMatrix = A.*A;
3      equivalent_stress = sqrt(3/2* sum(aMatrix(:)) );
4  end
```

C.2.7 material_curves

```
1  function [ePlRC, sRC, ePlPC, sPC] = material_curves(E, K, nRO)
2      % RC ... real curve (cyclic stress strain curve); Pl ... plastic
3      % PC ... pseudo curve;  e ... epsilon, s ... sigma
4      %% REAL CURVE
5      % 4 intervals for gamma and C and 1 corresponding to the yield
6      % strength  will be added later -> 5 invtervals == 5 backstress ...
           parts
7      ePlRC = [0.002 0.004 0.006 0.008 0.01]';
8      n = size(ePlRC,1); %number of discrete points on the curve
9      for i=1:n
10        sRC(i,1) = K*ePlRC(i)^nRO;
11     end
12
13     %% PSEUDO CURVE
14     ePlPC  = ePlRC;
15     for i=1:n
16       %sig_e   =        sig   *      eps_tot        *E
17       sPC(i,1) = sqrt( sRC(i)* (ePlRC(i)+sRC(i)/E) *E );
18     end
19 end
```

C.2.8 ramberg_osgood_coefficients

```
function [K, n] = ramberg_osgood_coefficients(eps, sig)
    f = fit(eps,sig,'power1');
    regCs = coeffvalues(f);
    K = regCs(1); %RO with Hollomon parameters: eps = sig/E + ...
        (sig/K)^(1/n)
    n = regCs(2);
end
```

C.3 Scripts

C.3.1 calc_rel_error

```
if useAluminum == 1
    e_exp_range = max(eps1Median_1)-min(eps1Median_1);
    g_exp_range = max(eps12Median_1)-min(eps12Median_1);

    conv = 1; % conversion
    const2 = 1;
else
    e_exp_range = max(e_exp)-min(e_exp);
    e_other_est_range = max(e_est)-min(e_est);
    e_rel_err_other = (e_other_est_range - e_exp_range)/e_exp_range ...
        * 100;

    g_exp_range = max(g_exp)-min(g_exp);
    g_other_est_range = max(g_est)-min(g_est);
    g_rel_err_other = (g_other_est_range - g_exp_range)/g_exp_range ...
        * 100;
    conv = 100;
    const2 = const;
end

e_pm_est_range = max(epsZz)-min(epsZz);
e_rel_err_pm = (e_pm_est_range*conv - e_exp_range)/e_exp_range * 100;
% pm ... proposed method

g_pm_est_range = const2*(max(epsYz)-min(epsYz));
g_rel_err_pm = (g_pm_est_range*conv - g_exp_range)/g_exp_range * 100;

fprintf('mu = %.2f\n', mu1);
if useAluminum≠1
    fprintf('RE axial other method: %.1f\n', e_rel_err_other);
end
fprintf('RE axial proposed method: %.1f\n', e_rel_err_pm);
```

```
if useAluminum≠1
    fprintf('RE shear other method: %.1f\n', g_rel_err_other);
end
fprintf('RE shear proposed method: %.1f\n', g_rel_err_pm);
fprintf(['cycles: ' int2str(num_cycles) '\n']);
```

C.3.2 define_notch_stress_inputs

```
if strcmp(path_name,'Ince_ksi')
    test_spcm = 'Ince_spc';
    num_cycles_text = '-';
    sigZzFI = 420 *[0   1   0   -1  0   1   0   -1  0   1   0   -1  ...
        0   1   0   -1  0   1   0   -1  0];
    sigYzFI = 222 *[0   0.2 0.4 0.6 0.8 1   0.8 0.6 0.4 0.2 0   ...
        -0.2    -0.4    -0.6    -0.8    -1  -0.8    -0.6    -0.4    ...
        -0.2    0];
    sigYyFI = 89  *[0   1   0   -1  0   1   0   -1  0   1   0   -1  ...
        0   1   0   -1  0   1   0   -1  0];

elseif strcmp(path_name,'Ince_N')
    test_spcm = 'Ince_spc';
    num_cycles_text = '-';
    sigZzFI = 420 *[0   1   0.333333333 -0.333333333    -1  ...
        -0.333333333    0.333333333 1];
    sigYzFI = 222 *[0   1   -1  1   -1  1   -1  1];
    sigYyFI = 89  *[0   1   0.333333333 -0.333333333    -1  ...
        -0.333333333    0.333333333 1];

elseif strcmp(path_name,'Ince_NV')
    test_spcm = 'Ince_spc';
    num_cycles_text = '-';
    sigZzFI = 420*[0    0.2 0.4  0.6    0.8 1   0.8 0.6 0.4 0.2 0   ...
        -0.2    -0.4    -0.6    -0.8    -1  -0.8    -0.6    -0.4    ...
        -0.2    0];
    sigYzFI = 222*[0    1   0   -1  0   1   0   -1  0   1   0   -1  ...
        0   1   0   -1  0   1   0   -1  0];
    sigYyFI =  89*[0    0.2 0.4  0.6    0.8 1   0.8 0.6 0.4 0.2 0   ...
        -0.2    -0.4    -0.6    -0.8    -1  -0.8    -0.6    -0.4    ...
        -0.2    0];

elseif strcmp(path_name,'Ince_S')
    test_spcm = 'Ince_spc';
    num_cycles_text = '-';
    sigZzFI = 420 *[0   1   -1  1   -1  1   -1  1];
    sigYzFI = 222 *[0   1   0.333333333 -0.333333333    -1  ...
        -0.333333333    0.333333333 1];
```

```
27      sigYyFI = 89  *[0   1   -1  1   -1  1   -1  1];
28
29  elseif strcmp(path_name,'Ince_square')
30      test_spcm = 'Ince_spc';
31      num_cycles_text = '-';
32      sigZzFI = 420 * [0  1  -1   -1   1];
33      sigYzFI = 222 * [0  1   1   -1  -1];
34      sigYyFI = 89  * [0  1  -1   -1   1];
35
36  elseif strcmp(path_name,'Ince_square_clock')
37      test_spcm = 'Ince_spc';
38      num_cycles_text = '-';
39      sigZzFI = 420 *[0 1  1 -1 -1];
40      sigYzFI = 222 *[0 1 -1 -1  1];
41      sigYyFI = 89  *[0 1  1 -1 -1];
42
43      %% LI ZHANG ...
           %%%%%%%%%%%%%%%%%%%%%%%%%%%%%%%%%%%%%%%%%%%%%%%%%%%%%%%%%%%%%%%%%%%%%%%
44  elseif strcmp(path_name,'Li_1070_C')
45      % counter-clockwise
46      test_spcm = '-';
47      num_cycles_text = '-';
48      sigZzFI = 420*[0 1 -1  1 -1 1];
49      sigYzFI = 222*[0 1  0 -1  0 1];
50      sigYyFI =  89*[0 1 -1  1 -1 1];
51
52  elseif strcmp(path_name,'Li_1070_N')
53      test_spcm = 'Li_spc';
54      num_cycles_text = '-';
55      sigZzFI = 420 *[0   1   0.333333333 -0.333333333    -1  ...
           -0.333333333    0.333333333 1];
56      sigYzFI = 222 *[0   1   -1  1   -1  1   -1  1];
57      sigYyFI = 89  *[0   1   0.333333333 -0.333333333    -1  ...
           -0.333333333    0.333333333 1];
58
59  elseif strcmp(path_name,'Li_1070_S')
60      test_spcm = 'Li_spc';
61      num_cycles_text = '-';
62      sigZzFI = 420 *[0   1   -1  1   -1  1   -1  1];
63      sigYzFI = 222 *[0   1   0.333333333 -0.333333333    -1  ...
           -0.333333333    0.333333333 1];
64      sigYyFI = 89  *[0   1   -1  1   -1  1   -1  1];
65
66  elseif strcmp(path_name,'Li_1070_square')
67      test_spcm = 'Li_spc';
68      num_cycles_text = '-';
69      sigZzFI = 420 * [0  1  -1   -1   1];
70      sigYzFI = 222 * [0  1   1   -1  -1];
71      sigYyFI = 89  * [0  1  -1   -1   1];
```

```
72
73 elseif strcmp(path_name,'Li_1070_square_clock')
74     test_spcm = 'Li_spc';
75     num_cycles_text = '-';
76     sigZzFI = 420 *[0 1  1 -1 -1];
77     sigYzFI = 222 *[0 1 -1 -1  1];
78     sigYyFI = 89  *[0 1  1 -1 -1];
79
80 elseif strcmp(path_name,'Li_1070_V')
81     % counter-clockwise
82     test_spcm = '-';
83     num_cycles_text = '-';
84     sigZzFI = 420*[0 1  0 -1  0 1];
85     sigYzFI = 222*[0 1 -1  1 -1 1];
86     sigYyFI =  89*[0 1  0 -1  0 1];
87
88     %% TAO - STEEL ...
          %%%%%%%%%%%%%%%%%%%%%%%%%%%%%%%%%%%%%%%%%%%%%%%%%%%%%%%%%%%%%%%%%%%%%%%
89 elseif strcmp(path_name,'Tao_1070_ksi')
90     test_spcm = '-';
91     num_cycles_text = '-';
92     sigZzFI = 366 *[0   1   0   -1  0   1   0   -1  0   1   0   -1  ...
          0   1   0   -1  0   1   0   -1  0];
93     sigYzFI = 193 *[0   0.2 0.4 0.6 0.8 1   0.8 0.6 0.4 0.2 0   ...
          -0.2    -0.4    -0.6    -0.8    -1  -0.8    -0.6    -0.4    ...
          -0.2    0];
94     sigYyFI = 77  *[0   1   0   -1  0   1   0   -1  0   1   0   -1  ...
          0   1   0   -1  0   1   0   -1  0];
95
96 elseif strcmp(path_name,'Tao_1070_N')
97     test_spcm = '-';
98     num_cycles_text = '-';
99     sigZzFI = 366 *[0   1   0.333333333 -0.333333333    -1  ...
          -0.333333333    0.333333333 1];
100    sigYzFI = 193 *[0   1   -1  1   -1  1   -1  1];
101    sigYyFI = 77  *[0   1   0.333333333 -0.333333333    -1  ...
          -0.333333333    0.333333333 1];
102
103 elseif strcmp(path_name,'Tao_1070_NV')
104    % Path NV;
105    test_spcm = '-';
106    num_cycles_text = '-';
107    sigZzFI = 366*[0    0.2 0.4  0.6    0.8 1   0.8 0.6 0.4 0.2 0   ...
          -0.2    -0.4    -0.6    -0.8    -1  -0.8    -0.6    -0.4    ...
          -0.2    0];
108    sigYzFI = 193*[0    1   0   -1  0   1   0   -1  0   1   0   -1  ...
          0   1   0   -1  0   1   0   -1  0];
109    sigYyFI =  77*[0    0.2 0.4  0.6    0.8 1   0.8 0.6 0.4 0.2 0   ...
          -0.2    -0.4    -0.6    -0.8    -1  -0.8    -0.6    -0.4    ...
```

```
        -0.2    0];

elseif strcmp(path_name,'Tao_1070_proportional')
    test_spcm = '-';
    num_cycles_text = '-';
    sigZzFI = 420  * [0   1  -1   1];   % axial direction
    sigYzFI = 222  * [0   1  -1   1];
    sigYyFI =  89  * [0   1  -1   1];  % tangential direction

elseif strcmp(path_name,'Tao_1070_S')
    test_spcm = '-';
    num_cycles_text = '-';
    sigZzFI = 366 *[0   1   -1  1   -1  1   -1  1];
    sigYzFI = 193 *[0   1   0.333333333 -0.333333333    -1  ...
        -0.333333333    0.333333333 1];
    sigYyFI = 77  *[0   1   -1  1   -1  1   -1  1];

elseif strcmp(path_name,'Tao_1070_square')
    % counter-clockwise
    test_spcm = '1070_steel';
    num_cycles_text = 'Tao';
    sigZzFI = 420 * [0  1  -1   -1   1];
    sigYzFI = 222 * [0  1   1   -1  -1];
    sigYyFI = 89  * [0  1  -1   -1   1];

%% ALUMINUM  -  FILLET NOTCH ...
    %%%%%%%%%%%%%%%%%%%%%%%%%%%%%%%%%%%%%%%%%%%%%%%%%%
elseif strcmp(path_name,'7')
    % Path "7";   F = 66kN, M = 329.133 kNmm, D 26mm
    test_spcm = 'f9';
    num_cycles_text = '1st 100 cycles';
    sigYyFI =  82 * [0   1  -1   1];  % tangential direction
    sigZzFI = 375 * [0   1  -1   1]; % axial direction,
    sigYzFI = 270 * [0  -1  -1  -1]; % FI as for incrementation

elseif strcmp(path_name,'circle_f7')
    % Path Circle;   F = 66kN, M = 329.133 kNmm, D 26mm
    test_spcm = 'f7';
    num_cycles_text = '1st 100 cycles';
    sigZzFI =   375 * [0    1    0.95    0.81    0.59    0.31    ...
        0.00    -0.31   -0.59   -0.81   -0.95   -1.00   -0.95   ...
        -0.81   -0.59   -0.31   0.00    0.31    0.59    0.81    ...
        0.95    1.00];
    sigYyFI =    82 * [0    1    0.95    0.81    0.59    0.31    ...
        0.00    -0.31   -0.59   -0.81   -0.95   -1.00   -0.95   ...
        -0.81   -0.59   -0.31   0.00    0.31    0.59    0.81    ...
        0.95    1.00];
    sigYzFI = (-270) * [0   0   -0.31   -0.59   -0.81   -0.95   ...
        -1.00   -0.95   -0.81   -0.59   -0.31   0.00    0.31    ...
```

```
          0.59    0.81    0.95    1.00    0.95    0.81    0.59    ...
          0.31    0.00];
149
150 elseif strcmp(path_name,'circle_1p73_f8')
151     % F = 101kN, M = 290 kNmm, D 26mm
152     test_spcm = 'f8';
153     num_cycles_text = '1st 100 cycles';
154     sigZzFI =  572 * [0 1   0.95    0.81    0.59    0.31    0.00    ...
            -0.31 -0.59 -0.81   -0.95 ...
155          -1.00   -0.95   -0.81   -0.59   -0.31   0.00    0.31    ...
                0.59    0.81    0.95    1.00];
156     sigYyFI =  125 * [0 1   0.95    0.81    0.59    0.31    0.00    ...
            -0.31 -0.59 -0.81   -0.95 ...
157          -1.00   -0.95   -0.81   -0.59   -0.31   0.00    0.31    ...
                0.59    0.81    0.95    1.00];
158     sigYzFI = (238)* [0 0   -0.31   -0.59   -0.81   -0.95   -1.00   ...
            -0.95   -0.81   -0.59 ...
159          -0.31   0.00    0.31    0.59    0.81    0.95    1.00    ...
                0.95    0.81    0.59    0.31    0.00];
160
161 elseif strcmp(path_name,'NV_f11')
162     % Path NV;  F = 66kN, M = 329.133 kNmm, D 26mm
163     test_spcm = 'f11';
164     num_cycles_text = '1st 50 cycles';
165     sigZzFI =   375 * [0.00 0.31    0.59    0.81    0.95    1.00    ...
            0.95    0.81    0.59 ...
166          0.31    0.00    -0.31   -0.59   -0.81   -0.95   -1.00   ...
                -0.95   -0.81   -0.59   -0.31   0.00];
167     sigYyFI =    82 * [0.00 0.31    0.59    0.81    0.95    1.00    ...
            0.95    0.81    0.59 ...
168          0.31    0.00    -0.31   -0.59   -0.81   -0.95   -1.00   ...
                -0.95   -0.81   -0.59   -0.31   0.00];
169     sigYzFI = (-270)*[0 1   0   -1  0   1   0   -1  0   1   0   -1  ...
            0   1   0   -1  0   1   0   -1  0];
170
171 elseif strcmp(path_name,'proportional_f3')
172     % F = 66kN, M = 329.133 kNmm, D 26mm
173     test_spcm = 'f3';
174     num_cycles_text = '1st 99 cycles';
175     %based on Kt
176     sigYyFI =  82  * [0   1  -1   1];  % tangential direction
177     sigZzFI = 375  * [0   1  -1   1];   % axial direction
178     sigYzFI = 270  * [0  -1   1  -1];
179
180 elseif strcmp(path_name,'proportional_f4')
181     test_spcm = 'f4';
182     num_cycles_text = '1st 100 cycles';
183     %based on Kt
184     sigYyFI = 125  * [0   1  -1   1];  % tangential direction
```

```
185     sigZzFI = 572  * [0   1  -1   1];   % axial direction
186     sigYzFI = 238  * [0  -1   1  -1];
187
188 elseif strcmp(path_name,'X_f5')
189     % F = 66kN, M = 329.133 kNmm, D 26mm
190     test_spcm = 'f5';
191     num_cycles_text = '1st 100 cycles';
192     sigYyFI =  82* [0   1   0   1   0   -1  0   -1  0];
193     sigZzFI = 375* [0   1   0   1   0   -1  0   -1  0];
194     sigYzFI = 270* [0  -1   0   1   0    1  0   -1  0];
195
196 elseif strcmp(path_name,'X_1p73_f6')
197     % F = 101kN, M = 290 kNmm, D 26mm
198     test_spcm = 'f6';
199     num_cycles_text = '1st 100 cycles';
200     sigYyFI = 125*  [0  1   0   1   0   -1  0   -1  0];
201     sigZzFI = 572*  [0  1   0   1   0   -1  0   -1  0];
202     sigYzFI = 238*  [0 -1   0   1   0    1  0   -1  0];
203
204 %% ALUMINUM  -  U NOTCH ...
    %%%%%%%%%%%%%%%%%%%%%%%%%%%%%%%%%%%%%%%%%%%%%%%%%%%%
205 elseif strcmp(path_name,'circle')
206     % Path Circle;  F = 66kN, M = 329.133 kNmm, D 26mm
207     test_spcm = 'u73';
208     num_cycles_text = '1st 100 cycles';
209     sigZzFI =   427 * [0    1   0.95    0.81    0.59    0.31    ...
            0.00    -0.31   -0.59   -0.81   -0.95   -1.00   -0.95   ...
            -0.81   -0.59   -0.31   0.00    0.31    0.59    0.81    ...
            0.95    1.00];
210     sigYyFI =   113 * [0    1   0.95    0.81    0.59    0.31    ...
            0.00    -0.31   -0.59   -0.81   -0.95   -1.00   -0.95   ...
            -0.81   -0.59   -0.31   0.00    0.31    0.59    0.81    ...
            0.95    1.00];
211     sigYzFI = (-291)* [0    0   -0.31   -0.59   -0.81   -0.95   ...
            -1.00   -0.95   -0.81   -0.59   -0.31   0.00    0.31    ...
            0.59    0.81    0.95    1.00    0.95    0.81    0.59    ...
            0.31    0.00];
212
213 elseif strcmp(path_name,'circle_1p73')
214     % F = 101kN, M = 290 kNmm, D 26mm
215     test_spcm = 'u7';
216     num_cycles_text = '1st 100 cycles';
217
218     sigZzFI =  652 * [0 1   0.95    0.81    0.59    0.31    0.00    ...
            -0.31 -0.59 -0.81   -0.95 ...
219          -1.00   -0.95   -0.81   -0.59   -0.31   0.00    0.31    ...
                0.59    0.81    0.95    1.00];
220     sigYyFI =  173 * [0 1   0.95    0.81    0.59    0.31    0.00    ...
            -0.31 -0.59 -0.81   -0.95 ...
```

```
221          -1.00   -0.95   -0.81   -0.59   -0.31   0.00    0.31    ...
                 0.59    0.81    0.95    1.00];
222      sigYzFI = (-257)* [0    0   -0.31   -0.59   -0.81   -0.95   ...
            -1.00   -0.95   -0.81   -0.59 ...
223          -0.31   0.00    0.31    0.59    0.81    0.95    1.00    ...
                 0.95    0.81    0.59    0.31    0.00];
224
225  elseif strcmp(path_name,'NV')
226      % Path NV;  F = 66kN, M = 329.133 kNmm, D 26mm
227      test_spcm = 'u4';
228      num_cycles_text = '1st 50 cycles';
229      sigZzFI =   427 * [0.00 0.31    0.59    0.81    0.95    1.00    ...
             0.95    0.81    0.59 ...
230          0.31    0.00    -0.31   -0.59   -0.81   -0.95   -1.00   ...
                 -0.95   -0.81   -0.59   -0.31   0.00];
231       sigYyFI =   113 * [0.00    0.31    0.59    0.81    0.95    ...
             1.00    0.95    0.81    0.59 ...
232          0.31    0.00    -0.31   -0.59   -0.81   -0.95   -1.00   ...
                 -0.95   -0.81   -0.59   -0.31   0.00];
233      sigYzFI = (-291)*[0 1   0   -1  0   1   0   -1  0   1   0   -1  ...
             0   1   0   -1  0   1   0   -1  0];
234
235  elseif strcmp(path_name,'NV_1p73')
236      % Path NV;  F = 101kN, M = 290 kNmm, D 26mm
237      test_spcm = 'u8';
238      num_cycles_text = '1st 42 cycles'; %it broke at 94
239      sigZzFI =   652 * [0.00 0.31    0.59    0.81    0.95    1.00    ...
             0.95    0.81    0.59 ...
240          0.31    0.00    -0.31   -0.59   -0.81   -0.95   -1.00   ...
                 -0.95   -0.81   -0.59   -0.31   0.00];
241      sigYyFI =   173 * [0.00 0.31    0.59    0.81    0.95    1.00    ...
             0.95    0.81    0.59 ...
242          0.31    0.00    -0.31   -0.59   -0.81   -0.95   -1.00   ...
                 -0.95   -0.81   -0.59   -0.31   0.00];
243      sigYzFI = (-257)*[0 1   0   -1  0   1   0   -1  0   1   0   -1  ...
             0   1   0   -1  0   1   0   -1  0];
244
245  elseif strcmp(path_name,'proportional_u11')
246      % F = 66kN, M = 329.133 kNmm, D 26mm
247      test_spcm = 'u11';
248      num_cycles_text = '1st 100 cycles';
249      sigYyFI = 113   * [0   1  -1   1];  % tangential direction
250      sigZzFI = 427   * [0   1  -1   1];   % axial direction
251      sigYzFI = 291   * [0  -1   1  -1];
252
253  elseif strcmp(path_name,'square')
254      % Path Square,  F = 66kN, M = 329.133 kNmm, D 26mm
255      test_spcm = 'u3';
256      num_cycles_text = '1st 100 cycles';
```

```
257     sigYyFI = 113* [0   1   1   1   0   -1  -1  -1  0  1];
258     sigZzFI = 427* [0   1   1   1   0   -1  -1  -1  0  1];
259     sigYzFI = 291* [0  -1   0   1   1    1   0  -1 -1 -1];
260
261 elseif strcmp(path_name,'uniaxial_u5')
262     % F = 86.25 kN, M = 0 kNmm, D 26mm
263     test_spcm = 'u5';
264     num_cycles_text = '1st 100 cycles';
265     sigYyFI = 148   * [0   1  -1   1];
266     sigZzFI = 560   * [0   1  -1   1];   % axial direction,
267     sigYzFI = 0     * [0  -1   1  -1];
268
269 elseif strcmp(path_name,'uniaxial_u9')
270     % F = 100.472 kN, M = 0 kNmm, D 26mm
271     test_spcm = 'u9';
272     num_cycles_text = '1st 100 cycles';
273     sigYyFI = 173   * [0   1  -1   1];
274     sigZzFI = 652   * [0   1  -1   1];   % axial direction,
275     sigYzFI = 0     * [0  -1   1  -1];
276
277 elseif strcmp(path_name,'X')
278     % F = 66kN, M = 329.133 kNmm, D 26mm
279     test_spcm = 'u2';
280     num_cycles_text = '1st 100 cycles';
281     sigYyFI = 113* [0   1   0   1   0   -1  0   -1  0];
282     sigZzFI = 427* [0   1   0   1   0   -1  0   -1  0];
283     sigYzFI = 291* [0  -1   0   1   0    1  0   -1  0];
284
285 elseif strcmp(path_name,'X_1p73')
286     % F = 101kN, M = 290 kNmm, D 26mm
287     test_spcm = 'u6';
288     num_cycles_text = '1st 100 cycles';
289     sigYyFI = 173*  [0  1   0   1   0   -1  0   -1  0];
290     sigZzFI = 652*  [0  1   0   1   0   -1  0   -1  0];
291     sigYzFI = 257*  [0 -1   0   1   0    1  0   -1  0];
292
293 end
```

C.3.3 elastic_region_solution

```
1 sigYPs(ii)  = sigYPs(ii-1)   + dSigYPs;
2 sigZPs(ii)  = sigZPs(ii-1)   + dSigZPs;
3 sigYzPs(ii) = sigYzPs(ii-1)  + dSigYzPs;
4 sigY(ii)    = sigY(ii-1)   + dSigYPs; % in elastic regime increments ...
      of real and pseudo stresses are equal
5 sigZ(ii)    = sigZ(ii-1)   + dSigZPs;
```

```
sigYz(ii)    = sigYz(ii-1)  + dSigYzPs;
sigReal = [0   0         0;
           0   sigY(ii)  sigYz(ii);
           0   sigYz(ii) sigZ(ii)];
SReal = sigReal - trace(sigReal)/3*eye(3);
dEpsXxE = 1/E * (-ny) * (dSigYPs + dSigZPs);
dEpsYyE = 1/E * (dSigYPs + (-ny) * dSigZPs);
dEpsZzE = 1/E * (dSigZPs + (-ny) * dSigYPs);
dGammaYzE = 1/G *  dSigYzPs;
dEpsYzE = dGammaYzE/ 2;
epsXxE(ii) = epsXxE(ii-1) + dEpsXxE;
epsYyE(ii) = epsYyE(ii-1) + dEpsYyE;
epsZzE(ii) = epsZzE(ii-1) + dEpsZzE;
epsYzE(ii) = epsYzE(ii-1) + dEpsYzE;
epsXx(ii) = epsXx(ii-1) + dEpsXxE;
epsYy(ii) = epsYy(ii-1) + dEpsYyE;
epsZz(ii) = epsZz(ii-1) + dEpsZzE;
epsYz(ii) = epsYz(ii-1) + dEpsYzE;
```

C.3.4 graphs

```
%% axial and shear strain graph
figure;
if plotExperiments == 1
    p1 = plot(eps1Median_1(1:end)*100,eps12Median_1(1:end)*100,'-',...
                    'color',[.929 .6940 .125],'LineWidth',1); hold on;
    p1.Color(4) = 0.5;
end

%% LOAD INCE'S DATA
if strcmp(path_name,'Ince_ksi')
    load(strcat(pwd,'/data_for_comparison/','Ince_1070_ksi.mat'));
elseif strcmp(path_name,'Ince_N')
    load(strcat(pwd,'/data_for_comparison/','Ince_1070_N.mat'));
elseif strcmp(path_name,'Ince_NV')
    load(strcat(pwd,'/data_for_comparison/','Ince_1070_NV.mat'));
elseif strcmp(path_name,'Ince_S')
    load(strcat(pwd,'/data_for_comparison/','Ince_1070_S.mat'));
elseif strcmp(path_name,'Ince_square')
    load(strcat(pwd,'/data_for_comparison/','Ince_1070_square.mat'));
elseif strcmp(path_name,'Ince_square_clock')
    load(strcat(pwd,'/data_for_comparison/Ince_1070_square_clock.mat'));
%% LOAD LI'S DATA
elseif strcmp(path_name, 'Li_1070_C')
    load(strcat(pwd,'/data_for_comparison/','Li_1070_C.mat'));
elseif strcmp(path_name,'Li_1070_N')
```

```
26      load(strcat(pwd,'/data_for_comparison/','Li_1070_N.mat'));
27  elseif strcmp(path_name,'Li_1070_S')
28      load(strcat(pwd,'/data_for_comparison/','Li_1070_S.mat'));
29  elseif strcmp(path_name,'Li_1070_square')
30      load(strcat(pwd,'/data_for_comparison/','Li_1070_square.mat'));
31  elseif strcmp(path_name,'Li_1070_square_clock')
32      load(strcat(pwd,'/data_for_comparison/','Li_1070_square_clock.mat'));
33  elseif strcmp(path_name, 'Li_1070_V')
34      load(strcat(pwd,'/data_for_comparison/','Li_1070_V.mat'));
35  %% LOAD TAO'S STEEL DATA
36  elseif strcmp(path_name,'Tao_1070_ksi')
37      load(strcat(pwd,'/data_for_comparison/','Tao_1070_ksi.mat'));
38  elseif strcmp(path_name,'Tao_1070_N')
39      load(strcat(pwd,'/data_for_comparison/','Tao_1070_N.mat'));
40  elseif strcmp(path_name,'Tao_1070_NV')
41      load(strcat(pwd,'/data_for_comparison/','Tao_1070_NV.mat'));
42  elseif strcmp(path_name, 'Tao_1070_proportional')
43      load(strcat(pwd,'/data_for_comparison/Tao_1070_proportional.mat'));
44  elseif strcmp(path_name,'Tao_1070_S')
45      load(strcat(pwd,'/data_for_comparison/','Tao_1070_S.mat'));
46  elseif strcmp(path_name,'Tao_1070_square')
47      load(strcat(pwd,'/data_for_comparison/','Tao_1070_square.mat'));
48  end
49
50
51  if  strcmp(path_name,'circle_1p73')
52          const = 1;
53  elseif strcmp(path_name, 'Ince_ksi') || strcmp(path_name, 'Ince_N')  ...
54      || strcmp(path_name, 'Ince_NV')  || strcmp(path_name, 'Ince_S') ...
55      || strcmp(path_name, 'Ince_square') || strcmp(path_name, ...
            'Ince_square_clock') ...
56      ...
57      || strcmp(path_name, 'Li_1070_C') || strcmp(path_name, ...
            'Li_1070_N')  ...
58      || strcmp(path_name, 'Li_1070_S') || strcmp(path_name, ...
            'Li_1070_square')...
59      || strcmp(path_name, 'Li_1070_square_clock') || ...
            strcmp(path_name, 'Li_1070_V') ...
60      ...
61      || strcmp(path_name, 'Tao_1070_ksi') || strcmp(path_name, ...
            'Tao_1070_N') ...
62      || strcmp(path_name, 'Tao_1070_NV') ...
63      || strcmp(path_name, 'Tao_1070_proportional') || ...
            strcmp(path_name, 'Tao_1070_S') ...
64      || strcmp(path_name, 'Tao_1070_square') ...
65          const = 2;
66          width = 2;
67
68        p1 = plot(e_exp,g_exp,'-k','LineWidth',width); hold on;
```

```
69          p2 = plot(e_est,g_est,'-r','LineWidth',1); hold on;
70  else
71           const = (-1);
72  end
73
74  p4 = plot(epsZz*100,const*epsYz*100,'--b','LineWidth',1);
75
76  % legend preparation
77  if plotExperiments == 1
78      lgd = legend(['experiment, ' num_cycles_text],['estimate, 1st ' ...
            int2str(num_cycles) ' cycles'],'Location','Best');
79  else
80      if  strcmp(path_name, 'Ince_ksi') || strcmp(path_name, 'Ince_N') ...
81       || strcmp(path_name, 'Ince_NV')  || strcmp(path_name, 'Ince_S') ...
82       || strcmp(path_name, 'Ince_square') || strcmp(path_name, ...
             'Ince_square_clock')
83          lgd = legend('experiment (1070 steel)','Ince''s ...
                estimate','proposed method','Location','Best');
84
85      elseif strcmp(path_name, 'Li_1070_C') ||  strcmp(path_name, ...
            'Li_1070_N')  ...
86          || strcmp(path_name, 'Li_1070_S') ||  strcmp(path_name, ...
                'Li_1070_square') ...
87          || strcmp(path_name, 'Li_1070_square_clock')  || ...
                strcmp(path_name, 'Li_1070_V')
88              lgd = legend('experiment (1070 steel)','Li''s ...
                    estimate','proposed method','Location','Best');
89
90      elseif strcmp(path_name, 'Tao_1070_ksi') || strcmp(path_name, ...
            'Tao_1070_N') ...
91          || strcmp(path_name, 'Tao_1070_NV')  || strcmp(path_name, ...
                'Tao_1070_proportional') ...
92          || strcmp(path_name, 'Tao_1070_S') ||  strcmp(path_name, ...
                'Tao_1070_square')
93              lgd = legend('experiment (1070 steel)','Tao''s ...
                    estimate','proposed method','Location','Best');
94      end
95  end
96
97   grid on;
98   xlabel('axial strain [%]'); ylabel('shear strain [%]');
99
100  set(gca,'fontsize',18);
101  lgd.FontSize = 16;
102
103  %% setting axes
104  if strcmp(path_name,'7')
105     x1 =0;     incx =1;    x2 =4;
106     y1 =-0.8; incy =0.4; y2 =0.8;
```

```
107  elseif strcmp(path_name,'Ince_ksi') || strcmp(path_name,'Ince_S') ...
108                       || strcmp(path_name, 'Tao_1070_proportional')
109     x1 =-0.3; incx =0.1;  x2 =0.3;
110     y1 =-0.5; incy =0.25; y2 =0.5;
111  elseif strcmp(path_name,'Ince_N') || strcmp(path_name,'Li_1070_N')
112     x1 =-0.3; incx =0.1; x2 =0.3;
113     y1 =-0.4; incy =0.2; y2 =0.6;
114  elseif strcmp(path_name,'Ince_NV')
115     x1 =-0.3; incx =0.1; x2 =0.3;
116     y1 =-0.4; incy =0.1; y2 =0.5;
117  elseif strcmp(path_name,'Li_1070_C')
118     x1 =-0.3; incx =0.3; x2 =1.2;
119     y1 =-0.6; incy =0.2; y2 =0.4;
120  elseif strcmp(path_name,'Li_1070_V')
121     x1 =-0.4; incx =0.2; x2 =0.4;
122     y1 =-0.4; incy =0.2; y2 =0.6;
123  elseif strcmp(path_name,'NV_1p73') || strcmp(path_name,'X_1p73') ...
124                                     || strcmp(path_name,'X_1p73_f6')
125     x1 =-1.5; incx =0.5; x2 =1.5;
126     y1 =-1;   incy =0.5; y2 =1;
127  elseif strcmp(path_name,'square')
128     x1 =-1.5; incx =0.5; x2 =1.5;
129     y1 =-1.2; incy =0.6; y2 =1.2;
130  elseif strcmp(path_name,'Tao_1070_NV')
131     x1 =-0.3;  incx =0.1;  x2 =0.3;
132     y1 =-0.54; incy =0.18; y2 =0.36;
133  elseif strcmp(path_name,'Tao_1070_square')
134     x1 =-0.3;  incx =0.1;  x2 =0.3;
135     y1 =-0.63; incy =0.21; y2 =0.63;
136  else
137     x1 =-1.2; incx =0.6; x2 =1.2;
138     y1 =-1;   incy =0.5; y2 =1;
139  end
140
141  axis([x1 x2 y1 y2]);
142  set(gca,'xTick',x1:incx:x2);
143  set(gca,'yTick',y1:incy:y2)
```

C.3.5 increase_number_of_load_cycles

```
1  num_cycles = 1;
2  %% paths, end steps of which ARE the same as the first non-zero state
3  if  strcmp(path_name, '7') || strcmp(path_name,'circle_f7') ...
4   || strcmp(path_name,'circle_1p73_f8') || ...
       strcmp(path_name,'proportional_f3') ...
5   || strcmp(path_name,'proportional_f4') ...
```

```
6   ...
7   || strcmp(path_name,'circle') || strcmp(path_name,'circle_1p73') ...
8   || strcmp(path_name,'proportional_u11') || ...
        strcmp(path_name,'square') ...
9   || strcmp(path_name,'uniaxial_u5') || ...
        strcmp(path_name,'uniaxial_u9') ...
10  ...
11  || strcmp(path_name, 'Ince_N') || strcmp(path_name, 'Ince_S') ...
12  || strcmp(path_name, 'Li_1070_C')|| strcmp(path_name, 'Li_1070_N')  ...
13  || strcmp(path_name, 'Li_1070_S')|| strcmp(path_name, 'Li_1070_V') ...
14  || strcmp(path_name, 'Tao_1070_N') || strcmp(path_name, ...
        'Tao_1070_proportional') ...
15  || strcmp(path_name, 'Tao_1070_S')
16
17      yy = sigYyFI(3:end);
18      zz = sigZzFI(3:end);
19      yz = sigYzFI(3:end);
20
21      if strcmp(path_name, 'Ince_S') || strcmp(path_name, 'Ince_N') ...
22      || strcmp(path_name, 'Li_1070_C') || strcmp(path_name, ...
            'Li_1070_N')...
23      || strcmp(path_name, 'Li_1070_S') || strcmp(path_name, ...
            'Li_1070_V') ...
24      || strcmp(path_name, 'Tao_1070_N') || strcmp(path_name, ...
            'Tao_1070_proportional') ...
25      || strcmp(path_name, 'Tao_1070_S')
26          repetitions = 39;
27      elseif strcmp(path_name,'square')
28          repetitions = 106;
29      else
30          repetitions = 98;
31      end
32
33  %% paths, end steps of which are NOT the same as the first non-zero ...
        state
34  elseif strcmp(path_name,'NV') || strcmp(path_name,'NV_1p73') ...
35      || strcmp(path_name,'X') || strcmp(path_name,'X_1p73')  ...
36      ...
37      || strcmp(path_name,'NV_f11') || strcmp(path_name,'NV_1p73_f12') ...
38      || strcmp(path_name,'X_f5') || strcmp(path_name,'X_1p73_f6') ...
39      ...
40      || strcmp(path_name, 'Ince_ksi') || strcmp(path_name, 'Ince_NV') ...
            ...
41      || strcmp(path_name, 'Ince_square') || strcmp(path_name, ...
            'Ince_square_clock') ...
42      || strcmp(path_name, 'Li_1070_square') || strcmp(path_name, ...
            'Li_1070_square_clock') ...
43      || strcmp(path_name, 'Tao_1070_ksi') ||  strcmp(path_name, ...
            'Tao_1070_NV') ...
```

```
    || strcmp(path_name, 'Tao_1070_square')

    yy = sigYyFI(2:end);
    zz = sigZzFI(2:end);
    yz = sigYzFI(2:end);

    if strcmp(path_name,'NV') || strcmp(path_name,'NV_f11')
        repetitions = 48;
    elseif strcmp(path_name,'NV_1p73')
        repetitions = 41;
    elseif strcmp(path_name,'X')
        repetitions = 103;
    elseif strcmp(path_name,'X_1p73') || strcmp(path_name,'X_1p73_f6')
        repetitions = 99;
    elseif strcmp(path_name,'X_f5')
        repetitions = 98;
    else
        repetitions = 39;
    end
end

for i = 1:repetitions
        sigYyFI = [sigYyFI yy];
        sigZzFI = [sigZzFI zz];
        sigYzFI = [sigYzFI yz];
        num_cycles = num_cycles+1;
end
```

C.3.6 prealocate_variables

```
n = size(gPC,1);  % number of backstress parts
alfa = zeros(3,3);    % total backstress
alfa_part = zeros(3,3,n); % backstress parts
alfaPs = zeros(3,3);    % total pseudo backstress
alfa_partPs = zeros(3,3,n); % parts of the pseudo backstress
alfa_partPsI = zeros(3,3,n); % parts of the pseudo backstress at the ...
    beginning of the step
theta = ones(1,n);
SPs = zeros(3,3);
SPsStart = zeros(3,3);
SReal = zeros(3,3);
dEpsPl = zeros(3,3);
dEpsPlPs = zeros(3,3);
dp = 0;
if sigYyFI(length(sigYyFI)) == 0
```

```
15      % m = number of points in elastic range + number of points in ...
            plastic
16      %       range + one initial zero state
17      m = length(sigYyFI)-1 + incPerPlR*(length(sigYyFI)-2) + 1;
18  else
19      m = length(sigYyFI)-1 + incPerPlR*(length(sigYyFI)-1) + 1;
20  end
21  epsXx(1) = 0;   epsYy(1) = 0;   epsZz(1) = 0;   epsYz(1) = 0;
22  epsXxE(1) = 0;  epsYyE(1) = 0;  epsZzE(1) = 0;  epsYzE(1) = 0;
23  epsXxPl(1) = 0; epsYyPl(1) = 0; epsZzPl(1) = 0; epsYzPl(1) = 0;
24  sigY = zeros(m, 1); sigZ = zeros(m, 1); sigYz = zeros(m, 1);
25  sigYPs(1) = 0; sigYPs(2) = 0; sigZPs = zeros(m, 1); sigYzPs = ...
        zeros(m, 1);
```